THE THERMAL CONDUCTIVITY OF FILLER MATERIALS AND PERMEABILITY OF A CEMENT SEALANT FOR DEEP BOREHOLE REPOSITORIES FOR HIGH LEVEL NUCLEAR WASTE

By
Alex Salazar III

Submitted to the
DEPARTMENT OF NUCLEAR SCIENCE AND ENGINEERING

In Partial Fulfillment for the Degree of
BACHELOR OF SCIENCE IN NUCLEAR SCIENCE AND ENGINEERING

ARCHIVES

At the
MASSACHUSETTS INSTITUTE OF TECHNOLOGY

MASSACHUSETTS INSTITUTE OF TECHNOLOGY
JUL 16 2013
LIBRARIES

JUNE 2013

Copyright © 2013 Massachusetts Institute of Technology (MIT)
All rights reserved

Signature of Author: _____
Department of Nuclear Science and Engineering
May 10, 2013

Certified By: _____
Jacopo Buongiorno – Thesis Co-Supervisor
Associate Professor of Nuclear Science and Engineering

Certified By: _____
Michael J. Driscoll – Thesis Co-Supervisor
Professor Emeritus of Nuclear Science and Engineering

Certified By: _____
Thomas J. McKrell – Thesis Reader
Research Scientist for Nuclear Science and Engineering

Accepted By: _____
Dennis G. Whyte
Professor of Nuclear Science and Engineering
Chair, NSE Committee for Undergraduate Students

THE THERMAL CONDUCTIVITY OF FILLER MATERIALS AND PERMEABILITY OF A CEMENT SEALANT FOR DEEP BOREHOLE REPOSITORIES FOR HIGH LEVEL NUCLEAR WASTE

By Alex Salazar

SUBMITTED TO THE DEPARTMENT OF NUCLEAR SCIENCE AND ENGINEERING IN PARTIAL FULFILLMENT OF THE DEGREE OF BACHELOR OF SCIENCE IN NUCLEAR SCIENCE AND ENGINEERING ON MAY 10, 2013.

Abstract

The Department of Energy is contractually obligated to begin the removal of spent nuclear fuel from reactor sites by the year 2020 at the risk of increased liabilities. The Blue Ribbon Commission on America's Nuclear Future proposed in 2012 that further development is necessary for geological repositories for spent nuclear fuel (SNF) and high level waste (HLW). They also noted that deep boreholes drilled into granite bedrock may be a viable option. Among the major concerns regarding this type of repository are the retention of radionuclides and the tolerance of heat from the canisters in situ. As a barrier against buoyancy-induced flows of groundwater through the borehole, a special cement formulation has been proposed as a sealant for the waste emplacement zone. Such a sealant must be expansive to prohibit flow through lateral gaps and should have a permeability that is less than or equal to that of the surrounding bedrock. Tests of the cement cured under pressure were conducted using a pressure decay method and water as a pore fluid. Data indicate that bulk permeability of this ideal sample is on the order of $0.1\mu D$, which is sufficient to inhibit flow through the bulk material for the immense expanse of time needed for long-lived radioactive species (e.g. I-129) to decay. However, a less homogenous variation cured under atmospheric conditions indicated a two order-of-magnitude increase in permeability when subjected to increasing temperature and pressure. Furthermore, the harsh aquatic environment is likely to induce chemical changes that may impact longevity and durability.

The decay heat of the waste canisters is conceptually able to induce water flows through air gaps, cracks and voids in the borehole and can lead to enhanced degradation of the canisters themselves. Therefore, thermal conductivity tests have been performed in an apparatus simulating the annular gap between waste canisters and the borehole wall liner on materials that can function as fillers for the gap and canisters themselves. These include mixtures of bentonite and crushed granite, bentonite mud, salt, and dehydrated borax. The effects of air and helium as fillers for the void space of porous materials was also analyzed, along with convection effects in vertical and horizontal orientations. The procedure involved controlling the linear power (13, 50, and 190 W/m) of a rod-shaped electrical heat source surrounded by an annulus of material in an insulated steel pipe and measuring the average temperature change across the gap at steady-state. These data have promoted a 3:7 mixture of bentonite and granite as an optimal gap filler with a value of thermal conductivity at 0.30 W/m-K

and adequate absorptive characteristics when in contact with water. Furthermore, helium enhances the thermal conductivity of anhydrous borax, a candidate for a canister filler, by a factor of 1.9, and water increases that for bentonite (in the form of clay) by a lesser degree. Data overall indicate that the horizontal orientation of a canister is optimal at increasing the thermal conductivity of the filler due to enhanced convective heat transfer, which favors slanted borehole designs.

The findings of this thesis can be used in future studies involving computational fluid dynamics of the system as a whole, and future work is suggested in the analysis of compacted materials, corrosion inhibitors, and variations on the cement formulation that optimize swelling/voiding at high pressures and temperatures. The latter would involve varying curing temperatures and pressures and employing X-ray crystallography to analyze the phases that are present.

Thesis Co-Supervisor: Michael J. Driscoll
Title: Professor Emeritus of Nuclear Science and Engineering

Thesis Co-Supervisor: Jacopo Buongiorno
Title: Associate Professor of Nuclear Science and Engineering

Thesis Reader: Thomas J. McKrell
Title: Research Scientist for Nuclear Science and Engineering

Acknowledgments

The author would like to acknowledge a number of esteemed individuals in the department and elsewhere from whom he received invaluable assistance, guidance and encouragement throughout the formation of this thesis. Dr. Thomas J. McKrell provided extensive support and advice in developing experiments relevant to this thesis in a safe and efficient manner in the Laboratory for Thermal Hydraulics of Nanofluids. PhD candidate Ethan Bates played a valuable mentoring role throughout my research, assisting in the formulation of the hydraulic cement and the development of other procedures. Professor Brian Evans and Dr. Ulrich Mok from MIT's Department of Earth, Atmospheric, and Planetary Sciences provided crucial input on the permeability aspects of the borehole system. I am very much indebted to Dr. Mok's services over Independent Activities Period in obtaining permeability data for the cement sealant. I would like to thank Michael Mahoney of the Fletcher Granite Corporation for providing a tour of the Westford, MA location and samples of granite filings, which were valuable in serving as real industrial byproducts. Experimental costs were borne by deep borehole contracts under Sandia and NEUP/DOE auspices. Lastly and most importantly, Professors Michael Driscoll and Jacopo Buongiorno were an indefatigable source of information on the borehole concept and collection of relevant data and I am greatly indebted to their roles as advisers from the beginning. Thank you.

Contents

List of Figures

List of Tables

Chapter 1

Introduction

1.1 Objective of the Thesis

The objective of this thesis is to analyze the bulk permeability of hydraulic cement under conditions present in a deep borehole repository and to characterize the thermal conductivity of materials to be used in the borehole gap. These objectives are necessary to understand the integrity of the overall system in meeting safety requirements. The criterion of a cement sealant to be used above the waste emplacement zone must extend beyond ensuring an expansive seal and must guarantee functionality in retarding fluid flow through sufficiently low permeability and durability in a hydrologically and thermally stressful environment. Gap materials must demonstrate the ability to effectively dissipate heat from spent nuclear fuel canisters so as to reduce material stresses that can lead to the eventual degradation of the canisters and augment the risk of exposure. An in-depth analysis of the fluid flow and the risk assessment involved with environmental exposure are beyond the scope of this thesis. However, pressure-induced and thermally-induced changes to bulk permeability and the variation of thermal conductivity at different linear powers will be assessed to determine whether material criteria are upheld in the geological environment. Data from experiments will illustrate the general properties or property changes of the materials under set conditions and will be used to qualify or readjust criteria for borehole requirements. Furthermore, data obtained in the process will be used for studies involving computational fluid dynamics (CFD) and other methods of thermal-hydraulic analysis.

1.2 Topic Motivation

The motivation behind current deep borehole research is based primarily on legislation requiring the Department of Energy (DOE) to ensure that the ~70,000 MT of spent nuclear fuel (SNF) from all civilian reactor sites is removed by the year 2020 or else face further legal damage awards to taxpayers. Deep boreholes drilled into granitic bedrock have been proposed as geological repositories to serve as a permanent storage solution. The Nuclear Waste Policy act of 1982 required the government to take the initiative of removing SNF from reactor sites. In response to the recent demise of the Yucca Mountain repository, the Secretary of Energy assembled a blue ribbon commission to review the policies behind the management of the back end of the fuel cycle and to conceive recommendations for solutions to the issue of SNF (also called used nuclear fuel: UNF)

Some have argued that spent nuclear fuel presents a significant risk of public harm and biosphere contamination when housed in SNF pools for extended periods of time [7]. There are risks of zirconium fire that the NRC has determined cannot be neglected. There is the option of moving SNF to interim dry cask storage but the financial incentives to the operating utilities are limited. It is estimated that an annual cost of up to $550 million may be incurred protecting spent nuclear fuel at 70 shutdown reactor sites in the future [8]. Therefore, it is expedient to devise a long-term solution that avoids unnecessary time spent in fuel pools and dry storage.

Deep borehole repositories have been recognized by the Blue Ribbon Commission on America's Nuclear Future as a potentially promising long-term solution for the disposal of high level wastes due to their effectiveness at isolating HLW[8]. However, as is the goal of this thesis, more information must be obtained to validate their technical feasibility, particularly in their effectiveness at preventing the exposure of long-lived radionuclides to the biosphere for long periods of time.

1.3 Overview

The system of interest is shown in figure 1-1, showing a borehole drilled 4-5 km deep into

crystalline granitic bedrock. The hole is approximately 45 cm in diameter, and its depth is determined primarily by economics. It is assumed that a drop-in model will be used where the terminal velocity of the canisters is low enough to prevent significant damage, using water to first flood the hole [9].The canisters themselves are around 34 cm in diameter, allowing the accommodation of a typical 21 cm x 21 cm PWR assembly.

Cement is poured to line the bottom of the hole as the first barrier to interaction with groundwater. A pilot canister (or possibly a few of them) holding no radioactive material is the first to be inserted, and bentonite mud is poured in the gap around each of them once the 2-3 km emplacement zone is filled with ~200 SNF canisters. A steel liner is used as a structural aid. A perforated guidance liner has been proposed to facilitate the filling of the gap between the canister and the steel liner. An expansive cement sealant is then poured to create a 200 m barrier above the emplacement zone. Another such barrier is poured 600 m above a layer of granite sand (drilling cuttings). The last kilometer consists of overburden used to refill the hole and coarser granite gravel, and the hole is capped with cement as a barrier to outside intrusion.

The future retrieval of SNF for purposes of reprocessing is not a key concern considering both the economics of reprocessing and its current prohibition in the United States. Furthermore, although fissile material from SNF can be used to assemble crude nuclear weapons,[10] the radioactive environment and engineered deterrents pose significant risks and hindrances to terrorists seeking its use. However, this self-protecting quality of the waste is only effective enough for a few hundred years, which gives incentive to providing a physical barrier that cannot be compromised. In case the site cannot be maintained permanently, signage will exist as a deterrence to future generations living in proximity to the borehole against interacting with the material buried underneath. This is a measure of intergenerational responsibility that will also ensure the viability of the current industry.

An array of 20 x 40 boreholes should be adequate to store approximately 80,000 MT of waste, or a capacity similar to that of Yucca Mountain. To avoid thermal interference, each borehole is spaced at least 50 m apart (preferably 200 m),[11] resulting in a minimum $2\,km^2$ land occupation. Excessive thermal loading has certain materials consequences on the surrounding granite and borehole materials that may be unfavorable. For example,

excessive thermal stress (corresponding to a canister temperature of 200-250 °C) coupled with the pressures of the borehole, can cause microfractures in the granite that enhance permeability.[12] The bentonite buffer is subject to cementation and illitization (the transition to a non-swelling clay) at temperatures of 150 °C within a period of 100 years.[13]

1.4 Arrangement of Thesis

The thesis will cover the following items of interest:

1. Thermal conductivity of materials that can be placed in the the gap between SNF canisters and the borehole liner or wall.

2. Bulk permeability of the expansive cement proposed as a sealant above the waste emplacement zone.

3. The viability of said sealant when water is passed through as a pore fluid in relevant conditions of temperature and lithostatic pressure.

The ultimate goal is to qualify or disqualify the use of certain materials as gap fillers or sealants and provide a background for future studies which can optimize the selection of such materials. Therefore, the thesis will conclude with a suggested body of future work to be completed by researchers aiming to enhance understanding and technical feasibility of the borehole system.

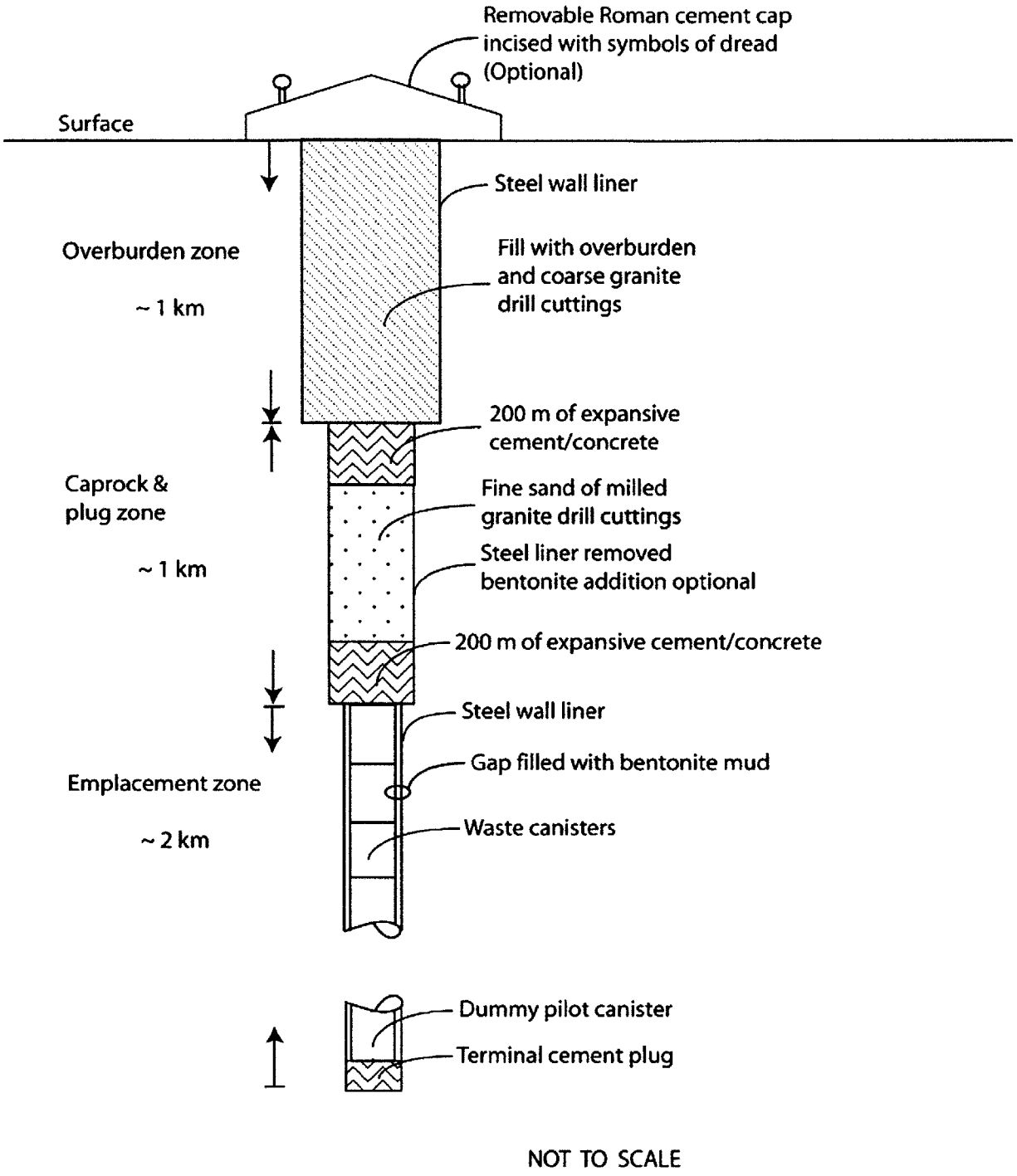

Figure 1-1: Schematic of deep borehole. Note that the emplacement zone contains on the order of 200 SNF canisters of 5 m length, and that a repository site will likely consist of a 20 x 40 grid of these boreholes separated by about 200 meters apart. This thesis concerns the layers of expansive concrete, for which custom cement formulations are tested and evaluated, and the gap filled with bentonite mud or other fill materials.

Chapter 2

The Borehole System

2.1 Groundwater and Host Rock

The interaction of the borehole system with groundwater provides the ultimate rationale for finding a strong sealant. A source of groundwater, commonly referred to as an *aquifer*, is the water saturated in the pores of soil and fractures of rocks underlying an extensive land area that interacts with water at the surface. These saturated water sources interact based on natural pressure gradients, and it is undesirable that, once a borehole is drilled, the pressure gradient causes such water to come into contact with the canisters and their radionuclides. Therefore, such applications of geoengineering must consider the hydraulic consequences posed by these lithostats both in the soil and bedrock. Permeability is a major concern as it indicates the ease at which groundwater travels with a given pressure gradient.

The geology of a repository can have permeabilities that vary over orders of magnitude with depth,[14] which in turn vary considerably with temperature and pressure.[15] Adding SNF canisters introduces a thermal environment that may cause permanent changes to normal groundwater flow processes, where permeability increases and buoyancy-induced flows become two major factors that compromise repository performance. Altogether, thermal, hydrological, and structural processes are coupled phenomena that must be analyzed to fully understand the effects of an engineered system on host rock and other solid barriers. In fact, the fluid flow and mechanical aspects are stress-dependent and dictated heavily by the presence of permanent cracks,[16] and sites that are deemed to be very solid and free of these

cracks and voids are most prone to the negative effects of thermal loading.[17] This thesis will focus more on the hydraulic consequences in the form of measuring permeability changes, although qualitative indicators of stress-related deformations must be taken into account. Furthermore, the material that will be tested is intended to have an inherently lower degree of permeability than solid granite.

The Drift Scale Test (DST) of the Yucca Mountain repository explored the accelerated effects of electric joule heating and resultant natural convection on fractured ambient host rock beginning in 1997.[18] The study employed air-injection as a means of testing permeability changes through the host rock in an offshoot of the shallow mined repository at relatively low-depth (250 m) in volcanic tuff. Initial solid rock matrix permeability was identified as being in the 10 μD range while that of the overall fractured material was much higher at 0.1 D. After the eight year experiment, it was observed in some experimental trials that irreversible changes incurred in the host rock in the form of increased fracture aperture and shear, resulting in higher permeability. Other trials revealed non-elastic surface asperity shortening, which resulted in permeability decreases. Nonetheless, it could not be guaranteed that such effects could be significant in a repository considering the failure of experiments conducted at high stress (130 ^{o}C and 10 MPa). Chemical effects such as dissolution were deemed to be the most significant for the long term, and permeability increases around horizontally oriented repositories are short-term effects that are insignificant over time.[17]

Granite is a hard, dense igneous rock comprised mainly of quartz (SiO_2), mica (a sheetlike mineral) and feldspar, and has a very minimal pore space. Alumina (Al_2O_3) and other oxides are also present in the chemical composition. As crystalline bedrock, its permeability is expected to be in the range of 1 μD to 100 mD,[19] although some granites have been observed to have values as low as 1 nD.[20] Although it is difficult to predict the specific permeability, this geology is in general suitable for use as a repository site, and the United States has several locations with outcrops of crystalline granite and other tough minerals, including the Cascade Mountains in northern Washington state, the eastern Sierra Nevada, the Rockies, New England, and the southern extent of the Appalachian mountains stretching into Alabama.[21] However, many important considerations come into play when siting, including seismically and volcanic activity, along with economic and political considerations

such as competition with existing coal mines and public acceptance of the repository. The latter is often the limiting factor in any case, although this can be alleviated with public outreach programs and perhaps tax incentives, like those given to residents near the Waste Isolation Pilot Plant (WIPP) in New Mexico.

2.2 Drilling Techniques

Deep borehole repositories have the advantage of being based on heavily researched and proven industrial technologies along with specific pilot systems demonstrated in Europe. Wells have been drilled to depths matching and exceeding 4 km, such as the geothermal application in Soultz, France, by the European Hot Dry Rock Program, which features a 5100 m deep borehole,[22] and the 12.5 km drillhole at Kola Peninsula in Russia.[23] In fact, exploration for the geothermal industry has provided a great deal of data for boreholes several kilometers deep and has inspired a number of different components in the overall design of the deep borehole repository, along with insight into the use of certain materials.

A consistent design issue has been the ability to provide the appropriate width for the canisters, which have a minimum 34 cm diameter.[24] Nonetheless, the natural gas and oilfield service industries can be presumed to benefit from further research and development that can alleviate this concern and provide the framework for repository specific development. For example, ARPA-E has been funding advanced research on laser-assisted drilling technology to avoid the wear associated with grinding through tough rock like that proposed to host a repository.[25]

An advantageous development in regards to analyzing the deep borehole geological environment is the Stripa project in Sweden. This consists of a mine in crystalline bedrock on the site of an abandoned iron mine that was assessed specifically for its properties at housing radioactive materials. Small boreholes were created and the parameters that were tested included the extent of fractures in the caprock, the interaction with groundwater, the migration of nuclides, and the use of bentonite clay as a backfill material.[26] Albeit a shallow mined repository in design, it demonstrated the feasibility of customizing borehole diameters and drilling through tough crystalline bedrock.

Although Yucca Mountain was dismissed as an option, the Waste Isolation Pilot Plant in southeastern New Mexico has been successful. This shallow mined repository was sited in deep salt beds to provide a favorable thermal and chemical environment for the transuranics produced during the Cold War weapons program. Site evaluation began in 1975 per the recommendations of the U.S. Geological Survey[27] and after congressional approval the facility began receiving waste in 1999. The geology of the repository location was favorable, and unlike the site proposed in Lyons, Kansas during the 1970s, this site was not plagued with openings caused by industrial surveys. Following this example, the testing of rock salt to model heat dissipation in salt beds is promoted for experimentation.

2.3 Spent Nuclear Fuel Canisters

The canisters to be inserted into the borehole are designed to contain one standard 17x17 PWR assembly of 21 cm width or three BWR assemblies (with channels) along with packing material. Consolidation of the fuel rods has also been considered as a space-saving measure. Design considerations must take into account the interactions between the casings and irradiated host rock, which presents a tough chemical environment that can result in embrittlement. SNF contains practically the entire periodic table in the form of fission products from ^{235}U; some of these nuclides, such as ^{99}Tc and ^{129}I, have half-lives on the order of a 10^5 to 10^7 years, posing long-term threats to exposure long after their formation. These fission products necessitate a canister design that can resist radiation damage for a long period of time and can resist breakage (either via emplacement or high pressure) to prevent leakage. Therefore, cast iron is the major component of their design due to its structural integrity and shielding, along with its ability to conduct heat.

In general, canisters designed to hold SNF are meant to be durable and part of an overall design that is safe for transport. The nuclear industry has successfully demonstrated the safety of SNF casks used for transport by land and the existing infrastructure is poised to accommodate similar procedures for repository-specific transportation operations. However, there are some vulnerabilities in design, mostly stemming from the structural resistance to impacts from other canisters upon emplacement and the chemical vulnerabilities of the

copper used to coat the cast iron.

Emplacement Zone

Once a plug of cement is cured at the extreme of the borehole, the first 2 km are prepared for the emplacement of the spent fuel canisters. It has been proposed that the borehole first be flooded with water so that the canisters can be simply dropped-in from a crane or transport vehicle.[9] The conservation of momentum forces the water to move much faster through the gap than the canister itself such that the terminal velocity of the canister is low enough to safely impact other ones already in place.

The gap formed between the canisters and borehole liner is filled with bentonite to serve as both an absorber of radionuclides and a medium of dissipating heat into the host rock. The goal of this thesis is to test the effective thermal conductivity of bentonite along with other possible fillers to verify that heat is adequately removed from the emplacement zone.

2.4 Rationale for Choice of Repository

There are several advantages for choosing this type of geologic repository over other available options, and the full consideration of these proponents exceed the scope of this thesis. For one, the environment of the borehole is highly reducing (as opposed to the oxidizing surroundings within Yucca Mountain) which reduces solubility of radionuclides in water.[11] More of these nuclides are absorbed in the fuel and thus mobility through dissolution is limited. Furthermore, the bentonite clay proposed for use as a gap filler is highly absorbent and can readily trap nuclides in its solid matrix.

The materials used in the borehole, whether fillers or sealants, are readily available and consist of natural, non-organic materials that can withstand the test of time. For example, crushed granite is a byproduct of cutting and processing at quarries and can be shipped from those sites at low cost. Portland cement that can be used for sealing consists of natural limestone ($CaCO_3$), sand (SiO_2), and gypsum ($CaSO_4 \cdot 2H_2O$),[28] all of which are found from natural sources like shale. This lends great economic feasibility to the design.

Granitic bedrock is prevalent throughout the continental United States, such as the White

Mountains of northeast Washington state. The permeability of bedrock is known to vary by orders of magnitude with respect to depth, with crystalline rock ranging from $1\mu D$ to $1\ mD$ (where $1\,D \approx 10^{-12}\,m^2$) [19]. This range is highly suitable for restricting fluid flow in man-made geological systems for many thousands of years and placing reliance mainly on the sealants used for these systems. It is of note that the salt bed repository that was proposed for Lyons, KS in the seventies was abandoned because of previous drilling on the property that compromised the isolatedness of the facility and vastly increased permeability. Therefore, proper geological siting, such as that conducted at WIPP, can lead to choosing optimal bedrock sites with minimal fracture presence.

Lastly, existing drilling technology and the research and development sponsored by the natural gas and oilfield industries provide a greater degree of feasibility at constructing these repositories and offers a reasonable outlook in terms of the construction period. This RD&D also provides insight as to the innovative use of certain materials such as backfills and sealants. The depth at which these holes are drilled provides an effective barrier to tampering and vastly reduces the potential for proliferation, and the layout of each hole allows for low maintenance and remote monitoring (i.e. by satellites.)

2.5 Summary

Granite is a prime candidate for host rock due its low permeability and reducing environment, which decreases the solubility of radionuclides in groundwater and retards the flow of water to the surface. The deep borehole repositories engineered for this host rock have an overall capacity similar to shallow-mined repositories and suggest high technical and economic feasibility. Cast iron canisters can be used to store individual spent PWR assemblies and about 200 can be placed within each hole at the lower 2 km extreme. However, once the hole is drilled, its effectiveness at preventing the migration of potentially contaminated water is dependent on the permeability of the sealant used to seal the zone containing the canisters.

Chapter 3

Expansive Sealant

3.1 Rationale for choosing an expansive sealant

Among other materials-based concerns, the use of a sealant that self-pressurizes upon setting is a crucial factor. In the event of the upward flow of groundwater through the borehole, such a sealant is needed above the waste emplacement zone so it can expand and form a tight fit with the borehole wall or liner. It is also necessary that the bulk permeability be less than or equal to the permeability of the surrounding granitic bedrock, such that in the event of leakage flow is forced through the larger extent of bedrock rather than the seal, allowing for greater protection of the biosphere.

Darcy Permeability

Darcy's Law for volumetric flow through the axial length of a cylinder of material is given by equation (3.1), where $\kappa$is the permeability, μ is the dynamic viscosity of the fluid, D is the diameter of the plug, and ΔP is the pressure change across a length ΔL. For a fluid acting upon a material of set geometry and given external pressures, the flow rate is proportional to permeability; therefore, in systems that require fluid retardation, permeability must be as low as possible. The parameter $\kappa$is of key interest for the sealant as it cannot be considered independent of surrounding pressure and temperature and may in fact vary when subjected to these stresses in the borehole environment. The goal is not to ascribe an empirical model to

permeability data, but to understand the general behavior and orders of magnitude involved.

$$Q_P = \frac{\pi}{4} D^2 \frac{\kappa}{\mu} \left(\frac{\Delta P}{\Delta L}\right) \tag{3.1}$$

Also of importance is the minimization of borehole gaps. A variation on Darcy's law for an annular gap of width δ can be obtained by solving the Navier-Stokes equations for laminar flow in the gap and results inequation (3.2), where τ is the tortuosity, or twistedness, of the flow path. Since the gap is a small open space, it does not depend on κ.

$$Q_a = \frac{\pi}{12} \frac{D}{\tau} \frac{\delta^3}{\mu} \left(\frac{\Delta P}{\Delta L}\right) \tag{3.2}$$

The ratio of equation (3.1) and equation (3.2) results in equation (3.3), which demonstrates the extreme sensitivity of gap flow to the width of the gap. This sensitivity indicates that width differences as low as 1 μm have impact on flow of several orders of magnitude. The parameters for Darcy flow are illustrated in figure 3-1. Since the gap essentially makes concentric pipes out of the cylinder and wall, an analysis of the hydraulics of the gap will follow using the conservation laws.

$$\frac{Q_a}{Q_P} = \frac{1}{3} \frac{\delta^3}{D\kappa\tau} \tag{3.3}$$

Flow in a concentric annulus

It is important to understand the hydraulics of a gap to realize the conditions affecting fluid flow when a seal is breached. This involves knowing fluid, kinematic and geometric parameters that affect the overall flow rate. It is implied that with very low velocity, the flow in the annulus created by a gap between the canister and borehole liner will be laminar. Assuming the fluid breaching the seal is incompressible and that flow is restricted to the z-direction with constant viscosity, the conservation of momentum holds that

$$\frac{D}{Dt} v_z = \frac{\partial v_z}{\partial t} + (\mathbf{V} \cdot \nabla) v_z = -\frac{1}{\rho} \frac{\partial P}{\partial z} + g_z + \nu \nabla^2 v_z \tag{3.4}$$

where ν,ρ, and v_z are the kinematic viscosity, density, and velocity of the groundwater,

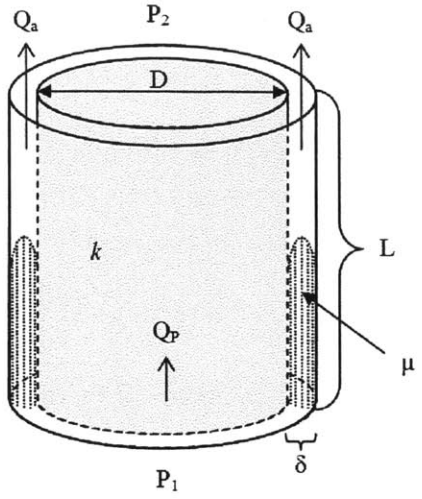

Figure 3-1: Diagram of Darcy flow parameters for a material with gap of width δ. ΔP is defined here as $P_1 - P_2$. Flow in the gap is laminar and has a half-toroidal shape.

V is the velocity vector, P is the external pressure and g is gravitational acceleration. We know that $\nabla^2 v_z = \frac{1}{r}\frac{d}{dr}\left[r \cdot \frac{dv_z}{dr}\right]$, since flow is assumed to be fully developed (parabolic) and laminar, implying that angular and longitudinal components can be ignored. Making a steady-state assumption, this equation is simplified and integrated twice with respect to r to give velocity in the form

$$v_z(r) = \frac{1}{4\mu} r^2 \frac{d}{dz}\left(P + \rho g z\right) + C_1 \ln(r) + C_2 \tag{3.5}$$

where μ is the dynamic viscosity and C_1 and C_2 are constants of integration. For a borehole of radius a and canister of radius b, the boundary conditions of the gap are as follows:

$$\begin{cases} v_z(r = a) = 0 \\ v_z(r = b) = 0 \end{cases} \tag{3.6}$$

These are known as no-slip boundary conditions. Applying these boundary conditions and solving for the constants, equation (3.5) becomes

$$v_z(r) = \frac{1}{4\mu}\left[-\frac{d}{dz}(P+\rho gz)\right]\left[a^2 - r^2 + \frac{a^2-b^2}{\ln(b/a)}\ln\left(\frac{b}{r}\right)\right] \tag{3.7}$$

Applying the conservation of mass, the flow rate Q is determined by integrating 3.7 over the annulus to get

$$Q = \int_b^a v_z(r) * 2\pi r dr = \frac{\pi}{8\mu}\left[-\frac{d}{dz}(P+\rho gz)\right]\left[a^4 - b^4 - \frac{(a^2-b^2)^2}{\ln(a/b)}\right] \tag{3.8}$$

which makes sense since there should be no flow if there is no gap ($a = b$). The sensitivity to the relative magnitudes of a and b (the gap width) is noticeable.

Let's presume that $G = \left[a^4 - b^4 - \frac{(a^2-b^2)^2}{\ln(a/b)}\right]$, a coefficient based entirely on the annulus geometry. Using a canister diameter of 0.386 m ($b = 0.193\,m$), as proposed by Hoag[24] for BWR assemblies, the effect of increasing the radius of the gap a on G is shown in figure 3-2. This demonstrates the large sensitivity of increasing the gap width: a $10\,\mu m$ increment results in a two order of magnitude increase in G and thus Q. This correlates with the analysis based on Darcy's Law and the Navier-Stokes derivation.

Due to the sensitivity of flow rate to gap width, it is extremely important to select materials that can eliminate the presence of such a gap. The following section will discuss criteria for an ideal sealant and materials that can satisfy them when employed in the borehole.

3.2 Overview of candidate materials

This section addresses the different sealant candidates for obstructing flow in the borehole. The following are major criteria that are used to determine their usability:

1. The ability to expand and press against the surface into which they are inserted
2. Very low permeability less than or equal to that of the host rock (no greater than 1 mD)
3. Resistance to chemical degradation from water and low solubility
4. Structural resistance to cracks

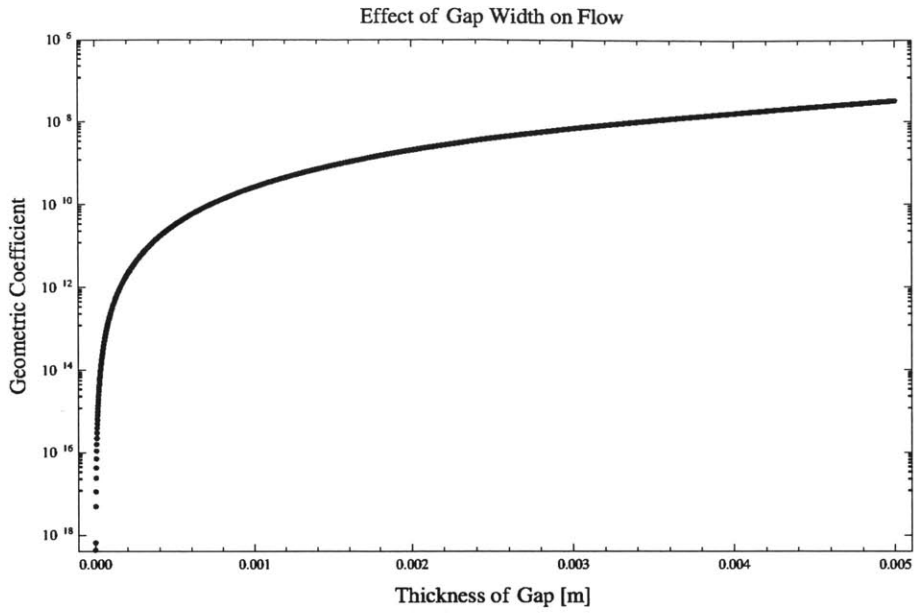

Figure 3-2: The effect of increasing the gap width to 1 cm on the annular geometric term of equation (3.8). Data points are in steps of microns.

The one millidarcy requirement is used in accordance with the upper range of permeabilities of crystalline bedrock, as previously mentioned. Although a proper analysis of item 4 is beyond the scope of this thesis, it is nonetheless an important factor that can at least be qualitatively assessed on the laboratory scale. Fractures have long-term implications on the viabilities of certain materials, and in a system meant to last for very long periods of time, this should not be an aspect for compromise.

3.2.1 Sodium Silicate

Sodium silicate gels have been proposed as sealants for open spaces in earth formations.[29] Samples were tested in the lab with the composition detailed in table 3.1, which consists of components that can be found readily in geologic formations or from industry. Calcium chloride ($CaCl_2$) is extracted from limestone or as a byproduct of the ammonium-sodium process and is usually in the form of flakes. Sodium silicate (Na_2SiO_3) can be prepared with sand in an alkaline process and it has seen applications as a a cement accelerator with slurries containing CMHEC retarder.[30] This particular composition was very exothermic when water was added to the other components and depending on the extent of mixing, the

Component	w/o
Quikrete® All-Purpose Sand	6
Calcium Chloride ($CaCl_2$)	5
Sodium Silicate (Na_2SiO_3)	41
Water (H_2O)	48

Table 3.1: Expansive mixture of sodium silicate and calcium chloride.

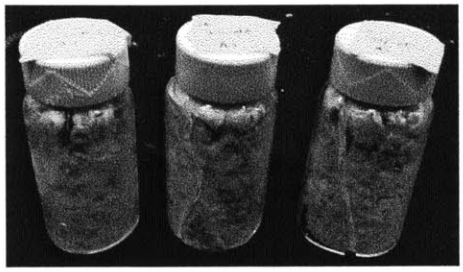

Figure 3-3: Hardened laboratory samples of the sodium silicate mixtures.

slurry would begin hardening within ten minutes to an hour. When confined to a specific volume, which included plastic centrifuge tubes and glass vials, the mixture would expand and cause fissures in the tubes or break the vials. The crystallized samples were very hard, the glass vials cracked as quickly as 5 days. However, when the mixture was placed in an open vessel, such as a plastic pipe open at one end, the mixture formed bubbles overnight and the resulting product had the consistency of wax or hard gelatin. It was therefore assumed that this particular sealant would not have sufficient long-term durability or resistance to hydraulic flow and was removed from consideration pending future experiments able to replicate it-situ conditions.

3.2.2 Borax

Sodium tetraborate ($Na_2B_4O_7{\cdot}10\,H_2O$) (STB) has been considered for use in wellbores as a downhole water-swellable component for certain applications[31]. It has the advantage of a high melting point, low rate of dissolution, and markedly different interactions with water in its hydrated and anhydrous forms. Both forms of borax were tested in glass vials immersed with deionized water. 15 g of anhydrous borax was used to fill about half the vial, while 7 grams of the decahydrate (20 Mule Team® Borax) was used due to the lower bulk density.

Adding water to anhydrous borax in small glass vials was noticeably exothermic, while no changes in temperature were observed in the other set. In fact, hydrated borax does not react with water and retains a "slush" consistency. The results are shown in figure 3-4, where some of the originally anhydrous samples expanded and cracked the vial in as little as three days, forming a hard, dense plug.

Borax was placed in another medium to test expansiveness and acquire a general understanding of permeability. This was for ascertaining its dual use as a canister filler in the event of fluid penetration. A hole of 3.13 mm diameter was made 15 mm from the base of a small aluminum can (2" OD by 3.75" length). 100.14 g of anhydrous sodium tetraborate was measured to occupy about a third of the given volume (or twice the axial height of the hole). Once inserted, dyed water was used to fill the can several times and the penetrant was observed to leak copiously through the hole. Therefore, the STB was allowed to sit overnight with the mouth of the can and the hole sealed.

The borax was measured to have been saturated with 15.00 g of water, implying a porosity of ~0.35. Since $\rho_{bulk} = 1.5(6)\, g/cm^3$ and $\rho_{solid} = 2.367\, g/cm^3$), this agrees with the calculated porosity of 0.34. Since the STB mesh is US #16 (1.7 mm), and employing the calculated void ratio (0.52), the Kozeny-Carmen correlation predicts a permeability of 870.29 D $\pm$ 564.85. After four days of "curing" the permeability of the now hardened borax mixture was tested using a falling head of water occupying the empty space in the can. Due to the uneven surface of the bed (caused by the dye penetrant) a dip stick was used to measure the actual height for the fluid head (L). The initial bed height was 2.9 cm and the initial head space was 5.7 cm, and the bed was pre-saturated (only absorbing 1.12 g H_2O this time). The empty space was filled with water with the hole held plugged, and then water discharge was measured on a scale while being timed. As trials progressed, a popping sound could be heard inside of the can, which may have been indicative of expansion caused by hydration.

Data indicated that over six trials the flow rate decreases by order of magnitude. However, using equation (3.1), permeability was determined to be in the hundreds of Darcy, which is not adequate for sealing criteria. It was therefore removed from consideration as a main sealant for the actual borehole. Further experiments on the STB perhaps after a more extensive hardening period may reveal even more reductions in permeability, which may

Figure 3-4: Top Row: Three vials of anhydrous sodium tetraborate left in contact with a head of water overnight. All three would eventually crack. Bottom Row: Hydrated borax left overnight with the same conditions. All three samples retained a "slushy" consistency.

be promising for the canister fill. Nonetheless, as shown in 3-5, when the STB is fully hardened, the material was able to expand enough to break the aluminum can as opposed to an expansive mixture of cement (explained later).

3.2.3 Cement

Among the considerations for a sealant are long-term durability and resistance to wear from a potentially aqueous and reactive environment. Cement has been demonstrated to last for long periods of time underwater, with examples found submerged and intact at the ancient Roman port of Caesarea in modern Israel: the single greatest application of concrete in antiquity.[32] Its applications in modern times are extremely diverse and serve as hallmarks of industrial infrastructural development. The oilfield services industries have employed specific formulations of cement to meet their engineering needs. Therefore, cement serves as the most obvious candidate for use in our deep borehole repository, which presents stressful and demanding conditions that require specific manipulation of its constituents.

Cement is prepared in the form of a two-phase slurry that can be poured into a deep well and, depending on the components of the mixture, cured over a certain period of time

Figure 3-5: Aluminum cans with hydrated sodium tetraborate (left) and cured expansive cement (right). Slightly visible is the pin hole used to flow water through the solid bed of STB.

into a hardened form. The hardening occurs through hydration reactions in which carbon dioxide is released and crystals begin to form and interlock, and the process time is dependent upon water content, additives, the method of stirring, and external temperature and pressure.[30]ASTM type I/II cement from Quickrete® was used as the default Portland cement component that served as the foundation for the different mixtures employed in all experiments. According to the standard, this cement can be used to attain special properties, and has the phase composition of 59% $3\,CaO \cdot SiO_2$, 11% $2\,CaO \cdot SiO_2$, 5% $3\,CaO \cdot Al_2O_3$ and 10% $4\,CaO \cdot Al_2O_3 \cdot Fe_2O_3$. By test, it is shown that the overall chemical composition is 63% calcium oxide (CaO), 21% silica (SiO_2), 4.4% alumina (Al_2O_3) and no more than 6.0% magnesium oxide (MgO) with a maximum porosity of 12%.[33]

3.3 Cement Additives

Several additives have been tested by many industries to suit various purposes, to the extent that competition amongst them has resulted in patents and private methodologies. Typical Portland cement is not adequate on its own for serving as a sealant because it in fact shrinks upon curing, as shown in figure 3-6. Therefore, additives must be used in formulations with Portland cement to improve mechanical stability, to resist chemical wear and most importantly to expand. This section summarizes a range of materials that can be used to achieve these desired results.

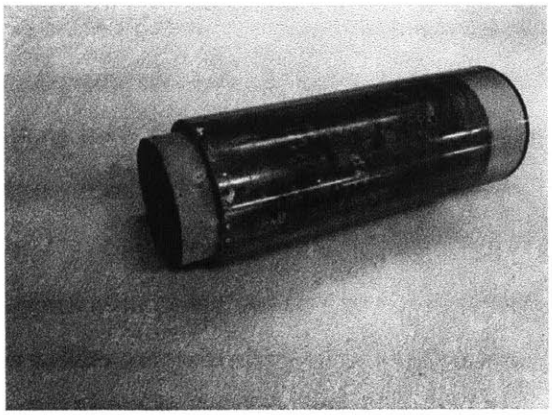

Figure 3-6: A sample of Portland cement cured in 2" PVC pipe demonstrates shrinkage after curing.

Sand

Sand, comprised primarily of SiO_2, has low reactivity with cement and decreases the overall specific heat capacity and increases the thermal conductivity in the aggregate[34]. In general, the lower total interface area of the sand particles relative to more homogeneously diffused substances (e.g. silica fume) creates the slippage characteristics with the cement matrix that results in these properties. Furthermore, this results in increased mechanical stability of the material, including greater resistance to shrinkage.

For reproducibility, sand to be used in cement aggregates was sieved with a W.S. Tyler RO-TAP model RX-29 sieve to defined ranges of particle sizes using standard U.S. meshes, as shown in figure 3-7. Individual meshes were weighed using a Mettler-Toledo model PB3002-S/FACT scale. Figure 3-8 compares the fractional amount of sand passing through the sieves with data recognized in the ASTM C-33 standard. Both figure 3-7 and figure 3-8 demonstrate that intermediate particle ranges form the majority of particles passing through the sieves, and that the bulk sample used in the laboratory conformed to the finer meshes of the accepted standard. U.S. Mesh 100, identifying particles between 150 and 300 μm, was chosen as the procedural sand additive for experimental mixtures due to its fineness and practical on-site obtainability.

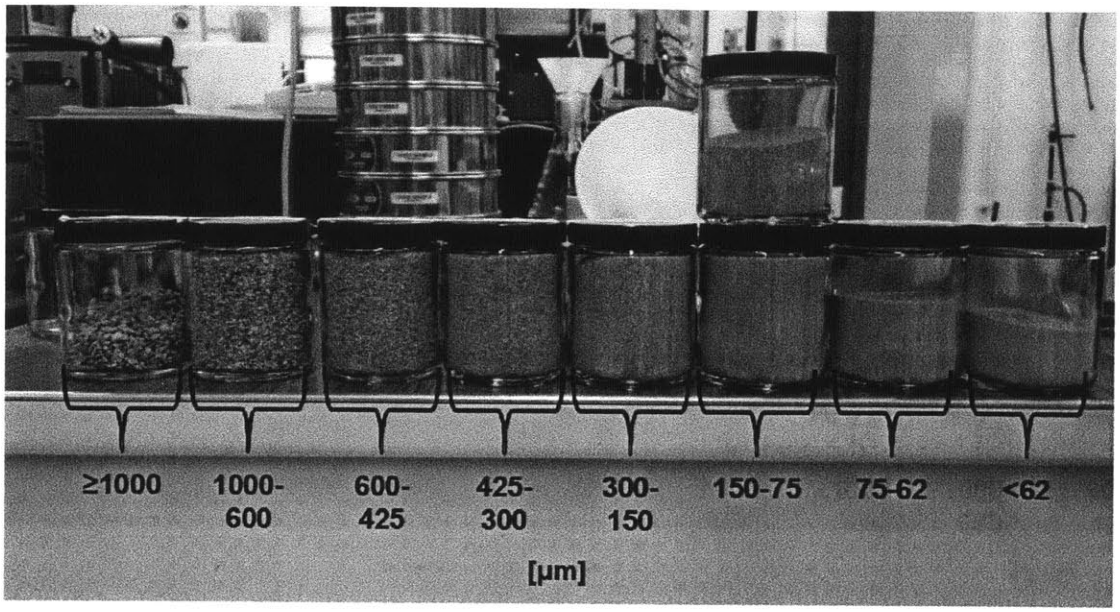

Figure 3-7: Sieving of Quickrete® sand using standard U.S. sieves. Particle size bins in micrometers are indicated.

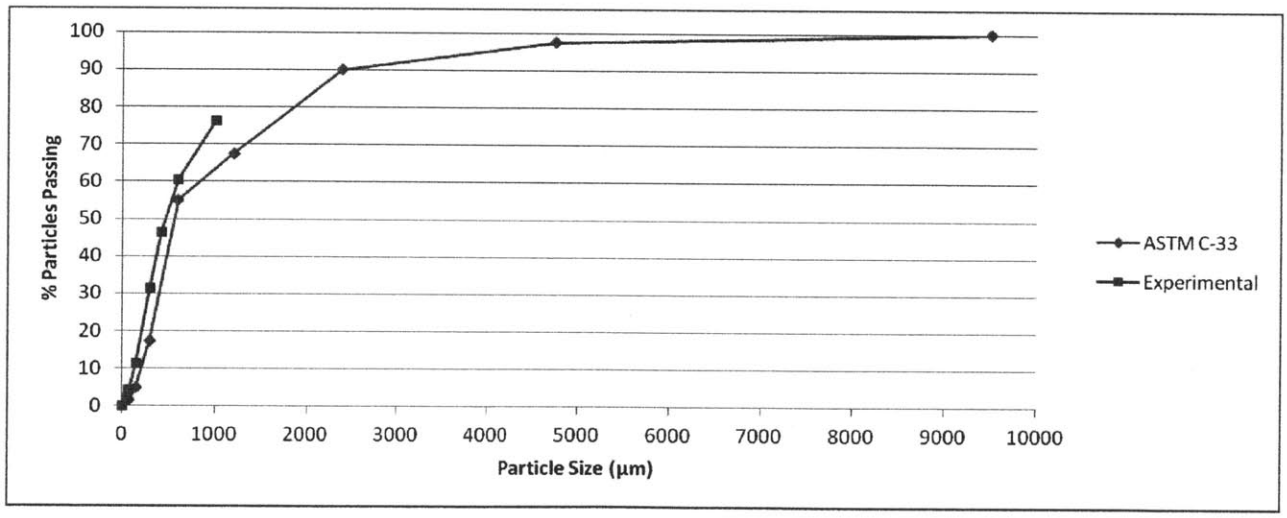

Figure 3-8: Fractional amount of particle sizes passing through standard U.S. sieves for Quickrete® sand compared to ASTM C-33 standard.

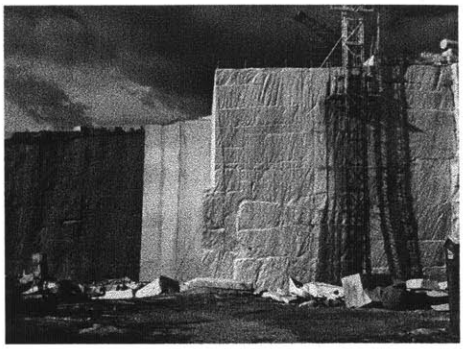

(a) Photograph of bleached granite at the Fletcher Quarry (Westford, MA).

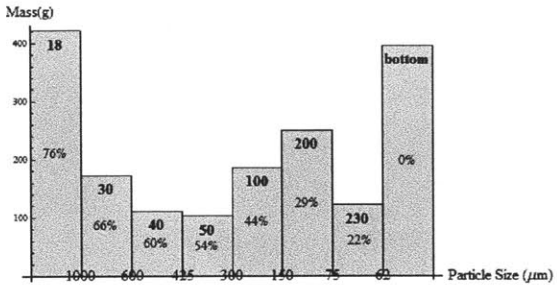

(b) Histogram of particle size distribution of granite filings obtained from Fletcher Quarry, with sieve and associated passing percentages.

Figure 3-9: Characterization of crushed granite.

Crushed Granite

To provide greater economic flexibility, fine sand can be provided as a cement component for the borehole in the form of crushed granite from nearby quarries or as a byproduct from the drilling process itself. Crushed granite was obtained as an on-site byproduct from the nearby Fletcher quarry in Westford, MA (3-9a) and a histogram of particle sizes obtained from a sieving is shown in figure 3-9b. As mentioned earlier, granite consists primarily of quartz (SiO_2) and contains mica, feldspar, alumina (Al_2O_3) and other oxides, which makes it chemically similar to sand.

Magnesium Oxide

The potential use of magnesium oxide was inspired by drilling applications in the natural gas industry.[35][36] This is found in nature as the mineral periclase and undergoes an expansive hydration reaction forming magnesium hydroxide: $MgO + H_2O \rightarrow Mg(OH)_2$. Therefore, this additive was one of immediate consideration, and the result of formulation tests yielded a composition, shown in table 3.2, that consistently cracked its containers. It became the "optimal mixture" that was selected for permeability testing despite further work yielding other potential candidates. The unusual numbers in the table are the result of the conversion to mass percents. Initially, the procedure varied *volumetric* percents of just the solid materials, allowing water (typically 30% of the total solid mass) to be adjustable to have a slurry

Component	w/o
Portland Cement	31
MgO	26
100-Sieve Sand	20
H_2O	23

Table 3.2: The expansive mixture with magnesium oxide, used as the subject material for the permeability experiments.

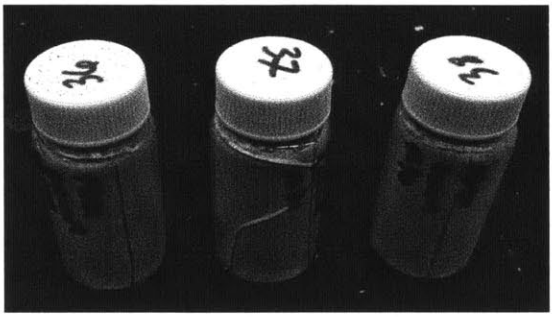

Figure 3-10: Vials containing expansive mixture of table 3.2 with crushed granite instead of fine sand, which were still able to expand around the same period of time (~10 days).

that was not too fluid or too viscous. The MgO used in experiments was Alfa Aesar® 95% minimum 140-325-Mesh powder, which had a solid density of 3.58 g/cc. Due to the chemical similarity between crushed granite and sand, along with the similar fineness of particle size (figure 3-9b and figure 3-7), this same composition is successful replacing one with other, and the results are shown in figure 3-10.

Pumice

A volcanic, pozzolanic material, pumice is comprised primarily of silica (SiO_2) alumina (Al_2O_3) and iron oxide (Fe_2O_3) and serves as a light, economic and inert filler for cement.[37] As a pozzolan, it can react with calcium hydroxide ($CaOH$) in the presence of water to form cementitious compounds, and improve mechanical durability in the overall cement composition.[38] In fact, pozzolanic cements have been shown to have lower permeability and greater resistance to chemical degradation, which is especially advantageous for use in the borehole environment.[39] Mixtures of 65-74% Portland cement, 3-12% pumice, and 23% water were prepared in the laboratory, with the slurries inserted into large glass vials.

None of these mixtures were able to expand and crack their vessel, as was the case for the optimal MgO-based mixture cured in the same vessel. However, one of these cured samples (12% pumice, 65% Portland, and 23% water) was submerged underwater, and yielded better resistance to degradation by water than the optimal mixture, as will be shown later.

Gypsum

Gypsum ($CaSO_4 \cdot 2H_2O$) commonly referred to as plaster of Paris, is typically used as a cement accelerator for shallow, low temperature (~100 ^{o}C) formations and a light expansive and gelling agent.[30] This allows for quick cementing applications that build up as much as 500 MPa of stress in as short a time as 5 minutes.

The expanding mixture of magnesium oxide is not affected by the addition of gypsum in place of sand, and the composition ("Gypsum Mix 1") is shown in table 3.3a. In fact, adjusting this composition to include fine sand, accommodated by decreasing the ratios of other solid constituents evenly, also produces an expansive mixture and this composition ("Gypsum Mix 2") in is neighboring table 3.3b. In accommodating the sand, it was particularly important to maintain the same mass percent of water to retain the consistency of the slurry. The percentages of each original solid component was reduced by 5% to ultimately provide 15% of mass available for the sand.

One of the gypsum samples was discovered to have expanded and cracked its glass vial after a period of (at most) seven days, and overall the time to expand is approximately 9 days. This is comparable to the amount of time it took the optimal MgO mixture to expand.

As expected, the gypsum additives caused the cement to harden more quickly in comparison to the optimal MgO mixture. It is not certain whether this quality is conducive to the mixture being used as a sealant for a deep borehole repository. Since the borehole is so long relative to diameter, the slurry will need to have a delayed thickening to allow for complete coverage of the sealing zone. In fact, cement "accelerators" are meant for utilization in shallow systems, and premature drying in the borehole may result in complications during pouring such as an incomplete seal and voids above the emplacement zone.

After curing, it is imperative that the samples be submerged in water to test aquatic viability. It is possible these sample types may exhibit better water resistance than the current

Components Mix 1	w/o
Portland Cement	30
MgO	25
Gypsum	20
H_2O	25

(a)

Components Mix 2	w/o
Portland Cement	25
MgO	20
Gypsum	15
100-Sieve Sand	15
H_2O	25

(b)

Table 3.3: Expansive mixtures with magnesium oxide and gypsum. Mix 2 in 3.3b was derived from Mix 1 (3.3a) by compensating amongst the existing solid components but maintaining the same water content, which was crucial to maintaining the form of the slurry.

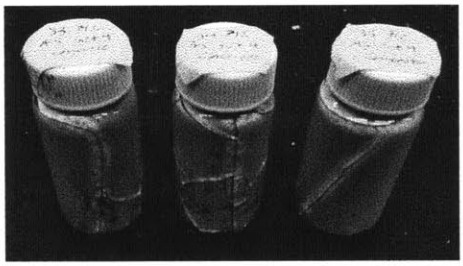

Figure 3-11: Vials of expansive cement with gypsum additive from table 3.3b.

samples that are submerged. This mixture was excluded from permeability measurements due to the limitations of time, but it has been proposed as a viable candidate for future studies.

Asphalt

Gilsonite, a natural form of asphalt, is an inert additive that is lightweight and acts as a lost-circulation agent, which prevents the contamination of drilling mud.[30] An old patent claims gilsonite imparts greater structural integrity, lower density and flash setting to well cement.[40] This allows the cement slurry to stay in place within the well, but to achieve this flash setting, it reduces the thermal conductivity of the cement slurry, which may have an impact on the heat transfer characteristics of the cured product. Although the SNF canisters interact with the cement sealant at one interface, it would not be a desirable quality to restrict heat dissipation in the axial direction. If the cement cannot dissipate heat, it can undergo structural degradation.

For a deep borehole, a light cement that hardens quickly is not desirable for sealing as it cannot be guaranteed that the slurry will reach the bottom quickly; in fact, a densifier should be use if anything. Furthermore, organic compounds are not warranted to last for geological expanses of time, and asphalt in particular is known to be degraded by aerobic microorganisms.[41] A bactericide, such as phenols and formaldehyde, may not be a solution to avoiding this issue given the long periods of time involved. Therefore, it was determined that asphalt should not be used for this particular long-term application.

3.4 Procedure for selecting among candidates

Glass Vials

Small glass vials of approximately 25 mL volume were used as sample vessels. The procedure consisted of inserting the slurry in three separate vials for triplication and for curing to take place with the vial cap screwed-on. A mixture was determined to be expansive if all three vials cracked upon curing; however, it is important to understand the structural mechanics qualifying that assumption. With a radius-to-thickness ratio of 12.28, thin-shell models can be used to quantify the minimum hoop stress of the expanding cement upon shattering the vials.[1] This hoop stress is analogous to what can be expected in the borehole with the cement pressing against a borehole liner. The three steel casings for the borehole proposed in Hoag[24] also fit thin shell criteria, although their yield strengths are obviously much higher than glass.

The following equations illustrate stresses on a thin cylindrical shell in cylindrical coordinates, which are illustrated in figure 3-12:

$$\sigma_z = \frac{(P_{inner} - P_{outer})R}{2t} \tag{3.9}$$

$$\sigma_\theta = \frac{(P_{inner} - P_{outer})R}{t} \tag{3.10}$$

[1] A thin shell is typically defined as having $R/t > 10$.

$$\sigma_r = -\frac{(P_{inner} - P_{outer})}{2} \tag{3.11}$$

The threshold of permanent, plastic yielding of a material is then defined according to the Tresca Stress criterion (equation (3.12)) where S_y is the yield stress.

$$S_y < \max\{|\sigma_\theta - \sigma_z|, |\sigma_\theta - \sigma_r|, |\sigma_z - \sigma_r|\} \tag{3.12}$$

Since the vial wall undergoes an abrupt expansion, the corresponding strain relationships are not important. However, when considering the potential deformations on surrounding liners, these are obviously matters of consideration. With strain being inversely proportional to the Young's modulus, minimizing such deformations depends on the materials used. Furthermore, these relationships cannot be used when analyzing the effects of cement in direct contact with the borehole wall.

The yield stress of glass is around 4 GPa.[42] Given the radius-to-thickness ratio and equation (3.10), it is implied that a minimum of ~320 MPa is needed to break the glass vial, which gives a minimum *hoop stress*. Given that cracks are always found running axially along the lateral surface, expansion is indeed demonstrated in the radial direction. However, some cracks were found in rings (the $\hat{\theta}$ direction) which suggest large axial stresses (see figure 3-11 and figure 3-13). In the laboratory experiment, the outer pressure was constant at 1 atm, but it could not be determined if the inner pressure exerted axially was the same as that exerted radially. Thus, future work must quantify the difference in axial and radial expansion during curing. In the borehole, the outer stresses exerted on the cement or borehole liners will vary depending on depth due to the lithostat. Therefore, future sample-based applications in the laboratory should strive to emulate these conditions.

Selection

With the criteria established that a cracked vial is indicative of an expansive mixture, the formulation process consisted of varying compositions of cement with the listed additives until one was able to consistently break for all sample sets. As indicated previously, from the onset, this was found to be the mixture in table 3.2 with magnesium oxide and sand/granite. Figure

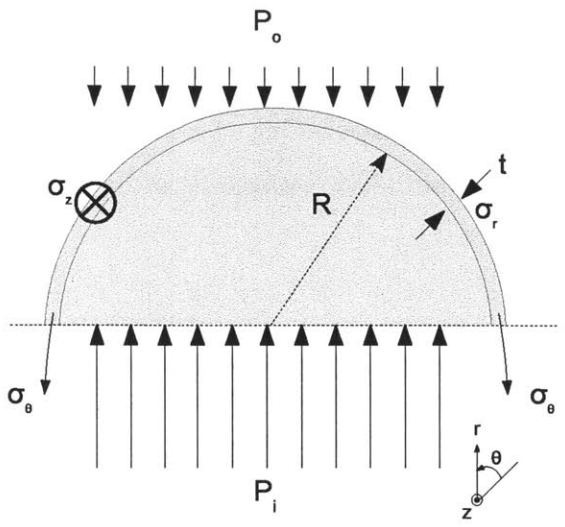

Figure 3-12: Diagram of stresses on a thin cylindrical shell, where $R/t > 10$. It should be noted that for σ_z the inner and outward pressures are still opposing but the outer pressure is in the $-\hat{z}$ direction.

3-13 shows two vials of Portland cement with dye penetrant and two vials of the expansive mixture with cracked vessels. It is extremely important to emphasize the shrinking nature of Portland cement and the difference an additive can make if it involves a volume-increasing chemical reaction.

In the process, some "sub-optimal" compositions were found with intermediate percentages of certain components. For example, of the MgO iterations, the sample set consisting of 52% Portland, 25% MgO and 23% water did not crack the vial but as figure 3-14 shows, these vials (the ones farmost to the right) are able to retard dye penetrant much better than Portland by itself. One has surface texture that exhibits a limited diffusion of the dye while the other hinders flow past the mouth of the vial. Therefore, it can be assumed that MgO as an additive even meets baseline standards for prohibiting flow through a gap.

3.5 Summary

A cement-based material was chosen as the material to seal the canister emplacement zone in the borehole. Standard Portland cement undergoes shrinkage upon curing, but a particular

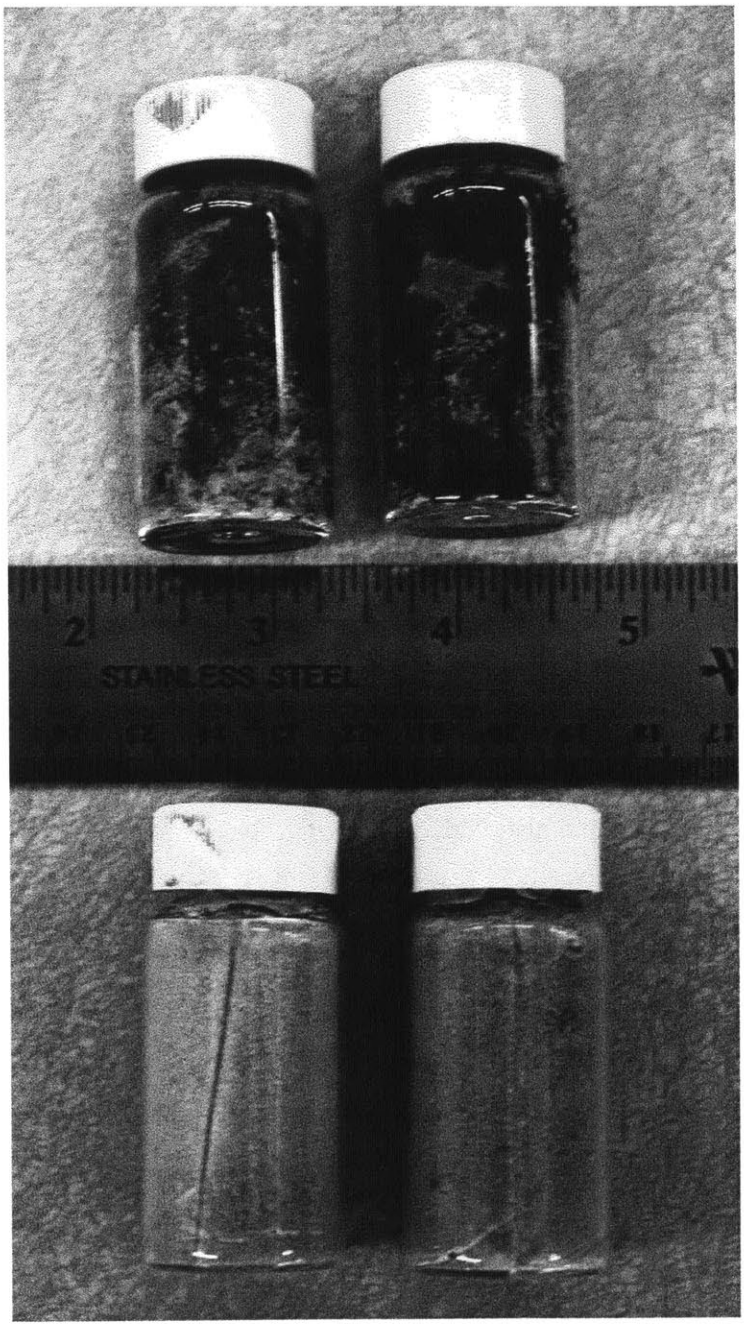

Figure 3-13: Comparison of vials of Portland cement (top) with dye penetrant and the optimal expanding cement, which has cracked vials.

Figure 3-14: Comparison, from left to right, of pairs of vials of the optimal mixture (with cracks), Portland cement, and a sub-optimal mixture containing magnesium oxide that was not able to crack its container. Dye penetrant placed into the uncracked vials reveals that dye flows in channels along the outer surface of the Portland sample while it undergoes a diffused or retarded flow in the sub-optimal mixture. This indicates that MgO is adequate at providing even a baseline resistance to gap flow.

formulation with magnesium oxide and fine sand as additives consistently demonstrated the ability to expand by cracking small glass containers. It was this formulation that proceeded to the permeability experiments, although other expansive cement candidates were identified. These were left to analysis in future work.

Before providing details on the permeability experiments with the optimal cement, the examination of materials that can be used to fill the gap between the SNF canisters and borehole wall will be expounded.

Chapter 4

Thermal Conductivity of Gap Materials

4.1 Introduction

The borehole approach requires that decay heat from SNF canisters can be dissipated at such a rate that the following phenomena are mitigated:

1. damage to the canister materials
2. natural convection and the onset of buoyancy-induced flows of groundwater
3. damage to the host rock.

This chapter describes the experiments designed to analyze effective thermal conductivity of materials proposed to meet these criteria. Prior to describing materials considered for use in the borehole, information about the source of heat from radioactive decay will be given along with the thermodynamics of its transfer from the canisters.

4.2 Experimental Setup

4.2.1 Apparatus

The apparatus used in the measurement of thermal conductivity was previously used by Novak[1] and Shaikh[43] and is shown schematically in figure 4-1. It consists of a long 1" diameter steel rod containing an electric resistive heater and eight K-type thermocouples,

the leads of which protrude through the top of a magnesium oxide plug to be connected to a Simpson® AC voltmeter and ammeter along with a voltage source in the form of a Staco® 3PN1010B variable transformer. The lower portion consisted of a concentric steel pipe of 2" inner diameter and 1/8" thickness bolted to the rod at a welded Varian® conflat, which allowed the rod to extend 63 cm into the pipe, forming an annulus. To maintain the concentric alignment and prevent the axial loss of heat, a annular ceramic Macor® spacer was positioned on the portion of the rod within the pipe, making the heated length 45.7 cm and leaving 5.4 cm of empty space on the bottom of the pipe.[1] The pipe had 1/32" ringed grooves on the outside that aligned with the thermocouples fastened inside the heater rod (see figure 4-1). Heat paste was applied to these grooves, and then three Omega® K-type thermocouples of 1/32" thickness and 32" length were fastened. A special heat-activated adhesive and aluminum shim was used to secure the thermocouples in place, and worm drives were tightened around each of them.

The electric heater consisted of a 29.25" long unheated length, an 18" heated length, and a residual 0.75" unheated length, leaving only the annulus exposed to the heat. Its power output is controlled by the setting on the variable transformer in terms of the percent voltage applied. The bottom of the pipe was sealed with a conflat, and both sets of conflats used copper O-rings to ensure a liquid-tight seal at the flanges. Also, near these conflats were two clamping flanges made of stainless steel and teflon along with silicone sleeves, all meant to reduce axial heat loss. To further provide against the loss of heat through the axial portions of the apparatus and the outside of the pipe, fiberglass insulation was applied by hand and fastened with wire.

The apparatus was grounded to a nearby metal rack in the event of a current leak from the heater. The upper extreme of the apparatus consisted of a Varian conflat perforated at the edges with threaded holes, into which two eye screws were fastened opposite from each other along with the grounding wire. Tethers were connected to a perforated steel rack using the eye screws so that the apparatus could be suspended vertically as shown in figure 4-2. To accommodate a horizontal orientation, two fire bricks were grooved and spaced apart on

[1] Another cylindrical spacer was originally used on the lower extreme of the pipe in Novak's[1] experiment for the same purposes, but this was not available at the time.

a bench to allow the rod and pipe to rest in this position.

4.2.2 Data Acquisition

Data was acquired using an Agilent 34980A Multifunction Switch/Measure Mainframe with corresponding 34921A 40-Channel Armature Multiplexer, using BenchLink data acquisition software on the Windows operating system. The software configuration measured temperature from all thermocouples and the voltage directly from the variable transformer. An alternative arrangement was to employ the manual reading of voltage from an ACV meter upon steady-state, but this was a less precise method and only used in early experiments. The data acquisition unit could not be used to measure current as the multiplexer had a 1 A limitation, and experiments exceeded this limit at 10% and 20% voltage. Therefore, the ACA meter made a considerable reduction on the number of significant figures that could be used in calculations, being precise to only two decimal places.

4.3 Decay Heat from Spent Nuclear Fuel

The amount of heat generated from nuclear fuel for a time t seconds after operating a reactor for t_0 seconds is represented in equation (4.1), where $\dot{Q}_0$ is the original reactor power in megawatts-thermal. The decay heat from the fuel assembly ($\dot{Q}_d$) versus the reactor lifetime (t, the amount of time in years from an initial fuel loading) is graphed in figure 4-3; it should be noted that the curve plateaus as operating time approaches infinity.

$$\frac{\dot{Q}_d(t)}{\dot{Q}_0} = 0.066[t^{-0.2} - (t + t_0)^{-0.2}] \tag{4.1}$$

A canister should be able to fit at least one standard PWR fuel assembly, which is typically 4 m in height. A Westinghouse AP1000™ has 157 fuel assemblies and operates at 3415 MWt in an 18 month fuel cycle[44]. Considering that SNF remains on-site for at least ten years in fuel pools prior to insertion into long-term repositories, the amount of heat that should be expected in one canister should therefore be around 790.0 W, with 197.5 W/m as a maximum value for linear power. Nonetheless, given the history of the current industry

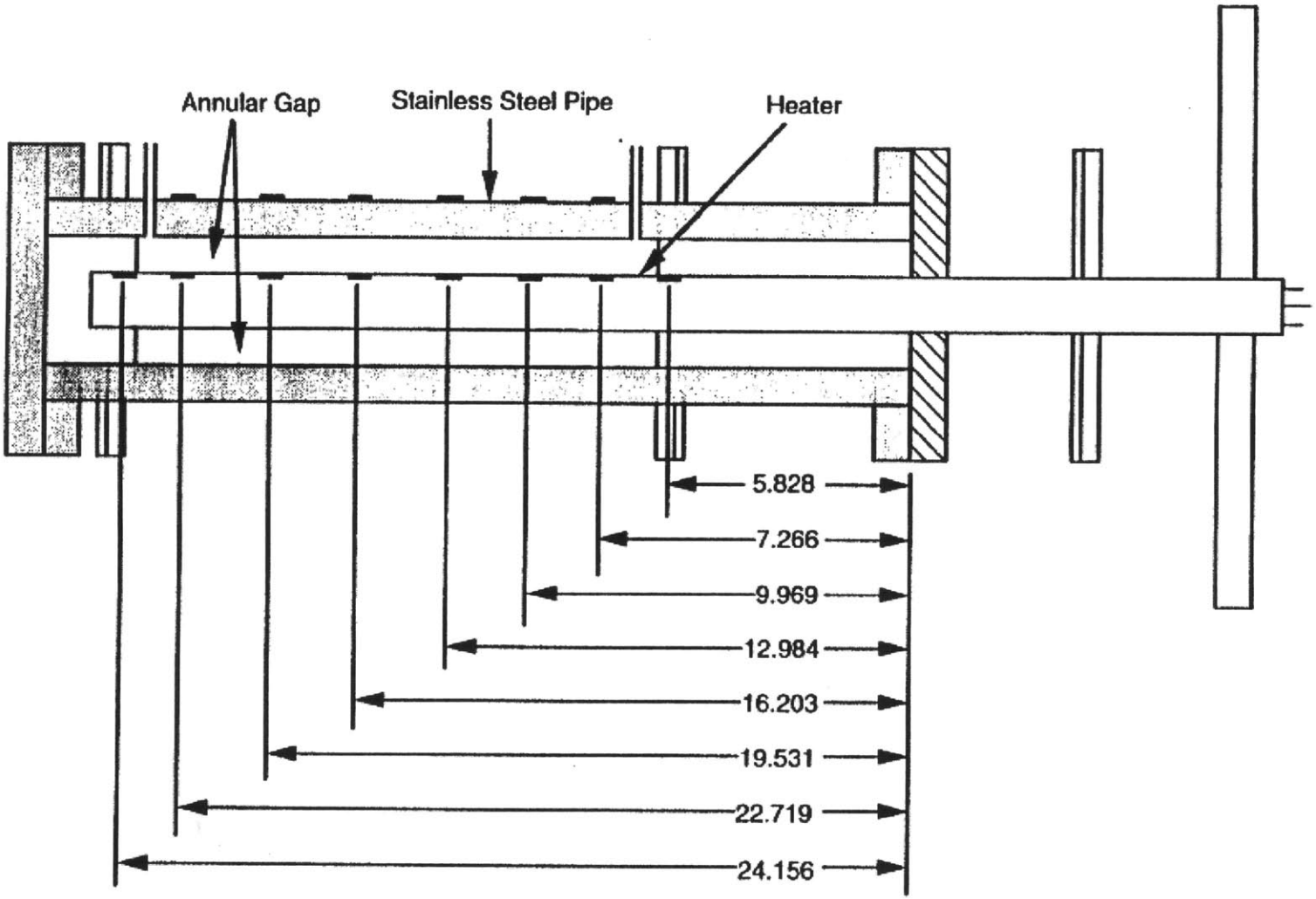

Figure 4-1: Schematic of thermal conductivity apparatus with thermocouple locations in inches. The leftmost four and rightmost one featured on the steel pipe were not employed in the experiments. From right to left, the inner thermocouples are numbered 1-8, while the external thermocouples are numbered 9-14. Three external thermocouples were used in the experiments that resulted in the following pairings: #3-#10, #4-#11, and #5-#12. The heated length begins after thermocouple #1 and stopes after #8. Image from Novak[1].

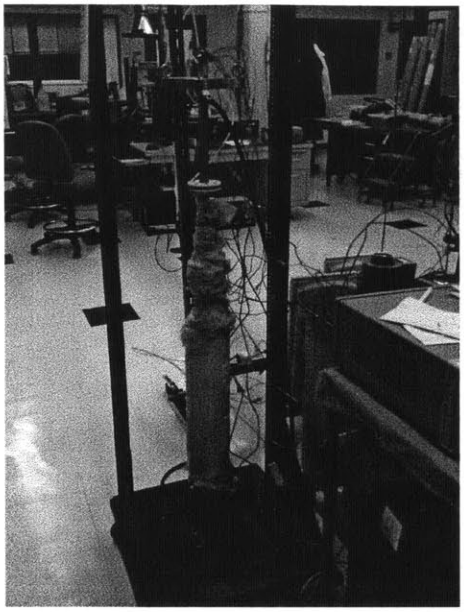

Figure 4-2: The thermal conductivity apparatus with insulation. The black cable connected to the top disk is a ground wire and the machine mounted on the cart to the right is the data acquisition system to which the thermocouples are connected. The grey variable transformer is visible on the table on the middle right.

where plant site operators have left spent fuel underwater (in in subsequent storage in dry casks) for much longer periods of time, it is safe to utilize experimental values that are under this maximum.

4.4 Effective Thermal Conductivity

Thermal conductivity (k) is calculated using Fourier's Law as applied to an annulus (equation (4.2)), where r_o is the the outer radius, r_i is the inner radius, L is the length and $\dot{Q}$ is the heat transferred radially through the annulus (figure 4-4). T_i and T_o correspond to the temperatures measured at the surface of the rod and the inner surface of the outer pipe, respectively. Since electric resistance is the source of heat in the experiments, $\dot{Q} = I \times V$, where I is the current flowing into the heater and V is the corresponding voltage. These parameters are controlled by the variable transformer in terms of the percent total voltage allowed into the heater (5, 10, and 20% were the values used in this project).

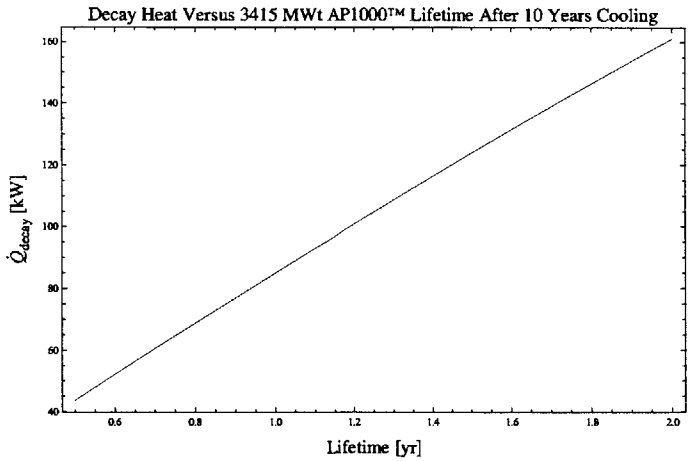

Figure 4-3: The decay heat of a Westinghouse AP1000™ after 10 years of cooling.

$$\dot{Q} = 2\pi k L \frac{(T_i - T_o)}{\ln(r_o/r_i)} \tag{4.2}$$

The small pipe thicknesses separating the thermocouples from the annular region of the apparatus present thermal resistances to annular heat conduction. The thermal resistances can be modeled as

$$R_{tot} = R_{st,shell} + R_{ann} + R_{st,rod} \tag{4.3}$$

where the contributions from the pipe and rod are defined as

$$R_{st} = \frac{\ln(r_o/r_i)}{2\pi L \cdot k} \tag{4.4}$$

such that $r_o - r_i = t$, where t is the particular pipe wall/thickness of the components (1.5 mm for the rod and 3.1 mm for the outer pipe). The overall resistance contributed by the annulus is defined as

$$R_{ann} = \left(\frac{1}{R_m} + \frac{1}{R_{rad}}\right)^{-1} \tag{4.5}$$

where R_m can correspond to $R_k = \frac{\ln(r_o/r_i)}{2\pi L \cdot k}$, which is a purely conductive resistance, *or* $R_h = \frac{1}{h \cdot A}$, which is the convective resistance employing the heat transfer coefficient h. Either do not occur in parallel in the annulus and it will be demonstrated that the latter

can dominate at higher temperatures. $R_{rad} = \frac{1}{4A\cdot\epsilon\cdot\sigma\cdot(\frac{T_i+T_o}{2})^3}$ is the resistance from thermal radiation, where σ is Boltzmann's constant and ϵ is the emissivity of steel. This term does not exist when the annulus is filled with a solid or opaque liquid and only becomes significant at very high temperatures.

These resistances are corrected in equation (4.6), where "rod" refers to the heater, "shell" refers to the part of the outer pipe between the thermocouple and the annulus, r is an outer (o) or inner (i) radius, and k is a thermal conductivity of the annular region (ann) or steel (as a function of temperature). This equation applies only to the majority of materials analyzed by experiment, which were solid beds. For transparent fluids, the contributions from convection and thermal radiation must be taken into account.

The thermocouples inside the heater rod are assumed to be flush with the inner wall and the annular material is assumed to be symmetrically homogeneous such that temperature readings are not affected by the specific rotation of the heater when inserted into the heated section.

$$k_{ann} = \ln\left(\frac{r_{ann,o}}{r_{ann,i}}\right)\left[\frac{2\pi L_{rod}\Delta T}{\dot{Q}} - \frac{\ln\left(\frac{r_{rod,o}}{r_{rod,i}}\right)}{k_{steel,rod}(T_i)} - \frac{\ln\left(\frac{r_{shell,o}}{r_{shell,i}}\right)}{k_{steel,shell}(T_o)}\right]^{-1} \tag{4.6}$$

The thermal conductivity of steel is known to vary with temperature. The relation used for the correction, from Bailey [45], is shown in 4.7, where k is in W/m-K and T is in units of °C.

$$k_{steel} = 14.6 + (1.27 \times 10^{-2})T \tag{4.7}$$

Error was propagated using equation (4.10). The potential errors in length measurements associated with the apparatus were assumed to be negligible due to manufactured precision. δV was obtained from the standard deviation of data points from the last 15 minutes of steady-state operation using the data acquisition unit. Similarly, δT was the standard deviation of the last 15 minutes of steady-state temperatures for either set of three thermocouples, for a total of 45 data points.

The data acquisition unit was limited to a 1 amp maximum of measurable current, which

is below the maximum current that is achieved given the experimental parameters. Therefore, a less-precise external ACA unit was attached in series with the heater and was used to log current manually at the end of an experiment. The unit was precise to two decimal places and four significant figures, therefore limiting the precision of data conducted at 5% voltage (typically around 0.82 A). A Fluke® 80J-10 10 A 100 mV current shunt was used to calibrate the meter. This involved connecting the current shunt in series and recording a 1 minute log of voltage (through the shunt and through the heater) using the DAS and simultaneously logging the reading on the ACA meter for 5, 10, and 20% Variac percentages. These data were used to obtain δI for particular applied powers in the most practical manner.

Letting

$$\tau = \Delta T_{avg} = T_{i,avg} - T_{o,avg} \tag{4.8}$$

such that the error is defined as the standard deviation of the measured temperature difference between each set of thermocouples (4.9),

$$\delta\tau = \delta((T_3 - T_{10}), (T_4 - T_{11}), (T_5 - T_{12})) \tag{4.9}$$

we have

$$\delta k = \|k\| \sqrt{\left(\frac{\delta I}{I}\right)^2 + \left(\frac{\delta V}{V}\right)^2 + \left(\frac{\delta \tau}{\tau}\right)^2} \tag{4.10}$$

since factoring thermal resistances employs both the inner and outer annulus temperatures, equation (4.11) is used to modify the error propagation. This also assumes negligible error in measured apparatus dimensions.

$$\delta k_{ann} = \|k_{ann}\| \sqrt{\left(\frac{\delta \dot{Q}}{\dot{Q}}\right)^2 + \left(\frac{\delta \tau}{\tau}\right)^2 + \left(\frac{\delta T_i}{T_i}\right)^2 + \left(\frac{\delta T_o}{T_o}\right)^2} \tag{4.11}$$

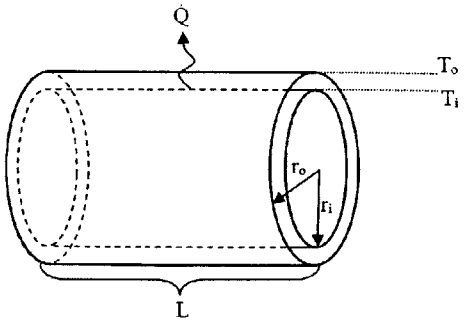

Figure 4-4: Geometry of annular heat transfer.

4.5 Convection in Horizontal Orientation

The non-linear, cosine-shape of the temperature profile of the heater implied that some difference in density would exist in the wetting fluid, leading to natural circulation. This is not easily solved due to the unique geometry of the annular gap.

The heat transfer correlation for natural convection between horizontal concentric cylinders is shown in 4.12[46]

$$\frac{k_{eff}}{k} = 0.386\left(\frac{Pr}{Pr+0.861}\right)^{1/4} Ra_{cyl}^{1/4};\ 10^2 < Ra_{cyl} < 10^7; 0.7 \leq Pr \leq 6000 \tag{4.12}$$

where k is the thermal conductivity and the Rayleigh number of the cylinder is defined as

$$Ra_{cyl} = \frac{[\ln(D_o/D_i)]^{1/4}}{\left[\frac{1}{2}(D_o - D_i)\right]^3 \left(D_o^{-3/5} + D_i^{-3/5}\right)^5} Ra_L \tag{4.13}$$

where the coefficient of Ra_L is the dimensionless "characteristic length" (or radius) of conduction in the annulus.

The dimensionless parameters, such as the Prandtl number, are obtained from data tables for the substance at the average annulus temperature: $\bar{T} = (T_i - T_o)/2$. The Rayleigh number demonstrates the dominance of buoyancy forces over viscous forces, and the Prandtl number indicates the relative development of the momentum boundary layer relative to the thermal

boundary layer. Since $Ra_L = PrGr = \left(\frac{\nu}{\alpha}\right)\left(\frac{\beta\Delta T \cdot gL^3}{\nu^2}\right) = \frac{\beta\Delta T \cdot gL^3}{\alpha\nu}$, where ν is the kinematic viscosity, α is the thermal diffusivity, and β is the volumetric expansion coefficient ($\sim 1/T$ for gases), it can be shown that effective thermal conductivity in this case is proportional to $\Delta T^{1/4}$ and inversely proportional to $\nu^{1/4}$ and $\alpha^{1/4}$. For example, since air has a much higher kinematic viscosity than glycerine ($6.8 * 10^4 \gg 8.9 * 10^2$) the effects of free convection per increasing ΔT should be somewhat more pronounced for glycerine. In any case, there is dependence on the competing forces of buoyancy and viscosity, along with momentum diffusivity and thermal diffusivity.

When in the horizontal orientation, fluid in the annulus moves upward along the side of the rod and descends down the inside surface of the outer pipe, as shown in figure 4-5. The amount of heat transferred between the two cylinders is governed by k_{eff}. The vertical orientation must have natural convection due to the density changes associated with the irregular temperature profile of the rod and heat rejection at either conflats of the apparatus, as will be demonstrated later. In designing this system, the presence of natural convection is a benefit because it allows a parallel means of transferring heat apart from conduction. Depending on the porosity of the material, which determines the extent of the solid matrix, natural convection may be of great benefit by removing energy from the fluid trapped in the pore space.

4.6 Buoyancy Induced Flow

Once a gap is available for the passage of water, the heat from the SNF canisters will generate buoyancy induced flow caused by a variation in the density of the fluid through an irregular temperature profile. Whenever there is an irregular or unstable temperature gradient, there is likely to be free convection. This mode of heat transfer is only negligible when when $Gr_L/Re_L^2 = \beta\Delta T \cdot gL/v^2 \ll 1$ while forced convection can be ignored when $Gr_L/Re_L^2 \gg 1$. (Conditions for mixed convection exist when $Gr_L/Re_L^2 \approx 1$, which has much significance in reactor design.) Because v is designed to be very low and flow is laminar, the effects of forced convection have little impact on heat transfer in the annulus. Furthermore, experiments involving annular channels that have varied Gr/Re have demonstrated that

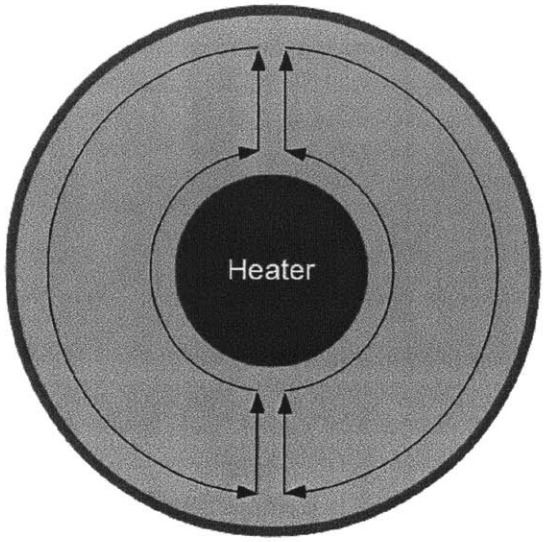

Figure 4-5: Diagram depicting natural convection in concentric pipes of the apparatus in horizontal orientation; more specifically when the annulus is filled with fluid. It is assumed the heater is on and the outer pipe is initially at a lower temperature. This figure is adapted from Incropera and Dewitt [2].

heat transfer is greatly increased proportional to that factor when flow is fully developed and surrounded by uniform heat fluxes.[47] This behavior is mostly applicable to an upward flow since forced and natural convection are in the same direction, and presents implications to the borehole gap. As opposed to groundwater flowing upward solely along geological pressure gradients, there is now an enhancement from the canister heat.

If one were to view the gap laterally as a rectangle, it is well known that if the inner surface (the canister) is hotter than the outer, fluid will move upward along the hotter surface and downward along the colder (Please see Figure 9.12 in Incropera[2]). It can therefore be assumed that a similar phenomenon occurs within the annulus. In fact, as a consequence of the conservation of mass, when Gr/Re increases, the buoyancy force causes flow reversibility at the outer wall due to the lower velocity.[47] Therefore, even though the apparatus does not employ a forced flow through an opening, flow can be induced anyway through the effects of buoyancy and natural convection, and this should be applicable to a tortuous pore space within a heated porous substance. For these reasons, it is important to understand the effective thermal conductivity of the materials used to fill the annulus relative to temperature to gauge both the degree of heat transfer and the positive feedback

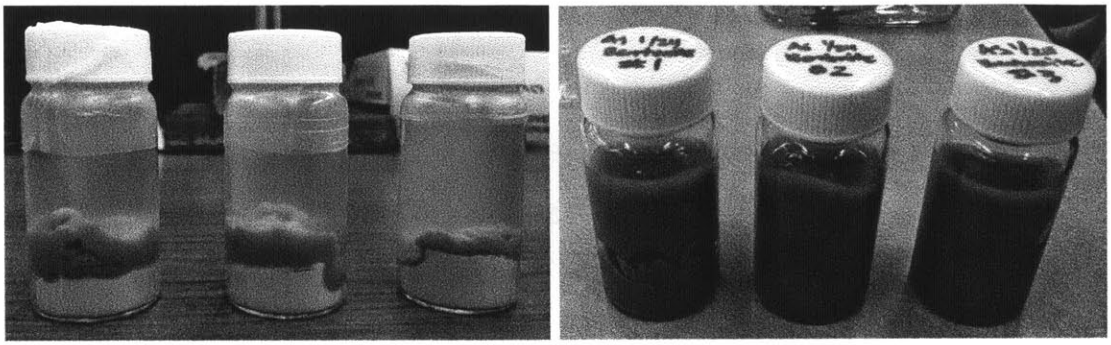

(a) Vials of 20.00 g of water added to 3.00 g of bentonite.

(b) The same three vials four days later with excess water removed. Bentonite is shown to expand greatly.

Figure 4-6: The saturation of bentonite.

of convection with increasing temperature.

4.7 Bentonite

Bentonite is an absorbent clay consisting of the mineral montmorillonite (a smectite) , and comes in forms where sodium or calcium are dominate chemical constituents. The calcium form, a fine light grey powder, was used for all laboratory experiments mentioned in this thesis. It has long been proposed for use as a buffer in repositories due to its high sorptivity, which would physically retard the migration of radionuclides through the borehole.[48] It has been known to impart significant viscosity and thixotropic properties to water and swell up to ten times its original volume, which has positive implications as a gap filler. It also has applications as a chemical-resistant and delaying agent for cement, although samples made in the laboratory were not expansive (even when packaged with MgO). Nonetheless, this material has an integral role in repository design due to these promising features and must be tested in thermal conductivity measurements to understand general heat transfer characteristics. Considering that it can be applied in a dry, powdery form which will inevitably transition to its natural colloidal clay form upon interaction with groundwater, both consistencies should be tested.

4.8 Granite and Sand

Granite and sand are physically and chemically similar with high contents of SiO_2, and the particles can be used interchangeably in the borehole system when of a common size. Rough granite filings are used as a backfill and finer, crushed granite or sand is used in the sealing zone. As detailed earlier, the two have also been successfully demonstrated as additives to expanding cement. Their continued application in the borehole system is as an additive to the bentonite canister buffer.

Bentonite and Sand/Granite Mixtures

The addition of crushed granite has the effect of increasing the thermal conductivity of a clay mixture, while maintaining mechanical stability and decreasing the potential for creep.[49][50] It also has the effect of decreasing porosity, as demonstrated in the laboratory data in table 4.1. This in turn inhibits mass diffusion, and with this decrease in the diffusion coefficient for the compacted clay, the addition of sand is considered beneficial to the buffer material.[49] Therefore, various proportions of these mixtures will be considered in experimentation so as to potentially find an optimal thermal conductivity.

The compacted density of 70/30 bentonite/granite filings is around 1.5 g/cc. In the laboratory, obtaining values for compacted densities of any merit was difficult. One method attempted was to use a hammer, piston and cylinder to manually compress the powder mixtures into a core so as to find the compacted density geometrically using a scale and its dimensions, but this sometimes resulted in easily-chipped solids that produced large systematic errors. In some instances, the bed would not compress at all and immediately break apart. A secondary approach was to take partially compacted masses, weigh them, and then use Archimede's test to find the volume. This method was too inaccurate to be of good use in experiments. Therefore, given these limited means, thermal conductivity experiments were conducted with non-compacted masses, which presents difficulties when comparing to published data which often features values for compacted beds. In reality, this is the most proper way to analyze the material, as the hydrostatic pressures of the borehole are likely to have large compressive effects.

Sample	ρ_{bulk} [g/cc]	Error	Porosity	Error	Void Ratio
100% Granite Filings	1.74	±0.03	0.122	±0.004	0.139
30% Bentonite 70% Granite Filings	1.60	±0.10	0.785	±0.004	3.64
50% Bentonite 50% Granite Filings	1.34	±0.07	0.873	±0.013	6.85
70% Bentonite 30% Granite Filings	1.22	±0.06	0.776	±0.008	3.47
100% Bentonite	0.97	±0.01	0.757	±0.008	3.12

Table 4.1: Bulk densities, porosities and void ratios for non-compacted mixtures of bentonite and granite. The porosity indicates the volume of void relative to the entire volume while the void ratio is only relative to the volume of solid. The 50/50 mixture has a high void ratio at 6.85, but the other mixtures involving bentonite have similar values.

As was conducted for bentonite, set proportions of granite in bentonite were immersed in water within vials to test the absorption of water. It is assumed that when such mixtures are poured into the gap between the canisters and borehole wall, water will eventually seep into the gap and be drawn into the solid bed, which will in turn swell and exert pressure on both sides of the gap. This will allow for enhanced thermal conductivity, as will be demonstrated when air is displaced in the pore space by other fluids. A photograph of the vials after a 3-4 days of immersion is shown in figure 4-7, which shows that swelling does occur for all mixtures containing bentonite. Since water can be assumed to occupy all of the pore space, changes in volume of the original immersed water were used to find the porosities and void ratios for each mixture, which are shown in table 4.1. Notice that as the granite does not visually appear to swell, its void ratio is very low, implying that it will be able to trap little water. However, all mixtures with bentonite have considerable void ratios that imply a great degree of retention for fluids including those with dissolved radionuclides.

Of further note, ferrous phosphate can be added to bentonite/sand mixtures as a deoxidant to ensure that a reducing environment is maintained despite the presence of air gaps formed in the filling process.[49] Furthermore, this additive will aid in the corrosion resistance of the canisters and reduce the solubility of radionuclides.[51] Therefore, a bentonite buffer with this additive should be considered for future work.

Figure 4-7: Vials of saturated granite with bentonite. From left to right: 100% , 70%, 50%, 30% and 0% granite in bentonite. Data from these vials (in triplicate) were used to form table 4.1.

4.9 Borax

As mentioned earlier, anhydrous sodium tetraborate ($Na_2B_4O_7$) (STB) is a dried form of decahydrate borax that resists buoyancy-induced flows through both a decrease in solubility and increase in density with temperature, therefore making it a candidate for a canister filler. It has also been considered as a corrosion inhibitor for bentonite, and borate is already employed as a neutron absorber in reactors. The material used in experiments was Alfa Aesar® 99.5% metals-basis anhydrous sodium tetraborate of US 12-mesh and solid density 2.367 g/cc. The hydrated form of STB is commonly sold as borax such as that from Twenty Mule Team®, where it used as a laundry detergent booster among a variety of other domestic uses. However, this was not used in the thermal conductivity apparatus to prevent moisture effects and to have a standard particle size as guaranteed by the laboratory grade material.

4.10 Helium

When replaced as the pore fluid in a solid bed, helium is known to increase thermal conductivity upwards of a factor of three.[52] Although this would obviously not be used in the gap, its addition into the SNF canisters would allow for a more more effective cooling of fuel assemblies in situ. This can be achieved by flooding the pore space of the packing material, for example, borax, with the gas to evacuate the air. This should mitigate the insulating effects of air and increase thermal conductivity. A special procedure for performing an experiment to analyze these effects on a solid bed will be explained in detail.

4.11 Experimental Procedure

4.11.1 Conventions

Experiments were organized by material and then by the percentage of voltage flowing through the variable transformer to the heater. For each of these percentages, there would be a "trial" denoting the main course of the individual experiment reaching steady-state and a "run" to differentiate between possible reiterations of data collection, for example, upon making an adjustment to the apparatus or changing the apparatus orientation. Since both the current and voltage consistently demonstrated some degree of fluctuation per set percentage on the variable transformer, experiments could not be classified by linear power. The duration of each run was monitored using the written start date and date of the final data acquisition scan logged in the data file.

4.11.2 Procedure for Testing New Material

1. With power off (heater unplugged) and the apparatus cooled to room temperature, disassemble apparatus, collect old material, and clean all surfaces until clean; allow surfaces to completely dry. It is advantageous to remove old material by removing the bottom conflat first and pouring into receptacle.

2. Prepare copper O-ring seal for upper conflat. The inside of the O-ring may have to be

filed to slide across the ceramic plug.

3. Tighten bolts of upper conflats by hand with wrenches. The use of fluids necessitates a tight fit.

4. Invert apparatus by suspending from cables on rack.

5. Insert well-mixed material into apparatus until sufficiently to the top and shake to ensure an even fill.

6. Clean annular area where flange is to rest.

7. Insert copper seal. Fill remaining space in annulus with material.

8. Apply bottom conflat and screw 6/8 bolts.

9. Remove apparatus from suspended position to horizontal and screw-on remaining bolts tightly.

10. Apply insulation to outer surfaces of apparatus, especially around the heated section (see 4-1 on page 54) and secure with wire.

11. If required, suspend apparatus on rack by connecting hooks of tether to eye bolts of apparatus.

12. Connect external thermocouples to the receivers connected to the terminal block of the data acquisition system.

13. Power on data acquisition system and computer.

14. Make sure variable transformer is at 0% and is connected to AC outlet. Plug in heater to variable transformer.

15. Turn on variable transformer.

16. Set variable transformer to the experimental voltage level.

17. Begin data collection with DAS. Record ACA meter and time. Keep in mind the length of scan intervals.

18. Continue heating until steady-state is achieved, and then make sure to record at least 15 minutes of steady-state. Steady-state is achieved when temperature does not fluctuate more than ±2°C in one hour. Graphically, in a chart of temperature versus time, this would amount to a plateau. If a DAS is not available and an analog readout is used instead, one has to wait until these conditions are met and then record temperatures perhaps every minute for 15 minutes.

19. Record ACA meter.

20. Stop DAS scanning.

21. Either

    (a) Turn dial on Variac to zero and switch to off. Allow apparatus to cool.

    (b) Change Variac to new setting and begin new experiment.

4.11.3 Procedure for analyzing data

1. Convert .csv file to Excel format, if necessary.

2. Identify columns corresponding to sets of inner and outer thermocouples, the voltage, and the time.

3. Average temperatures from each thermocouple and voltages from last 15 minutes.

4. Use current and voltage from last 15 minutes to derive the power, according to $\dot{Q} = I \times V$, and calculate standard deviation.

5. Average the inner and outer thermocouple temperatures, and find the difference between these two averages (ΔT). Find the standard deviation of both inner and outer temperatures.

6. Use length of heater ($L = 0.457\,m$), the radius of the heater rod r_i, the inner radius of the heated section r_o, the power $\dot{Q}$, and the temperature difference ΔT to find the thermal conductivity k with 4.2.

7. Propagate error according to 4.10.

8. To correct for thermal resistances, use apparatus dimensions and the average inner and outer temperatures to derive actual k according to 4.6. Assuming negligible error in apparatus dimensions and empirical model for steel thermal conductivity, propagate error according to 4.11.

9. Agglomerate data according to orientation and variac percentage.

10. Effective thermal conductivity can be found using the slope of a chart of ΔT_{avg} and q', where the latter is derived as $q\prime = k \times \Delta T_{avg}$. Note, that $q\prime$ is not properly a linear power, at least for this experiment.

11. Error bars on graph should represent whichever of the following is higher:

    (a) the built-in instrument error

    (b) the standard deviation (or propagated error)

4.11.4 Procedure for Measuring Effects of Flooding Solid Bed with Gas

These tests are designed to be conducted at atmospheric pressure.

1. Allow heater to reach steady-state at a particular Variac setting.

2. Fit valves to upper and lower plena of heated section.

3. Connect pressure tubing to valve outlets and tighten.

4. Insulate the surfaces.

5. Connect pressure tubing from Alcatel® M2004A vacuum pump to upper outlet on heated section. Make sure pump is vented in a fume hood.

6. Connect pressure tubing from pressure regulator on gas tank to lower outlet of heated section.

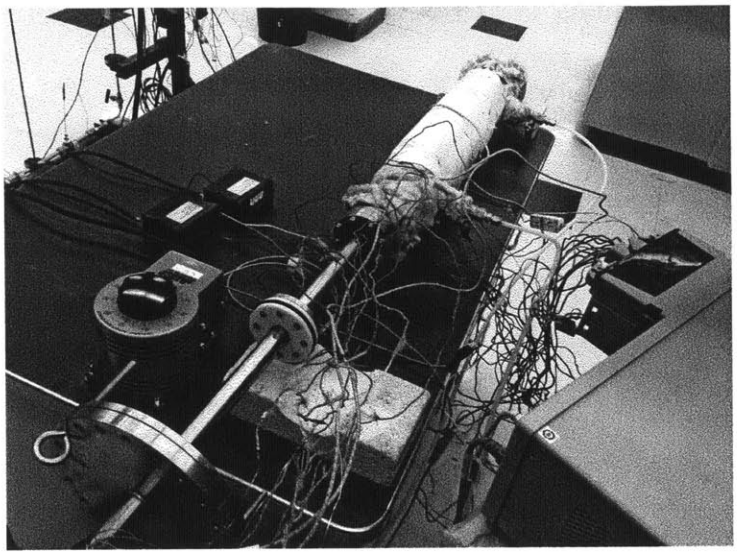

Figure 4-8: The apparatus in horizontal orientation with DAS, variable transformer, and meters visible along with hose connections at the extremes of the heated section.

7. Open valves.

8. Turn on vacuum pump.

9. Begin data acquisition.

10. Open regulator on gas tank for two minutes to test pressurize.

11. Close upper valve.

    (a) Close main valve of gas cylinder.

12. Empty gas trapped in regulator and close the lower valve to isolate the test facility. If the gas cannot empty (which is not likely, due to the poor sealing of the conflats) open the upper valve, empty again, and then close the upper and then lower valves.

Due to the immediate effects of helium, temperature was either measured overnight or until a steady-state was observed in the BenchLink chart. The lowest average temperature difference was found using a spreadsheet and 15 minutes of data including up to this value was used for analysis per the details in ??. Some of the connections described in this procedure can be seen in figure 4-8.

4.12 Summary

Measuring the thermal conductivity of a bentonite and granite-based filler is necessary to understand its capability at conducting the decay heat from the SNF canisters. Higher effective thermal conductivity will prevent overheating of the canisters and reduce the potential for upward, buoyancy-induced flows of groundwater through the gap. An apparatus comprised of concentric steel pipes will be be used to measure the thermal conductivity of an annulus of various mixtures of bentonite and granite along with other materials. It features openings for the injection of helium to test its effects on a solid bed, so as to assess the benefits of its use as a conductor within the canisters themselves.

Chapter 5

Permeability of Cement Sealant

5.1 Porosity

Unlike granite, cement is a more-or-less porous material since it is an aggregate of constituent materials that emits gas when curing. A porous medium consists of a volume of space occupied by a heterogeneous multiphase material, with at least one phase being solid [53]. The solid phase is the solid matrix and the rest comprises the pore space. Depending on the interconnectedness of these pores, the extent of flow of a fluid through the solid matrix will more or less depend on the hydraulic pathway provided by the pore space. The means of determining porosity employs the measured density of the porous substance (the bulk density) and the density of the material itself (the solid density), usually obtained through a high degree of compaction. Porosity (ϕ), defined as the ratio between the volume of the pore space over the total volume of the material, is calculated as using $\phi = \frac{V_{void}}{V_{total}} = 1 - \frac{\rho_{bulk}}{\rho_{solid}}$. This value has important implications on both the mechanical integrity of the material, the nature of fluid flow,[54] and the extent of plasticity when subjected to physical stresses and chemical reactions. In general, concrete for nuclear applications must have a very low porosity, and delays in reactor construction have been rooted in deviation from this standard. However, pores can be closed and not percolate, resulting in a loss of interconnected pores. Therefore, there is not necessarily a strict correlation between porosity and permeability, especially when considering large geological systems like caprock.

An associated value with porosity is the void ratio, or the ratio of the volume of voids

in the material to that of solids. It can be found as $VR = \frac{\phi}{1-\phi}$, and implies the extent to which the volume of a solid bed may increase or decrease under loading and the ease with which particles can flow through the solid matrix.

5.2 Preliminary Work with Coarse Aggregates

Large diameter gravel was first considered within the scope of possible cement additives. However, given the resources of the lab and the limited scale of experimentation with a falling head permeameter, this would eventually prove impractical to properly demonstrate on a small scale and fine additives were chosen instead. Nonetheless, the findings during these experiments gave valuable information on the material properties of cement and motivated the need to use advanced permeameters.

Sample Set

Table 5.1 shows the samples that were created at the very beginning of research on the cement-based sealant. Coarse sand and gravel were chosen as common additives suggested by cement manufacturers along with particular fractions of water in the slurry. Homax® Grade #0000 Super Fine Steel Wool was considered for its structural benefits as a reinforcing agent. Each was cured in a roughly 6" clear Harvel PVC pipe with 0.5 cm thick pipe walls for a height of approximately 6 cm. After one week of curing, these samples were to be used to test their resistance to a head of water.

Falling Head Permeameter

Darcy's Law (3.1) can be modified to represent the falling head $h(t)$ of fluid through a saturated sample where pressure is equivalent at both ends. The hydrostatic pressure over time is defined as

$$P(t) = \rho g \cdot h(t) \tag{5.1}$$

where g is the acceleration due to gravity. In order to use Darcy's law, the pressure prop

No.	Description	Total Mass Material (g) ±2.0 g
1	Concrete mix following manufacturer's guidelines of minimum water content (8.3% H_2O)	270
2	Concrete mix following manufacturer's guidelines of maximum water content (14% H_2O)	286
3	Portland cement mixed with sand and gravel using minimum H_2O ratio	218
4	Portland cement mixed with sand and gravel using maximum H_2O ratio	255
5	Portland cement mixed with sand, gravel, and steel wool using minimum H_2O ratio	232
6	Portland cement mixed with sand, gravel, and steel wool using maximum H_2O ratio	225
7	Pure cement at 36% H_2O	227

Table 5.1: Samples used for preliminary permeability experiments.

across the sample must be defined. Since the external pressure remains constant at 1 atm (P_{atm}), the thermodynamic properties of the pore fluid remain the same, and the change in pressure over time is therefore

$$\frac{dP(t)}{dt} = \rho g \frac{dh(t)}{dt} \tag{5.2}$$

From equation (3.1), the volumetric flow rate must equal

$$Q = \frac{\kappa A}{\mu} \cdot \frac{P(t) - P_{atm}}{L} \tag{5.3}$$

Volumetric flow can be defined as the velocity of a fluid passing through an area A, and since $v(t) = -dh(t)/dt$ (the velocity of the fluid head), the following equation for flow is obtained:

$$Q = A \cdot v(t) = -A \cdot \frac{dh(t)}{dt} \tag{5.4}$$

Rearranging terms inequation (5.2) and substituting the head velocity in equation (5.4) gives

$$Q = -A\left(\frac{dP(t)}{dt} \cdot \frac{1}{\rho g}\right) \tag{5.5}$$

Further equating equation (5.3) with 5.5 and canceling A gives

$$-\frac{dP(t)}{dt} = \frac{\kappa\rho g}{\mu}\left(\frac{P(t) - P_{atm}}{L}\right) \tag{5.6}$$

Isolating terms with $P(t)$ on one side, the following first order differential equation is obtained:

$$-\frac{dP(t)}{dt} - \frac{\kappa\rho g}{\mu L} \cdot P(t) = \frac{\kappa\rho g}{\mu L} \cdot P_{atm} \tag{5.7}$$

Let $P(t) = C_1 + C_2 e^{at}$, where C_1, C_2, and a are arbitrary constants; . Plugging this into equation (5.7), the following expression is obtained:

$$(1 + \frac{\mu L}{\kappa\rho g} \cdot a) \cdot C_2 e^{at} + C_1 = P_{atm} \tag{5.8}$$

Since P_{atm} is constant, equation (5.8) is only true if $a = -\frac{\kappa\rho g}{\mu L}$, which implies that $C_1 = P_{atm}$. Therefore, $P(t) = P_{atm} + C_2 e^{-\frac{\kappa\rho g}{\mu L}t}$. Assuming the initial pressure $P(t = 0) = P_{atm} + P_0$, where P_0 is the initial hydrostatic pressure, the following expression is obtained:

$$P(t) = P_{atm} + P_0 e^{\frac{-\kappa\rho g}{\mu L}t} \tag{5.9}$$

Plugging in equation (5.9) back into equation (5.3), we obtain equation (5.10), which defines the flow rate as an exponentially decaying function. This is experimentally advantageous in that it allows for the direct measurement of volumetric flow through the sample over time. The natural log of flow versus time can be plotted and the slope of the fit line will be equal to $-\frac{\kappa\rho g}{\mu L}$. Therefore, only the kinematic viscosity(μ/ρ) and with the length of the sample need to be known to solve for the permeability κ; P_0 does not need to be measured.

$$Q(t) = \frac{\kappa A}{\mu L}(P_0 e^{-\frac{\kappa\rho g}{\mu L}t}) \tag{5.10}$$

Samples 1 and 3 were the coarsest and porous among the set, and were chosen due to

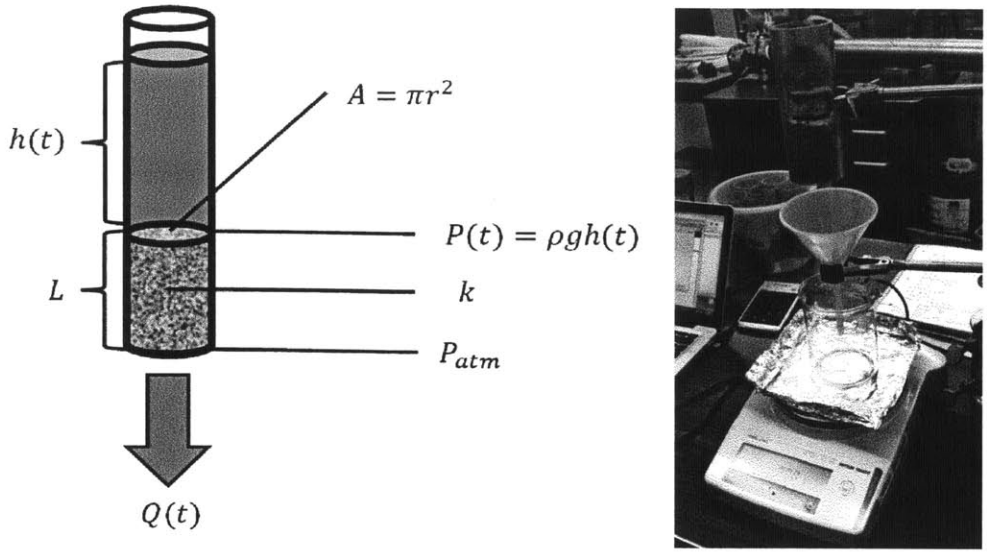

Figure 5-1: Left: Diagram of falling head permeameter used in the laboratory (drawing from Bates[3]). Right: Permeameter setup including scale used to measure flow rate in terms of mass. The scale has a serial connection to a computer, which is used to read mass data over time.

the practicality of obtaining data from fluid flow within a short time frame. Water was mixed with red food coloring to facilitate the viewing of fluid flow, and the data collection first involved manually measuring a flow rate of dye penetrant from the bottom of the PVC pipes using a graduated cylinder or (later) a scale while monitoring time. (The dye has no effect on the viscosity of water.) The next evolution involved acquiring the data automatically using a serial port connection from the Mettler Toledo scale to a computer with manufacturer's software. Data from falling head experiments is summarized in table 5.2, which indicate values that are three to four orders of magnitude higher than the highest allowable permeability of the cement seal.

Sample 7, being pure Portland cement, shrunk to such an extent that it became detached from the pipe wall. Initial falling head experiments confirmed that flow was restricted to the annular gap between the cement and the pipe, which does not account for bulk permeability. This sample was therefore removed from consideration. When a head of dye penetrant was added to the other sample pipes, fluid flow was completely blocked. Therefore, flow measurements had to be restricted to an overnight basis, where beakers would be used to account for flow rate overnight along with measuring the decrease in the fluid head (figure 5-

Sample	Permeability [D]
1	5.12
3	37.5

Table 5.2: Falling head permeability measurements for coarse aggregate samples 1 and 3.

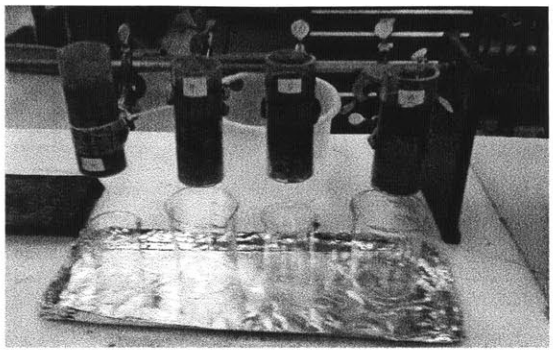

Figure 5-2: Samples 2,4,5, and 6 (the least permeable of the coarse aggregates) suspended above beakers in attempt to measure volumetric flow overnight.

2).

Over time, the fluid heads decreased and dye diffused through the upper extent of the material. However, at the same time moisture was observed at the bottom that could only have come from lateral annular gap flow, rendering measurements inaccurate. This required a new experimental method to probe the low permeabilities of these samples and inspired the development of an expanding cement formulation through an evolutionary formulation process, *without* coarse aggregates. It is presumed that coarse aggregates in contact with the tube introduced large gaps for flow.

5.3 Bulk Permeability

With the low permeabilities surmised from the other coarse aggregate samples, it became apparent that the only means of measuring outflow and deriving permeability would be to apply a pressure gradient across the sample above atmospheric. An attempt was first made using pipe fittings and available laboratory resources. However, the technical limitations and poor quality of data necessitated the use of a specialized precision instrument that was

available at a facility of the MIT Department of Earth Atmospheric and Planetary Sciences (EAPS).

5.3.1 Preliminary Pressurized Air Permeameter

Preliminary permeameter designs that actually employed a pressure gradient was built in the NSE Green Lab from pipe fittings. Two variations are shown in figure 5-3. Because the air inlet could not be regulated and the experiments relied only on gauge readings, sheet plastic was cut and assembled as a blast shield to surround the apparatuses in the event of pipe fitting failure. The expansive cement mixture was prepared in a thin plastic tube of 6 cm diameter to a depth of 1 inch, which corresponded with the thickness of the rubber sheath employed in the pipe coupler. Therefore, when fully cured, the sheath was fitted to the outside of the the cylindrical puck. This was advantageous by allowing the sheath to be constricted during pipe fitting such that it formed a lip at the surface of the puck. This was meant to prevent fluid from flowing through the sides of the sample, which interferes with bulk permeability measurement.

The least permeable coarse aggregate samples were also accommodated for testing inside the crude permeameter scheme. Since the coarse aggregates were already hardened in PVC pipes, a pipe coupler was used to connect the sample PVC pipe to the iron pipe with the pressure fittings. The Mettler-Toledo scale was initially employed to measure the flow rate, but these were typically too low to be convenient for overnight measurement. Furthermore, the rate of overnight evaporation exceeded the formation of droplets. Therefore, a different strategy was used to determine the flow rate via the change in pressure.

In experiments where the outlet pressure is not atmospheric, a derivation from Heineman[55] can be used that factors in an atmospheric flow rate. Assuming ideal gas behavior, equation (5.11) is obtained as below:

$$\kappa_a = \frac{2Q_a\mu L}{A}\frac{P_a}{P_1^2 - P_2^2} \tag{5.11}$$

where P_a is atmospheric pressure, Q_a is the flow rate at atmospheric pressure, P_1 is the inlet pressure and P_2 is the outlet pressure. In this experiment $P_2 = P_a$ because the pipe

apparatus flowed directly out to the environment. The relation can be used to find the permeability across a solid core placed in a permeameter.

These experiments faced a number of systematic difficulties that disqualified the data:

- The coupling of PVC and iron pipes does not provide an effective mechanical fitting and in fact demonstrated failure on many occasions (for both setup types). For this reason, we could not ensure that any loss of air or water occurred solely through the bulk material and not through the pipe coupling junction.

- Water was still observed to have seeped through the lateral gap of the puck.

- There was no discrete method of acquiring pressure gauge data (i.e. through pressure transducers).

Given the inadequacies of the design, a new experimental methodology was sought in order to properly quantify bulk permeability. Applications in geology-related research such as for the oilfield services industry were examined for their capabilities at measuring low permeabilities.

5.3.2 Final Experimental Apparatus (EAPS Laboratory)

Ultimately, the resources to conduct proper bulk permeability measurements were available at a laboratory of the MIT Department of Earth, Atmospheric, and Planetary Sciences. This laboratory featured a permeameter capable of probing the millidarcy range. It was constructed with stainless steel pipe fittings and consisted of a sample chamber surrounded by an external electric heater, an inlet and outlet for the pore fluid, a differential pressure transducer, a displacement transducer, and a confining pressure system (see figure 5-4). Bulk permeability measurements involved the sample being inserted into a sheath of Teflon (PTFE) and set in place with two steel plugs of equal diameter. The samples were either cured within the sheath as a slurry or drilled to the proper dimensions from a cured bulk sample. The connections to the pore pressure system were then connected to the steel plugs and the sample was secured by tightening the pipe fittings. The apparatus was then vertically oriented using a desktop laboratory stand.

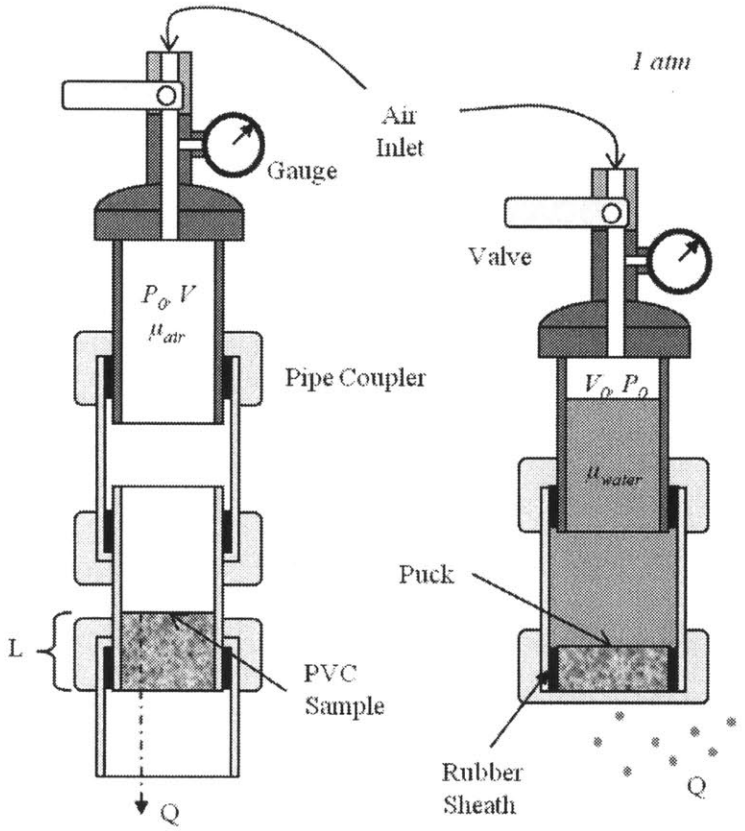

Figure 5-3: Cross sections of the pipe apparatuses for the PVC sample (left) and the puck sample (right). The puck apparatus contains both water and air.

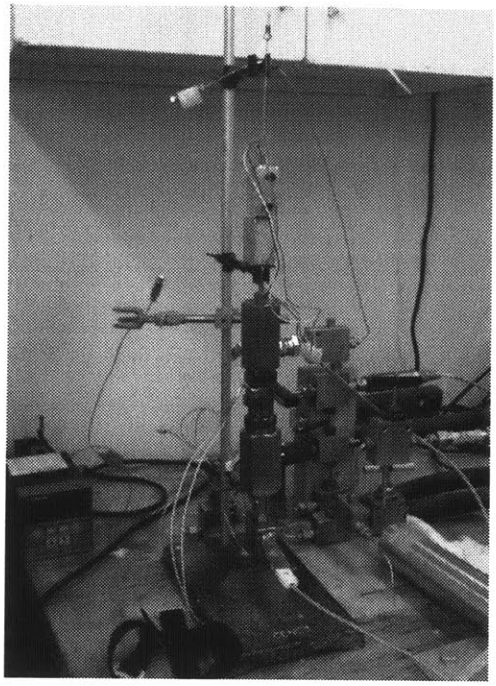

(a) The permeability apparatus.

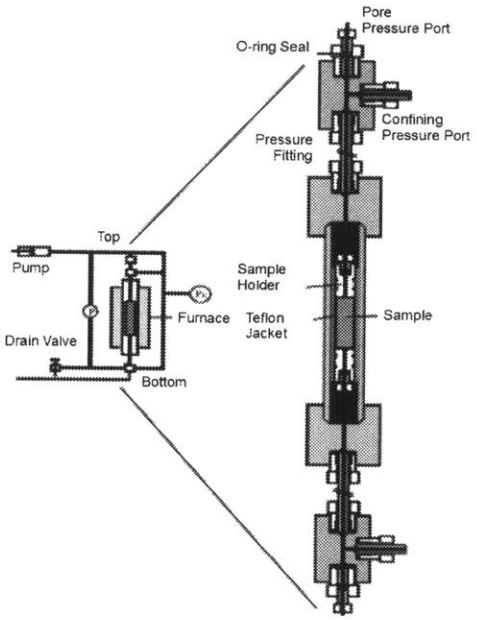

(b) Schematic of the apparatus, from Mok.

Figure 5-4: The EAPS permeability apparatus and corresponding schematic, from Mok.[4] The displacement transducer is visible as the instrument at the top of the sample container in 5-4a.

Sample Types

Two forms of cement were examined in the experiments. One consisted of the a bulk sample prepared under atmospheric conditions and room temperature in the laboratory. In order to have an upper bound to permeability measurements, a sample of the optimal mixture (see table 3.2) was prepared in the laboratory in a short 2" PVC pipe that was plugged on the bottom by a rubber stopper. About 6 cm of the pipe length was filled with the slurry, and paraffin was used to seal the mouth of the pipe to mitigate the loss of moisture. The sample was allowed to cure for two weeks, wherein it demonstrated the ability to remain firmly within the pipe despite earlier samples of Portland cement that were prepared in the same tubes and demonstrated shrinkage. The hardened mass (with a mass of 327 g) had to be removed forcefully using a saw to break the tube.[1] The next day the core was baked inside a furnace at 150 °C for three hours, after which it was observed that cracks had formed

[1]The PVC pipe was of the same variety used for the coarse aggregates. The cement did not expand enough to break the pipe or create fissures.

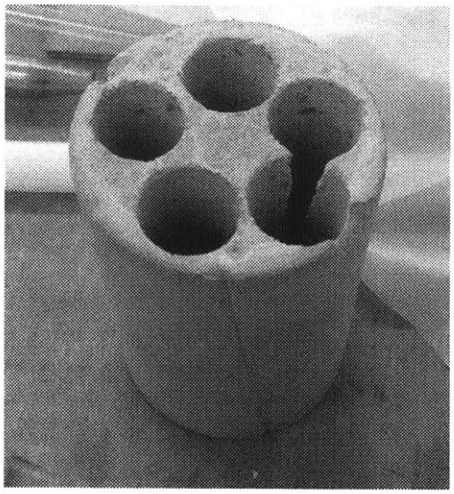

(a) The atmospheric sample was prepared in bulk and drilled into smaller cylinders were insertion into the Teflon sheath.

(b) The pressurized sample was prepared in a small quantity. It was held at 200 bar within this steel piston for 6 days, after which CO_2 bubbles were observed dissolved in the surrounding water.

Figure 5-5: Preparation of the two permeameter sample types.

from defects in the surface caused by removing the sample. It was determined that this mass was adequate for demonstrating an upper bound of permeability due to the conditions of preparation, cracks, and the likely presence of voids. The bulk cylinder was cut into smaller individual samples that could fit in the permeameter, as shown in figure 5-5a. Properties for each cylinder cut from the bulk sample are shown in section §B.1.

The other sample type was prepared in a very small batch and prepared within a Teflon sheath between two steel plugs to an approximate length of 2.5 cm. This was then placed in a steel chamber and pressurized with water to 200 bar for six days, as shown in figure 5-5b. This sample was meant to be indicative of cement cured within the borehole environment and was thus used as a representative of the lower bound of permeability. It was also considered to be much more homogenous than the room temperature sample and was used as a rough baseline for determining the porosity of those drilled slugs. Information for the pressurized sample is shown in section §B.2.

5.3.3 Method

The displacement transducer was placed upstream of the sample and the pressure transducers were placed in piping on both sides of the sample; both were connected to a data acquisition system and computer with a LabVIEW® user interface. Thermocouples also provided data for the experiments involving heating. The effective pressure is defined as the difference between the pressure of the pore fluid and the pressure used to confine the sample to the sheath (which prevents lateral leakage): $P_{eff} = P_{confining} - P_{pore}$. Distilled water surrounded the sample in the sheath and was used by the confining pressure system to pressurize the outside and prevent the lateral passage of fluid. The pore pressure should be at least 100 bar less than the confining pressure.

Values for permeability were obtained using the oscillating pore pressure technique as detailed in Kranz et. al.[5] The method involved oscillating the pore pressure at one extreme of the sample using a servo-controlled hydraulic intensifier, and using a Fourier-type analysis to measure the phase and amplitude shifts of the pressure wave at the other extreme, as shown in figure 5-6. This involves varying the period of the pressure wave to maximize the pressure output and then sampling various points of the output sinusoid at steady-state depending on the need for phase-shift resolution. This upstream/downstream analysis gives the pressure drop in equation (3.1), which in turn is used to solve for permeability. This technique is used as opposed to the transient method, which involves creating transient pulses and measuring pressure decay curves, and has the advantage of measuring permeability κ and the diffusion coefficient D simultaneously (although the latter is not of interest in these experiments).

Kranz et. al[5] used a graphical method to solve simultaneous equations with the measurement of the amplitude ratio R and phase shift δ in the downstream portion of the apparatus. Let $\alpha = \frac{\lambda}{(2\omega D)^{1/2}}$, $\gamma = \frac{\omega \cdot L}{(L\omega D)^{1/2}}$ and $\lambda = \frac{\kappa A}{\mu \beta V_{out}}$, where $V_{out}\,[cm^3]$ is the volume of the downstream reservoir, $\mu\,[Pa \cdot s]$ and $\beta\,[MPa^{-1}]$ are the dynamic viscosity and compressibility of the pore fluid, ω is the angular frequency of the measured pressure wave, and $D\,[cm]$, $A\,[cm^2]$ and $L\,[cm]$ are the diameter, endcap area and length of the cylindrical sample. The pressure wave function, $P(x,t)$, where x corresponds to the axial extent of the

sample and t is time, is determined through the diffusion equation:

$$\frac{\partial P}{\partial t} = D\frac{\partial^2 P}{\partial x^2},\ D > 0,\ 0 < x < L \tag{5.12}$$

This involves applying the boundary conditions requiring the upstream pressure to be a complex exponential (needed for the oscillations) and for $\frac{\partial P}{\partial t} + \lambda\frac{\partial P}{\partial x} = 0$ to be satisfied when $\lambda > 0$.

Directly measuring pressure at both ends of the sample, R is determined as the complex ratio $P(x = L, t)/P(x = 0, t)$, while $\delta = \arctan[\mathrm{Im}(R)/\mathrm{Re}(R)]$. Finally, equations for the output pressure amplitude and phase difference are obtained numerically as functions of α and γ in the form of equation (5.13) and equation (5.14), respectively.

$$\|R\|(\alpha, \gamma) = \left[\frac{4\alpha^2}{(2\alpha^2 + 1)\cosh(2\gamma) + (2\alpha^2 - 1)\cos(2\gamma)}\right]^{1/2} \tag{5.13}$$

$$\delta(\alpha, \gamma) = \arctan\left[\frac{\tanh[2\alpha\tan(\gamma) + 1] + \tan(\gamma)}{\tan(\gamma) - \tanh(\gamma) + 2\alpha}\right] \tag{5.14}$$

Therefore, from the measurement of amplitude and phase at steady state, α and δ can be determined graphically from the intersection of the lines $\|R\|(\alpha, \gamma)$ and $\delta(\alpha, \gamma)$. Therefore, via the defining equations, the diffusion coefficient can be determined from

$$D = \frac{\omega}{2}\left(\frac{L^2}{\gamma}\right) \tag{5.15}$$

and permeability can determined from

$$\kappa = \frac{\mu\beta V_{out}\alpha\omega L}{A\gamma} \tag{5.16}$$

as all the other parameters are known. Interestingly, none of the equations require knowledge of the upstream reservoir volume. However, because permeability is a function of *both*α and ω as opposed to diffusivity, the sensitivity required for it's measurement will be different for a given frequency. Therefore, obtaining quality data for κ involves finding an optimal ω at steady-state through successive iterations.

The pore pressure alone, being at a minimum of 100 bar, is quite stressful to cement

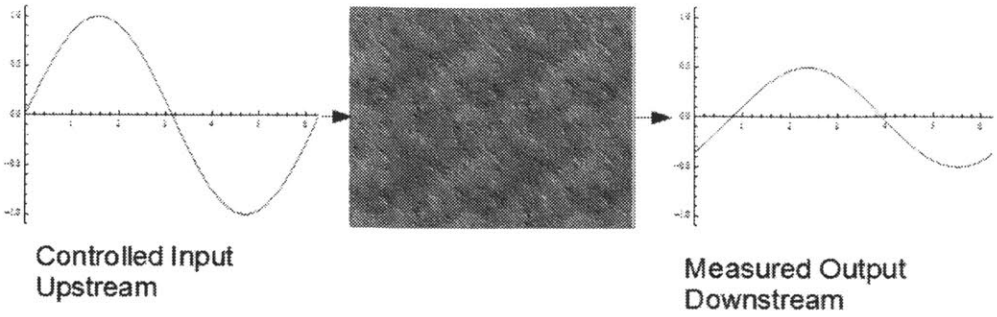

Figure 5-6: The oscillating pore pressure method, adapted from Kranz et al.[5] Upstream of the sample is a controlled pressure wave and downstream is a resulting pressure wave with a relative gain and phase shift that is used to deduce the permeability given the pore fluid parameters.

relative to normal atmospheric conditions (~1 bar), and the confining pressure will add onto the total effective pressure applied to the sample. The permeameter is advantageous in using a small sample size so that these conditions are feasible to provide. Furthermore, it is expected that higher temperature will enhance chemically reactive flows through the cement and cause changes in the crystalline composition. Calcium silicate hydrates, which are formed from the hydration reactions during curing and serve as binding phases, play a very important role in determining the strength and permeability of cement.[54] Their dissolution via the leaching of calcium ions in aqueous solution is a negative effect on material binding, which is obviously not favorable for use in the borehole. When temperature rises, there is positive feedback with both permeability and the diffusion coefficient, which can increase by 32% within a 20 to 80°C transition,[56] which in turn affects reaction rates in the material. It is therefore important to measure temperature effects on the expansive cement along with permeability. However, preliminary heating experiments should take place beforehand to understand material wear without a pressure gradient.

5.4 Tubular Heating Experiments

Hollow glass tubes were used to test the effects of a set temperature on both bentonite mud and cement prior to permeability experiments. Samples were prepared in clear tubular gauge glass from McMaster-Carr of 8" length and 3/4" outer diameter, with 7/64" wall thickness.

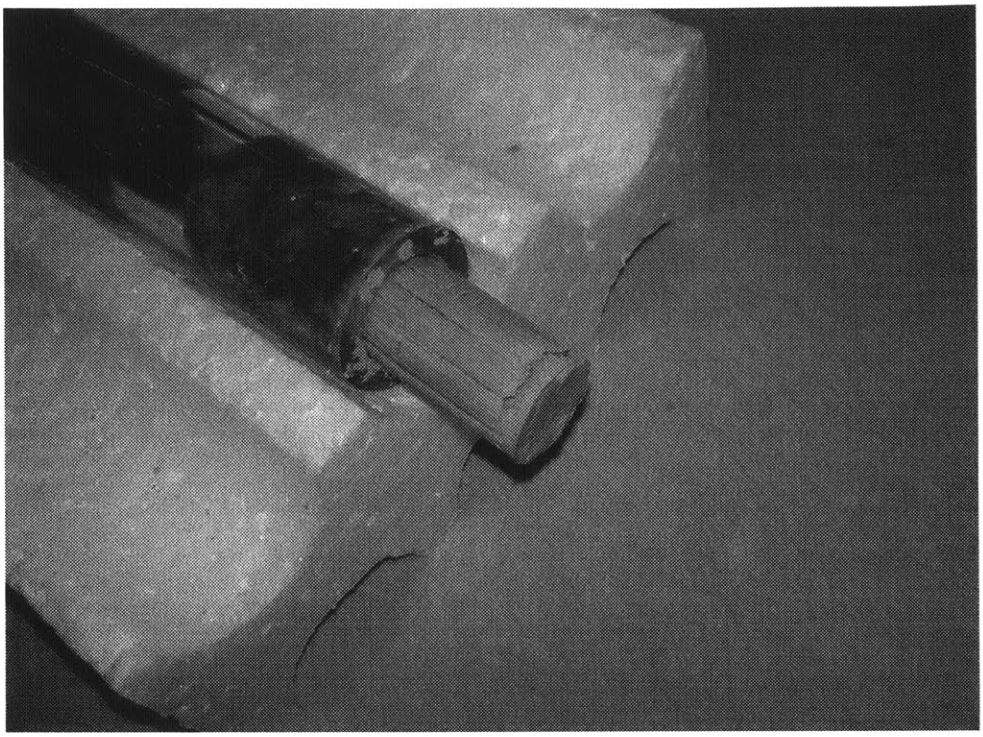

Figure 5-7: Sample #5 of freshly prepared 70/30 Bentonite/Water protruding after being heated in a furnace at 150 ^{o}C for 15 minutes.

The wall thickness was allowed to be excessive to place a bias on axial displacement upon expansion. A furnace was used to heat the samples to 150 ^{o}C. Due to the effects of moisture on the heating of bentonite mud, the tests for those samples were limited to 10 minutes. As shown in figure 5-7, the water trapped in the bentonite clay pushes the rest of the material axially outwards and forms air gaps in the tube. Given the intense pressure heads in the borehole, this behavior shouldn't be expected in such a dramatic form. Rather, this is an experimental inconvenience for this particular material at atmospheric pressure, and further heating experiments should be performed under more representative conditions and use a sampling procedure that guarantees uniformity.

The cement samples included the optimal mixture, Portland cement, and a mixture of Portland cement and fine sand. The optimal mixture was cured first in vertical orientation; the other two were allowed to cure horizontally because the water from the mixes began to flow downward. Each was heated at 150 ^{o}C for 15, 30, and 180 minutes and then an extended ($\tilde{}$1 wk) period of time, and results are shown in table 5.3. The initial objective was to test whether a clear line could be distinguished where moist material ended and dry

material began. However, this was made difficult with the inability to remove the cement from the tube without breaking it into small pieces. [2] Furthermore, visual comparison was practically impossible due to the overall homogenous color. Therefore, mass differences were used instead to understand the effects of heating.

One sample in each set was selected for an extended heating period. Sample 3 from the optimal mixture was heated for a total of 22 days over three trials, and the mass measurements made at the end of each trial indicated smaller decreases in mass until none was detectable. This indicated a complete loss of moisture locked into the solid matrix. Samples 5 and 8 were both heated initially for 15 minutes and then for 7.5 days, where it was shown that Portland cement loses a higher percentage of moisture over the longer period of heating compared to the sand mixture. Data for 180 minutes of heating also indicate Portland's higher susceptibility to losing moisture relative to the optimal mixture and set 3. Finally, the 60 minute tests show that the sand mixture undergoes a percent mass decrement lower than the other two sets. This implies that sand and MgO impact the extent to which water is retained in a mixture with Portland cement.

Heating produced 1-2 circular cracks in all sets at various longitudinal positions (although usually near the middle) which indicate expansion in the axial direction. The locations of the cracks were not consistent enough among samples of the same set to draw conclusions relating thermal stress with material failure.

5.4.1 Effects of heating on expansive seal

The heated expansive cement samples underwent testing with dye penetrant to understand the effects on the integrity of the seal. Due to thermal shock, the glass of some of these tubes cracked in the process and were excluded from the penetrant experiment. Sample 3 was selected due its time spent in the heater and was held vertically in place. Red food coloration was added to the top endcap of the tube until the dye maintained a somewhat constant head. The dye was then left overnight to penetrate the sample or dry out. When dry, the other endcap was also tested in the same manner. Like the glass vial samples of suboptimal mixtures, the dye diffused along the sides of the glass tube until it reached a

[2] cement does not have very good tensile qualities, and the glass tubes had a considerable L/D ratio.

Set	Formula	No	Trial	t (min)	M_i (g)	M_f (g)	ΔM(g)	$\Delta M/M_i$
1	31% Portland, 20% 100-Sieve Sand 26% MgO 23% Water	1	1	10	123.58	121.37	2.21	0.018
		2	1	60	118.36	111.75	6.61	0.056
		3	1	180	114.58	108.14	6.44	0.056
			2	20085	108.14	107.70	0.44	0.004
			3	11520	107.70	107.67	0.03	0.000
2	70% Portland 30% Water	4	1	60	121.47	114.38	7.09	0.058
		5	1	15	107.77	105.10	2.67	0.025
			2	10745	105.10	99.65	5.45	0.052
		6	1	180	114.43	106.74	7.68	0.067
3	27% Portland 53% 100-Sieve Sand 20% Water	7	1	60	119.05	113.34	5.71	0.048
		8	1	15	117.29	113.36	3.93	0.034
			2	10745	113.36	110.86	2.50	0.022
		9	1	180	118.27	112.00	6.27	0.053

Table 5.3: Results for the heating of cement mixtures in glass tubes at 150 ^{o}C.

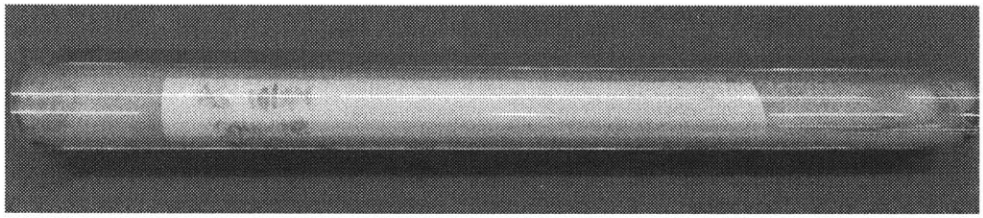

Figure 5-8: Extent of dye penetration on sample of heated expansive cement.

point of retardation. The penetration is visible in figure 5-8, where the dye permeated 48 ± 3 mm, while the opposite endcap had dye permeation 28.8 ± 0.2 mm in a more uniform manner. Therefore, it is implied that the effects of curing vertically were apparent in that voids along the outer surface were concentrated on the upper extent of the sample while the denser materials settled towards the bottom. These voids were caused by air trying to escape the glass as the cement cured, which produced a noticeably rough surface in the cured product. Therefore, these observations are not conclusive of an effect of heating on the expansive seal.

5.5 Summary

Falling head permeameters were inadequate at assessing the permeability of cement sealants due to the large time scales associated with low permeability and the unfortunate presence of lateral gaps in primordial coarse aggregate samples. Similarly, pressurized apparatuses

involving pipe fittings devised in the thermal hydraulics laboratory were yet inadequate due to the evidence of water seeping through the lateral gaps in the bulk material and the inability to ensure air-tight pipe junctions. An earth-sciences laboratory provided a permeameter that employed smaller sample sizes and a confining pressure system to prevent the seepage of pore fluid through the lateral gap. Permeability was obtained using the oscillating pore pressure method where the phase and amplitude shifts of pore pressure waves upstream and downstream of the sample were measured with a data acquisition system. This apparatus had precision beyond the range of $1\,\mu D$.

Chapter 6

Results

6.1 Thermal Conductivity

This section summarizes the data from the thermal conductivity experiments. A comprehensive set of charts are found in appendix A for all experiments. Beforehand, an explanation of possible deviations from the procedure will be explained.

6.1.1 Deviations from procedure

The primordial procedure called for averaging over four external thermocouples, as per the amount available when the apparatus was refurbished. However, factoring in the thermocouple closest to the top (#9) (see 4-1 on page 54) introduced anomalies to data as the position of this thermocouple was close to the ceramic plug, which had insulating effects. Also, its partner, thermocouple #2, was erratic in its temperature readings, which were sometimes close to room temperature or otherwise noticeably off from the other three sets by more than one standard deviation. Therefore, the pairing of #3-5 with #10-12 was employed for all data obtained for temperature differences in this thesis.

Deviating from averaging over these sets occurred when a thermocouple would break. Runs were still conducted while waiting for a replacement, but forcing the averaging of, for example, #4-5 with #11-12 would produce markedly different data and higher thermal conductivities. These data points were removed from the data sets. Furthermore, the original

design of the experiments did not employ insulation around the heated section of the apparatus and allowed cooling from fans or the ambient air. The use of cooling interfered with the accurate measuring of k because the temperature measured by the outer thermocouples could be easily reduced, especially with fans. Therefore, the numerous runs under these conditions were ignored and are not included at all in this thesis.

6.1.2 Convection Effects

Experiments with air had data that varied significantly in the horizontal orientation. The temperature differences measured between thermocouples decreased in this orientation due to the increased heat transfer from convection. This results in increased effective thermal conductivity relative to the vertical orientation due to the $k \propto 1/\Delta T$ proportionality. Data for air are shown in terms of linear power infigure A-4 and in terms of bulk temperature in figure A-5, where the horizontal orientation clearly exceeds the vertical in terms of k for all corresponding linear heats and temperatures.

The temperature profile of the heater rod is shown in figure 6-1 for experiments with air and bentonite clay. These charts demonstrate the remarkably different temperature differences between the two materials resulting from the insulating effects of air. The cosine-shaped temperature profiles strongly indicate that natural convection will in fact occur in the annulus for fluids and to some extent for the fluid in interconnected pore spaces. Density changes are expected to occur along the temperature gradient, and fluid will flow from areas of low density to areas of high density where heat is rejected. Even when insulated, the conflats and pipe openings of the apparatus serve as fins and allow this heat rejection to occur. The thermal conductivity of clay (which is essentially a solid) is not susceptible to the effects of natural convection and there was no incentive to test in the horizontal orientation.

When the air-filled apparatus is oriented horizontally, convection occurs as detailed in section §4.5. The fluid will not be driven so much by the irregular temperature profile considering the lack of a gravitational pressure drop, and the heater rod will be cooled in a radially-oriented convection loop (see figure 4-5). However, when oriented vertically, the fluid will be driven by gravity downward while the irregular temperature profile changes density all along the length of the rod, which moves the fluid upward and creates an axially-

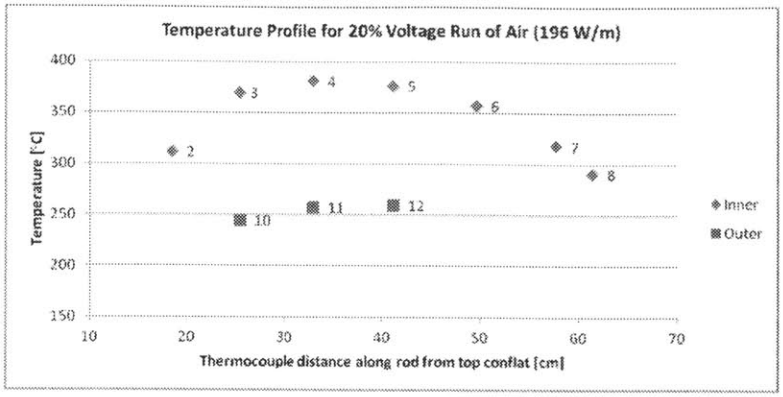

(a)

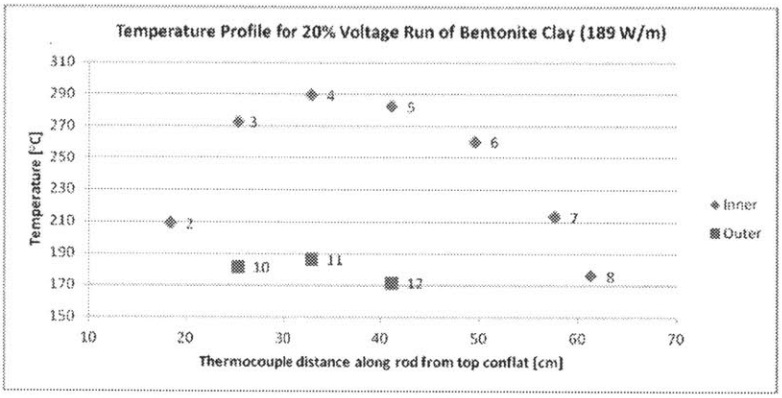

(b)

Figure 6-1: Plot of temperature versus thermocouple location for an experiment at 20% voltage for air and bentonite clay in the vertical orientation. The low thermal conductivity of air is evident through the greater temperature differences between inner and outer thermocouples, and the higher temperatures of the heater rod overall indicate an insulating effect.

oriented natural convection loop. Per given point along the rod, the fluid will spend less time transferring heat because it will always be moving axially. Therefore, less heat is removed from the rod, temperature differences across the annulus are greater and thermal conductivity is lower.

6.1.3 Bentonite and crushed granite

Individual experiments were conducted for bentonite, granite, and three particular mixtures of both. These mixtures were 30/70, 50/50, and 70/30 mass granite per mass bentonite, and results are shown in figure 6-2. The data points for each mixture were obtained as the average effective thermal conductivity for each individual set of experiments (shown in

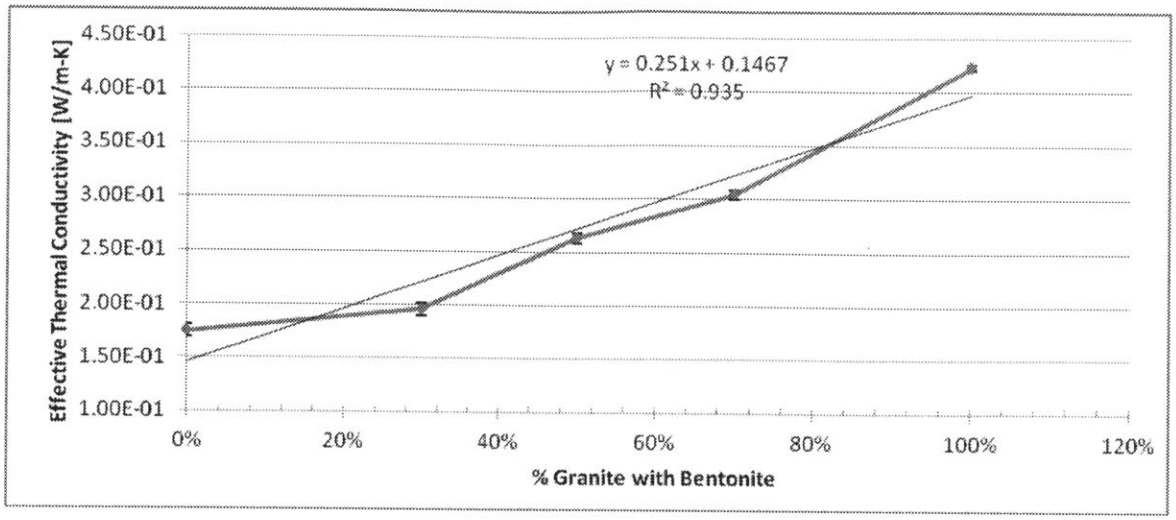

Figure 6-2: Chart summarizing thermal conductivity experiments for mixtures of bentonite clay and granite filings.

appendix A). As the percent composition of granite increases, the thermal conductivity of the mixture increases as well.

The density of each particular mixture was plotted with its effective thermal conductivity and compared to published data with the same percent compositions. The mixtures corresponding to the published data were more dense, and thus they exhibited a higher k than the powders employed in the apparatus. However, as figure 6-3 shows, there is a general trend in the data that may warrant further investigations into the effect of particle density (and porosity) on thermal conductivity.

6.1.4 Flooding Sodium Tetraborate with Helium

The thermal conductivity of sodium tetraborate was evaluated for both air and helium in the pore space. It should be noted that after adding helium to the solid bed of STB with the heater on, and then adding more helium not more than an hour later, there is effect on the temperature being read. This observation confirms that the gas itself has no convective cooling effects as would be expected with any room temperature fluid being passed through a hot pipe. Data shown in figure 6-4 indicate clearly that helium has an enhancing effect on the thermal conductivity of anhydrous borax, and this may be the case for similar materials as well. The thermal conductivity for STB with helium in the pore space is a factor of 1.7

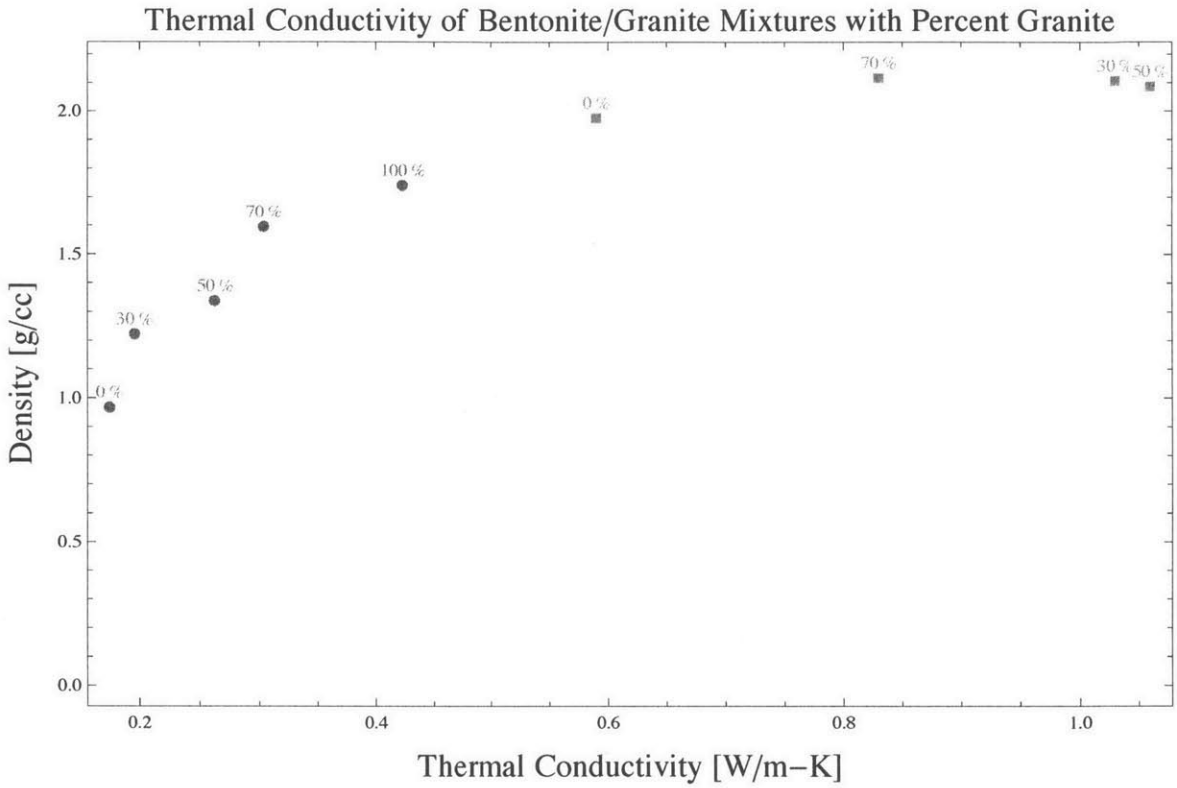

Figure 6-3: Chart relating thermal conductivity to bulk density of material, with the percentages of granite/sand in the mixture. Blue data points were obtained in the laboratory, while red data points for more compact samples were published by Moss et al.[6]

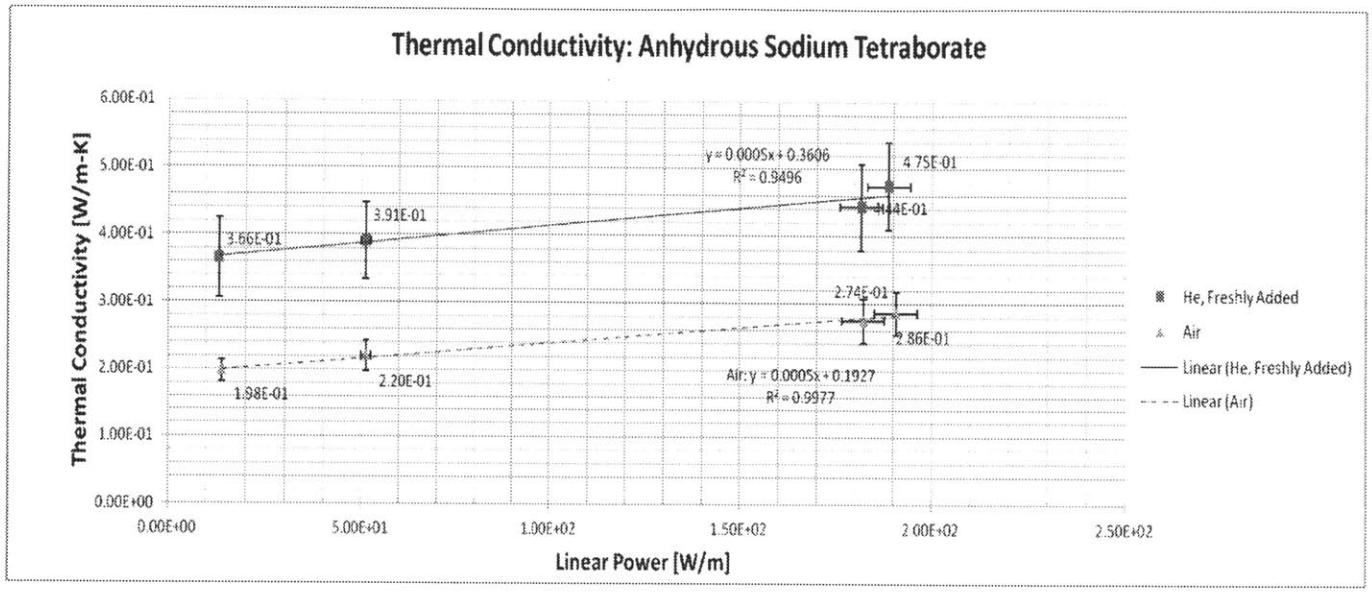

Figure 6-4: Data for sodium tetraborate flooding with both air and helium. Helium data is plotted both when freshly added to the solid bed and averaged at the end of a run overnight. The overnight helium data aligns closely with that for air, implying poor containment of the helium.

higher than when using air. It should be noted that for each test involving helium at a particular voltage setting, data was obtained overnight that indicated leaked of the light gas from the annulus. This was confirmed via the almost perfect overlapping of the overnight data curve with that of air.

6.2 Permeability

This section summarizes the experimental data from the permeability experiments. A set of data tables regarding the sample set are found in appendix B.

6.2.1 Sample Cured Under Pressure

Part 1

The temperature of the expansive cement was measured using a thermocouple over a curing period of six days, which is visible to the left of the pressurized sample in figure 5-5b. A maximum temperature of 29.72 ^{o}C was observed from the outset, after which the temper-

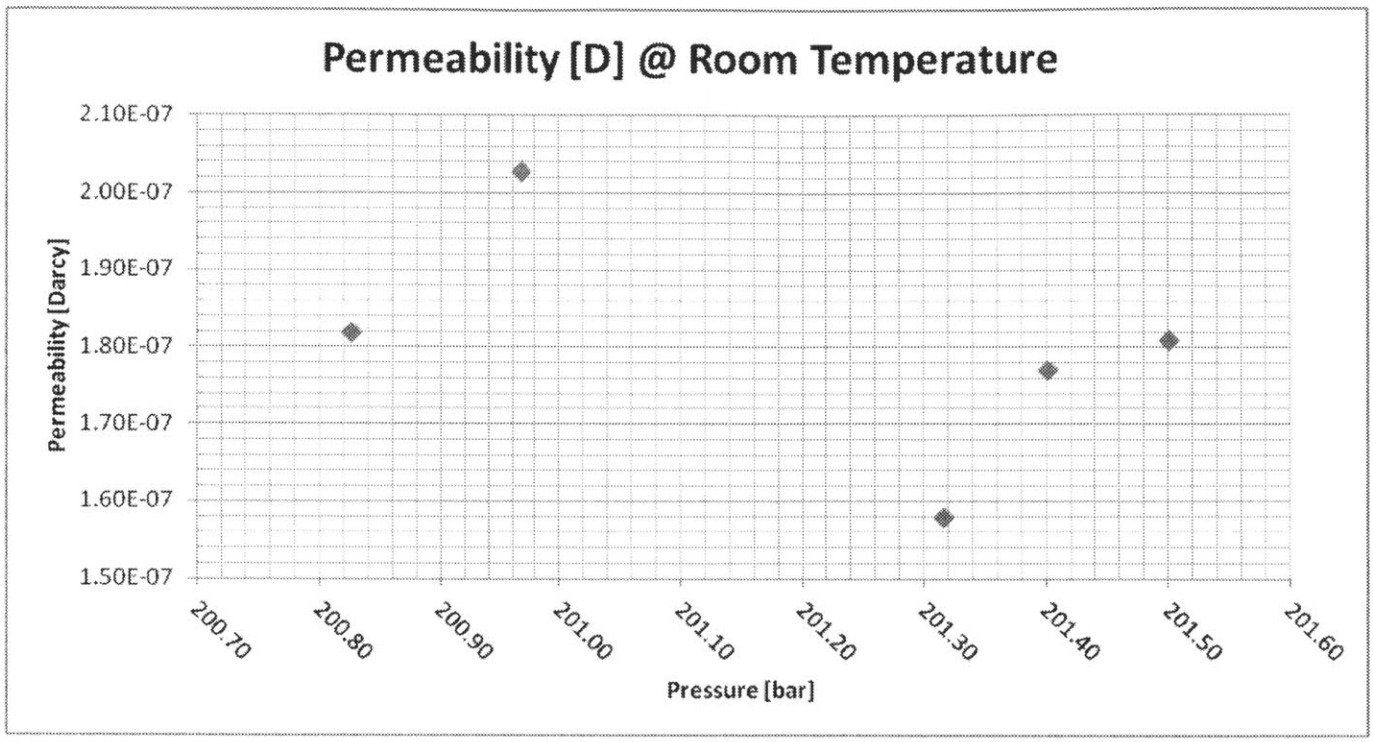

Figure 6-5: Permeability data for sample cured under pressure after six days of such curing. Data is truncated to the 200 bar range due to the poor resolution of the instruments at lower permeabilities when pressure was applied.

ature settled at or around room temperature. This was the only measured evidence of an exothermic hydration reaction, if not the heat from mixing the cement itself. However, this was not an important objective of the experiment.

The pressurized sample was allowed six days of curing under those conditions and was then implemented into the apparatus for testing at high pressure until possible failure. The experiment began at 200 bar and was to progress to an effective pressure as close to 900 bar as possible. However, when the pressure was increased, data could not collected as it appeared the material had exceeded the resolution of the permeameter (which would amount to being well into the nD range.) Therefore, upon the end of this run, it was assumed that the expansive formulation was effectively impermeable.

Part 2

The data featured in 6.2.1 is not the most representative set for the cured sample for the following reasons:

1. Although lab tests at room temperature suggested a time of about 7 days for the sample to expand, this is not necessarily indicative of the nature of curing under pressurized conditions. The curing was presumably incomplete and therefore the data shows effects on an uncured, more malleable sample, whose crystal structure was more susceptible to deformations favoring higher resistance to fluid flow.

2. The steel plugs used to contain the cement in the Teflon sheath created indentations on the endcaps of the cement due to its incomplete curing.

3. An extended range of pressures is needed to better match the conditions of the borehole and to possibly test for abrupt or microscale failure.

Therefore, three months and fives days after the sample was created, the tests in Part 1 were repeated at room temperature up to a confining pressure of 665 bar. However, this time 5.08 mm of the sample face was cut away to remove the glassy outer layer and expose the bulk of the material directly to the pore fluid. Data are shown in figure 6-6, where pressure is increased up to 650 bar. Notice the large break in the trend around 450 bar. Also, the low permeability data point at 300 bar was measured *after* the last data point measured at high pressure and may be the result of non-linear elastic effects.

6.2.2 Samples Cured at Room Temperature

To further probe the upper bound of permeability, with the understanding that temperature typically has negative effects on material structure and the chemical environment, one of the slugs drilled from the atmospheric sample was selected to undergo permeability measurement at high temperature. The apparatus featured a simple resistive electric heater to change the temperature, and the particular setup is shown in figure B-2. Once the sample was subjected to an effective pressure of 300 bar, temperature was varied over a period of 214 hours from 23 °C to 142 °C , although data was only reliable to 130 °C. During this period, the sample underwent remarkable plastic deformation, which is summarized in figure 6-7. Data are plotted in figure 6-8, which shows a two order of magnitude increase in permeability from the 0.1 μD range to tens of μD.

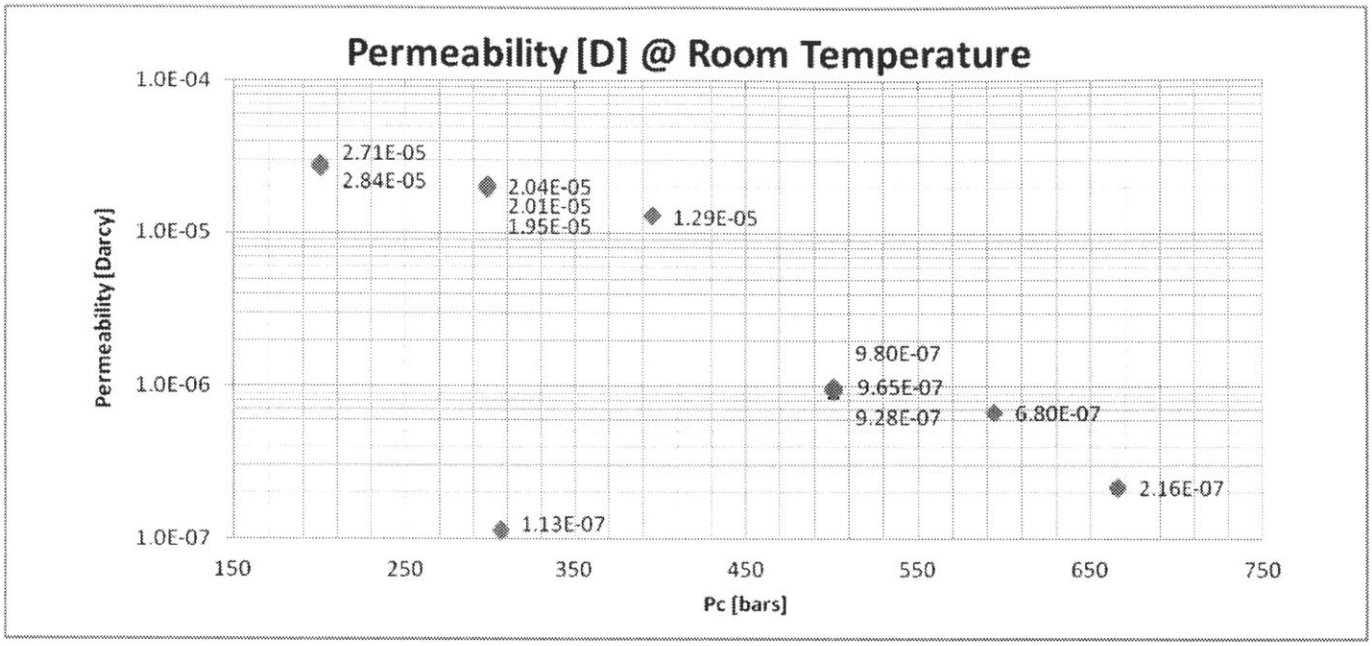

Figure 6-6: Permeability data for sample prepared under pressure after 3 months, 5 days of curing in general.

Sample Deformation Atmospheric Sample #2			
$\Delta D\,[mm]$	$\Delta L\,[mm]$	$\Delta M\,[g]$	$\Delta\rho\,[g/cm^3]$
0.89	2.86	0.4983	-0.268

Figure 6-7: Left-to-right: comparison of cement samples cured under high pressure and at atmospheric pressure, and an atmospheric sample after being stressed at high temperature and pressure. The ruler gives length in centimeters and the table on the bottom gives the measured deformations.

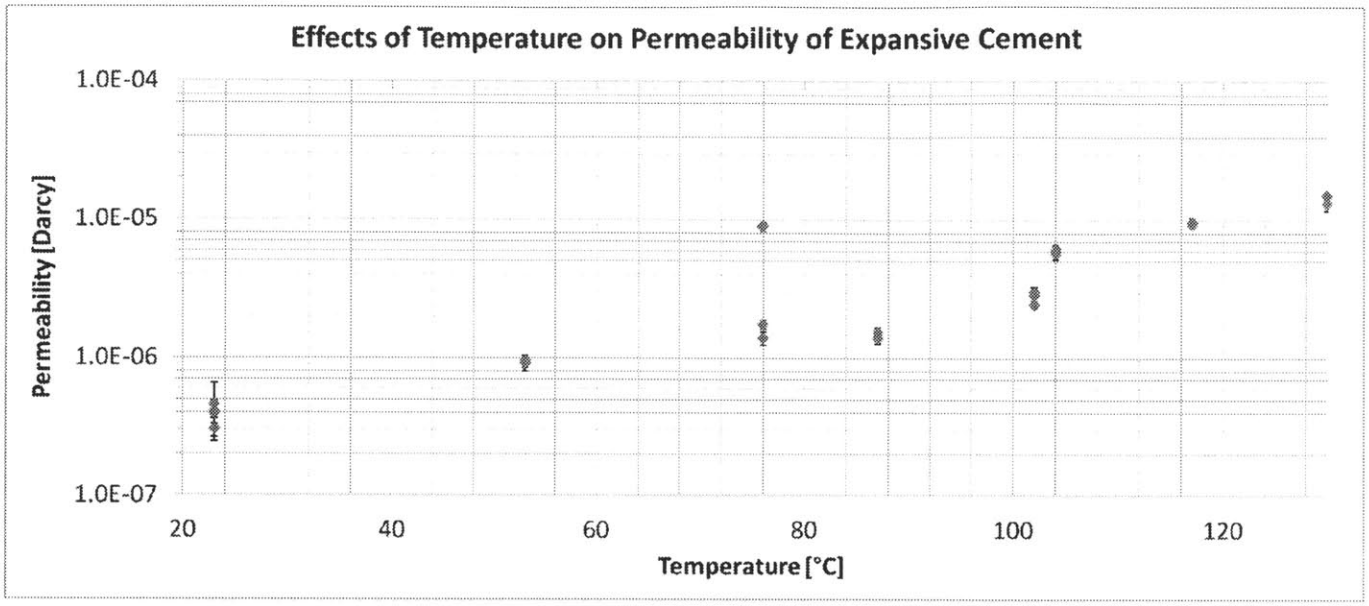

Figure 6-8: Permeability data for sample drilled from bulk laboratory preparation under atmospheric conditions. The confining pressure was increased to around 400 bar, while the pore pressure remained at around 100 bar. It was at this point that the temperature was varied for a total run time of 214 hours.

6.3 Summary

When used in mixtures of bentonite, granite increases the thermal conductivity in proportion to its percent weight composition. Experiments involving these mixtures were for non-compacted powder beds, as there was no practical means to compress the material within the apparatus. When these mixtures were compared with data for compacted mixtures of the same compositions, the trend for thermal conductivity was the same but the overall magnitudes were higher, which is more favorable for the borehole gap. When air is flushed with helium for a bed of anhydrous borax, the thermal conductivity increases by almost a factor of two. Due to the leakage of this pore fluid, experiments had limited duration when measuring steady-state. This necessitates hermetic tightness if canisters are to employ helium as a filler.

The pressurized expansive cement mixture at first exhibited permeability below the resolution of the permeameter due to the effects of incomplete curing. This suggests that plastic deformations of the mixture were the primary inhibitors of fluid flow. When tested three months after preparation, permeability decreased by two orders of magnitude from the mD

to 0.1 μD range after the effective pressure was increased to 500 bar. This sample exhibited hysteresis in not returning to higher permeability when the effective pressure was decreased.

The room temperature variation of the expansive cement were tested under high temperature, with the experiment conducted at 300 bar effective pressure. As temperature was increased to 130 °C, permeability increased from the 0.1 μD range to mD range, and the sample exhibited plastic deformations that were evident in changes in cylindrical dimensions and density.

Chapter 7

Discussion

7.1 Thermal Conductivity

The data from thermal conductivity measurements demonstrate the following key observations:

1. Increasing the weight percent of crushed granite in bentonite increases thermal conductivity and has minimal effects on water sorptivity.
2. Thermal conductivity increases linearly with linear power.
3. Apart from air, data for tests with the apparatus in the horizontal orientation indicate lower effective thermal conductivities than the vertical orientation.
4. Flooding the pore space of borax with helium increases thermal conductivity by a factor of two.

Due to measured ability to expand many times its original volume (see table 4.1), bentonite clay is an optimal gap filler in terms of retarding fluid flow. However, its candidacy can only be defended when mixed with a fraction of fine sand due to the need for mechanical stability and reducing shrinkage. The optimal fraction was determined to be 70% wt. sand in bentonite powder, which raised the thermal conductivity of bentonite 74% to 0.304 W/m-K. This value concerns a non-compacted powder as opposed to the compacted material in a borehole, which is likely to have higher thermal conductivity due to a lower porosity (which

reduces the insulating effects of air). Furthermore, as is demonstrated with bentonite clay (figure A-6) and bentonite powder (figure A-11), the addition of water increases thermal conductivity by forming a clay.

Borax has questionable use as a canister fill but has demonstrated that replacing the pore space of air with helium does in fact increase thermal conductivity as cited in the literature. The thermal conductivity was improved by a factor of 1.7 relative to air, although the literature reported much more dramatic increases. Due to difficulties of sealing the light gas (as was evident with its leakage in the conflats of apparatus) its practicality is low and may only be valid as a measure of leak detection. Nonetheless, the practice of surrounding SNF assemblies in dry storage casks with helium has been qualified as an effective means of dissipating heat.

7.2 Permeability

The data indicate that the cement formulation identified in the course of this project is not necessarily the best candidate for use in a borehole for the following reasons:

1. The roughly two order-of-magnitude increase in permeability with increasing temperature and decreasing lithostatic pressure, indicating vulnerability throughout the entire cement sealing zone to penetrability by groundwater and dissolved radionuclides. Note, however, that temperature and pressure in the caprock zone will not vary significantly, and when changes begin occurring, they will be very prolonged. Furthermore, in regards to temperature, it should be noted that the cement/emplacement zone interface is limited to one location and thermal stresses on the cement may be limited through the use of bentonite buffers.

2. Proof that major fractures form around 450 bar. Once again, it must be noted that pressures are not likely to be this severe in the sealing zone, but this must be considered on the grounds of a worst case scenario.

3. The changes in crystal structure implied by the physical deformation of samples that may have implications on both material durability and expansiveness.

4. The need to test other expansive formulations that may have better chemical resistance to water.

The expansiveness of the cement has not been negated, but the long-term materials consequences posed by experimental evidence are possibly not favorable and warrant future materials-focused investigations. Permeability has been identified below 1 mD and exceeding 1 μD, which meets and exceeds expectations, but it cannot be assured that the materials environment will not compromise this over long periods of time (hundreds of thousands of years.) Therefore, with all matters considered, it is important to develop a comprehensive list of future work in regards to these studies.

7.3 Recommendations for Future Work

The following sections suggest means to expand the studies initiated by this thesis with the goal of innovating the proposed sealant, developing a better understanding of the issues surrounding the sealing of the borehole in general, and providing better experimental data for thermal analyses.

7.3.1 Filler Materials

Further thermal conductivity experiments for the heater apparatus must establish the relationship between the measured values for the powdery beds of bentonite/granite/etc. and the related *compacted* densities. It is determined that the most practical applications of bentonite will be in compacted form and therefore experiments should be conducted on the material in such a state. Although Maxwell's model exists to correct for the solid conductivity for a given pore thermal conductivity [6], ideally, the test material should be subjected to the same lithostatic pressures present in the deep borehole, which are as high as 100 MPa [57] although more likely in the range of 14-41 MPa (2000-6000 psi) from top to bottom of the emplacement zone (see Figure 4 in Powley[14]). Either way, it is best to expose the material up to a plausible extreme to have relevance to its use in all parts of the system, even though the sealing zone is well above this level of pressure. A chart of thermal conductivity versus

pressure should then be made for certain temperatures present in the repository, e,g, 50, 100, and 150 ^{o}C, as it is known that contact pressures at interfaces increase thermal conductivity. However this may be impractical due to the volume of material needed (~900 cc) and the procedure used to compact the powder, which may cause damage to the apparatus. Practically speaking, a calibrated thermal conductivity instrument simulating concentric cylinders would be used on samples from a die press, like the machines used in some materials and radiochemistry laboratories for creating pellets. Another take on this suggestion would be to fill the annulus with such pellets of a defined volume and then applying Maxwell's model to correct for the contributions by air in the pore space.

Other materials that could be tested in the current apparatus include:

- Bentonite with graphene oxide, with the latter claimed to have promising absorptive properties [58].
- Bentonite with corrosion inhibitors
- Solid Portland cement, with a sample of the mix kept separately to analyze porosity

If cement is investigated as a backfill material, the effect of contact resistance would need to be accounted for. The expansive cement cannot be tested in the currently-used apparatus on the basis of repeatability, since once cured it would not be removable. Furthermore, making a solid annulus external of the device would require precise knowledge of expansion, and even when inserted there would be contact resistances and air gaps that would need to be corrected with heat paste or the like. It may be possible to cure plain Portland cement within the device since it has been proven to shrink, but as was mentioned, the air gaps created from this would need to be corrected. Furthermore, it may not shrink uniformly or in such a way as to make removal easy.

7.3.2 Modifications to the conductivity apparatus

If the apparatus is continued to be used, it is imperative that all outer thermocouples be utilized to provide a greater breadth of data points that correlate with the heated length. Having six temperature differences as opposed to three provides a more accurate picture of

thermal conductivity for a given material. The K-type thermocouples in use are satisfactory with regards to instrument-error, although J-type thermocouples (from the same manufacturer, Omega) can be used as well given the temperature range of the heater below at and below the 20% voltage setting. These have the same standard limits of error.[59] However, a potential source of systematic error is the interface between the thermocouple probe and the the outer pipe. The contact resistance between the two surfaces in the grooves of the pipe has to be a low as possible, and this is why conductive heat paste was used on the surfaces in the first place. Therefore, it may be advantageous to consider thermocouple designs that can fit perfectly in the grooves, although the existing 1/32" thick ones in use are already good candidates.

A detachable 5.4 cm ceramic plug must be ordered to fit exactly the inner diameter of the outer pipe minus a few microns, as such a plug was present in the initial applications of the apparatus.[1] This would be inserted right beneath the lower extreme of the rod before the conflat, and is the only effective means of preventing heat loss through both conflats. This would also allow for less of the material to be wasted on a section where no data is collected, and will prevent the conflats from acting as fins.

Foam insulation should be ordered to fit the exact outer diameter of the outer pipe with conduits for the thermocouples. The type used in the experiments was scrap material that was ill-fitting and more or less created an air gap. Nonetheless, fiberglass insulation can still be used as it was to cover other metal parts near the heated section. The inlet and outlet valves connected to the pipe fittings on the outer pipe function inadvertently as fins and should be reduced in size, if possible.

When applying helium as a void filler, the presence of leakage was evident by ear when the gas was heard flowing out of the top conflat and verified experimentally through overnight data acquisition. To improve future experiments with this gas, the apparatus should be modified to be more gas-tight at the conflats. However, this may be difficult and not realistic in representing actual canister conditions. Helium overall is very difficult to confine, and perhaps impossible in the high stress environment of the borehole.

7.3.3 Sealant

When focusing research on the product of an evolutionary process, as was done for the cement, results indicate whether the process should be altered or inclusive of new variables. Based upon the outcome of the experiments, it is clear that attention should focus on additives that not only lend to expansion but strengthen the mechanical integrity of the material. The cement did expand, and continued to do so under high stress. Nonetheless, the permeability was decreased by two orders of magnitude and the porosity noticeably augmented when temperature increased by 100 °C, which does not meet standards for a durable sealant.

There are certain compounds that impart greater structural integrity to the cement; however, these often involve unpublished trade secrets among competing industries. Certain companies have proposed "self-healing" materials and heavily wear-resistant formulations that are economic for industrial application, but have not been tested in geological settings. Other additives to test for improved mechanical stability include:

- Varying sand particle size per sample instead of using crushed granite. Sand itself is already known to increase stability, so it is postulated that there is an optimal particle size to volume ratio in terms of hardness and expansiveness.

- Gypsum, as this was demonstrated to retain expansiveness of cement when the existing formulation was modified to include it. This is a promising additive for deep well cementing as an inhibitor of flash setting, which lends a greater margin to the cementing period and reduces the potential for slurry thickening to impair the complete coverage of the sealing zone.

- Adding fine steel wool, carbon or glass fibers to provide reinforcement, with an effect presumed to be very similar to reinforced concrete. The fibers are presumed to improve the tensile qualities of the cured mixture, which may be important given the very large length-to-diameter ratio of the cement used to fill the borehole/liner wall gaps.

7.3.4 X-Ray Crystallography

Due to the remarkable changes to cement structure that were observed, it is imperative that X-ray crystallography be performed on the pre-tested and resultant material in testing orientations that are likely to cover the range of possible crystal species. This will clearly indicate the changes to crystalline structure, e.g. the formation of exotic, hydrous crystals, that may be detrimental to the stability of the material. Until then, the cement formulation cannot be promoted as having the optimal characteristics that were originally taken for face value. The radial expansion observed after stressing may not be emulated in granitic bedrock, considering the malleability of the Teflon sheath used in the experiment. Furthermore, even if the formulation was still expansive, the associated loss of impermeability may be a trade-off that is not commensurable.

7.3.5 Stress and Deformation Tests

Deformation measurements on the curing cement sealant are proposed as a means of quantifying its observed expansiveness in both the axial and radial directions. The previous sampling procedure only provided the minimum thin-hoop stress based on the known yield stress of glass. Also, the displacement transducer in the permeameter only provided axial measurements for cement that was already cured and only for stressed conditions.

An experiment is proposed where a piezoelectric sensor is planted in a sample of the expanding cement. Over a period of approximately 1 month, the depression of the sensor will result in force readings that can easily be converted to wall pressures. The vessel for the cement can be rigid enough to prevent cracking and will allow for tests beyond the minimum hoop stress estimated for the glass vials. Once radial elongation is measured, dimensional analysis can be used for the actual in-situ geometry to determine if the hoop stress is enough to counteract lithostatic pressure and the weight of the sealant itself. Furthermore, these measurements can be compared to the data obtained from the displacement transducer in the permeameter experiments.

Another means of testing expansiveness is using a "push-out" test as outlined in Akgün[60], where a steel piston is pressed against cement sealed to some extent in cored rock (preferably

granite) and the force is measured until the plug yields. This test would be especially applicable to the concept of cement "bridge plugs," which are layers of expansive cement installed between canisters to relieve stress. The load is measured using machine gauges and pressure transducers, and the sealant movements are detected using linear variable differential transducers. This type of test varies in time from minutes to a few days, and indicates whether failure lies mainly in the creep of the host rock or from the top-to-bottom failure at the seal interface, or a combination thereof. Therefore, the two stress tests mentioned here can be conducted in parallel.

The final outlook on the expanding cement was based on a conservative approach, and solutions can be found to mitigate the negative effects. For example, between the sealing and emplacement zones, materials can be used that have greater durability under stressful temperatures such as crushed granite. This would allow the cement to experience less of this thermal stress and be located further up the borehole near ambient temperature. The unfortunate trade-off is increased proximity to the biosphere, which increases the probability of exposure should the seal be compromised. Nonetheless, if the sealing zone consisted of a less stressful environment, the cement would still be recommended as an expansive seal with adequate permeability.

7.3.6 Irradiation

The environment near the upper extreme of the emplacement zone is considerably radioactive and presents materials stresses that warrant further investigations into the effects of radiation on sealant durability and the chemical environment. Experiments can be conducted using the spent fuel pool of the MIT Research Reactor, which gives the added advantage of controllable hydrological surroundings. The major considerations of such experiments would include

- radiation-induced voiding and segregation, which is likely to impact the permeability of the bulk sealant through a increase in porosity and formation of more extensive channels through which the pore fluid can pass more easily. Furthermore, although the average centerline temperature of the canisters may be low in this sense, the effect of swelling is further enhanced with temperature.[61]

- radiation-induced dissolution of iodine and other rock salts containing sodium and chlorine into the groundwater flooding the gap, augmenting the natural rate of dissolution and presenting a harsh oxidizing environment to the steel of the canisters. For example, hydrogen gas can be formed through the irradiation of such salts which can embrittle steel.[62]

7.3.7 Calibration

The use of propylene glycol (PG) to calibrate the temperature readings of the thermocouples will be a valid approach if the following adjustments are made:

1. The tubes are surrounded by insulation.

2. The fluid heating/pumping device can maintain the temperature of the fluid at a near constant

3. The temperature readout of the device is accurate to at least three decimal places

These reasons indicate the shortcomings that were experienced in an initial attempt to calibrate the thermocouples with PG. A Lauda® Ecoline 100-Series bath and immersion thermostat were connected to the apparatus through the inlet and outlet on the outer pipe using rubber hoses with no insulation. The heater was off but measurements with the DAS were conducted as usual for all thermocouples. As PG was pumped through the heated section from top to bottom, the measured temperatures were not uniform and did not match the set temperature within a reasonable margin of error. Switching to high or lower temperatures did not replicate the measured differences between neighboring thermocouples. The reference temperature also fluctuated from the original temperature set on the device because the machine switches heat on and off to prevent dry operation. These inconsistencies made the data difficult to use, as only set temperatures near the ambient room temperature were fairly consistent. Furthermore, the reference temperature of the thermostat would have reduced the significant figures used in analysis. Therefore, this calibration data was ignored.

The use of glycerine is still a valid means of calibrating the instrument for thermal conductivity at least at low linear powers where the effects from convection are minimal.

However, its use can be improved in the following ways:

1. Use the inlet and outlet valves to completely fill the annulus with the viscous fluid, e.g. by using a hand pump, and thus eliminating the air gaps likely to have been present using the previous method (inserting the fluid with the apparatus inverted and *then* applying/sealing the conflat.)

2. Test a finer range of linear powers, including those below 5% voltage down to 1%.

Ideally, a *solid* material would be used to calibrate the temperature readings. The issue with using waxes is the generally low melting point that would be effective only at probing low linear heats. Other moldable materials would require melting points that would be hazardous in application and would render their removal from the apparatus impractical or even impossible. A solid annulus of material that could be inserted as a sort of sleeve has the obvious setback of creating contact resistance and air gaps. Heat paste can be used to resolve this matter, but depending on the viscosity, it may create frictional resistance when inserted.

Steel balls of a precise volume can be used as a filler provided there is a dependable publication of thermal conductivity versus temperature for the particular type of steel, possibly from the manufacturer or a trusted industrial source. A model correcting for the void space can then be applied, which further necessitates that the volume of empty space in the apparatus is precisely known. This is more difficult than it seems, considering that purely geometric analysis did not compare well to the use of water as a test fluid. Steel beads were available in the lab during the period of these experiments, but their specific grade was unknown and they were oxidized in some places.

7.3.8 Miscellaneous

The following items may be of secondary importance to future studies:

- Measuring the heat of hydration for different cement formulations using a bomb calorimeter and finding a correlation between this and observed durability and expansiveness. It is suggested that a greater heat of hydration would result in the reduced formation

of hydrous crystals when penetrated with water. Furthermore, given the dependence of cement quality on a variety of factors apart from the inclusion of certain additives, intermediate-scale experiments should be conducted on cement slurries that monitor the heat of hydration, hardening time, cylindrical wall stress, and perhaps CO_2 buildup for a given external pressure and temperature and stirring time.

- Incorporating pressure and temperature controllability of apparatus to validate the onset of convection in the porous media that have so far been tested, with particular emphasis on crushed granite, to correspond with transient thermal computations in CFD models. This will involve refining the measurement technique for porosity.

- Testing the ability of bentonite to absorb iodine dissolved in water.

- Performing permeability measurements with a saline pore fluid of the type that would be expected in the borehole gap. This would involve using a solution with well-known thermodynamic properties.

7.4 Final Remarks

The expansive cement was qualified only to the extent of its highly suitable permeability under low stress. The measured changes in permeability under high temperature and pressure may have negative structural implications with plastic deformation and the formation of cracks. Further tests must be conducted that validate the self-pressurizing nature of the formulation and its durability under high stress conditions. If the material is structurally weak due to the changes in composition when subjected to stress, then other likely candidates should be considered as the borehole sealant must have ensured long-term viability. Greater understanding is achieved when the chemical changes in the cement are known, and crystallography experiments are highly encouraged to provide input for the inclusion or exclusion of certain additives in the future.

A particular mixture of bentonite with crushed granite was qualified for use in the borehole gap as the thermal conductivity was demonstrated to improve with the addition of that component. The high sorptivity of the swelling clay was not reduced relative to pure

bentonite and therefore the ability to trap radionuclides dissolved in water has not been compromised. It is likely that the granite will impart structural integrity to the filler such that swelling is not impacted over long periods of time. Further experiments should strive to emulate the compacted form of the filler as this would impart higher thermal conductivity and better represent the in-situ borehole gap conditions.

Appendix A

Thermal Conductivity Data

Introduction

This appendix consists of the thermal conductivity data obtained for some materials proposed as gap or canister fillers for the borehole system. It will first show the standard that was used to provide a basis of comparison for all data sets. It will then proceed to show graphs showing thermal conductivity versus linear power, as was determined to be the most concise and informative format to present the figures. Air and glycerine will also feature data in terms of bulk fluid temperature.

It should be noted that in some early experiments, two window fans or the ambient air were used to cool the outer pipe left bare without insulation. These numerous data did not conform to the ultimate standard procedure and were removed from consideration. Therefore, all data in this thesis was obtained from an insulated apparatus.

A.1 Glycerine Standard

In order to validate the data obtained from the thermal conductivity apparatus, a standard material with a defined thermal conductivity had to be measured and compared with published data. Glycerine ($C_3H_8O_3$) (also known as glycerol) was chosen as a standard for the thermal conductivity measurements because

1. it has a consistent and thoroughly published value for thermal conductivity. The Soap

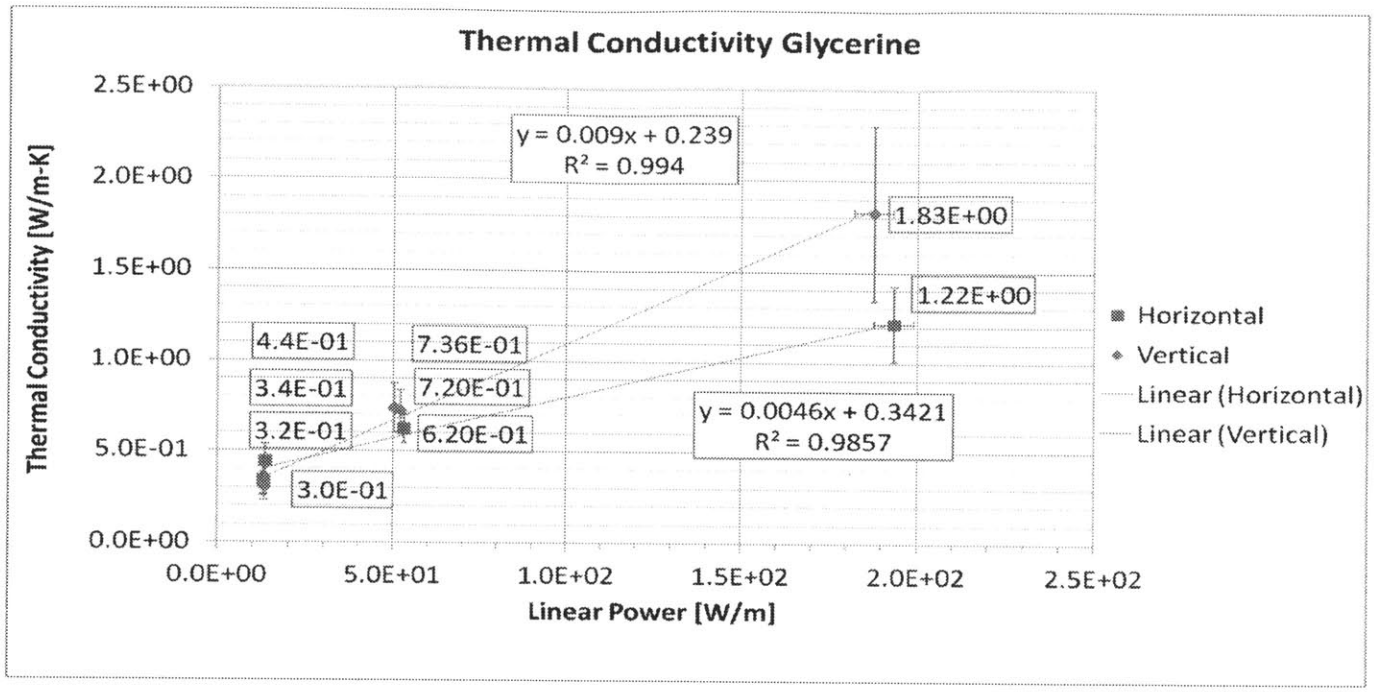

Figure A-1: Data for the thermal conductivity of glycerine in terms of linear power.

and Detergent Association[63] published the value $k = 0.289\,W/m \cdot K$, which is similar to other published values.

2. its high viscosity will resist convective heat transfer

3. as a fluid, it can fill the entire annulus without leaving pore spaces if poured slowly.

The glycerol used in this calibration was 1 L of Alfa Aesar® 99+% Glycerol. Data are plotted in figure A-1. It is apparent that at low linear power the data have a mild agreement with published data, as shown in the inset (figure A-2). At higher linear powers, convective effects dominate and enhance heat removal, thereby lowering temperature differences and dramatically increasing the effective thermal conductivities measured in the apparatus. Thus, for fluids, the apparatus is only valid for obtaining actual thermal conductivity values at low heat (around 5% applied voltage) while data obtained at higher power should be subject to the evaluation of a heat transfer coefficient. However, the apparatus should be validated for testing solids. There is also a linear relationship between thermal conductivity and the bulk temperature of glycerine, as shown in figure A-3.

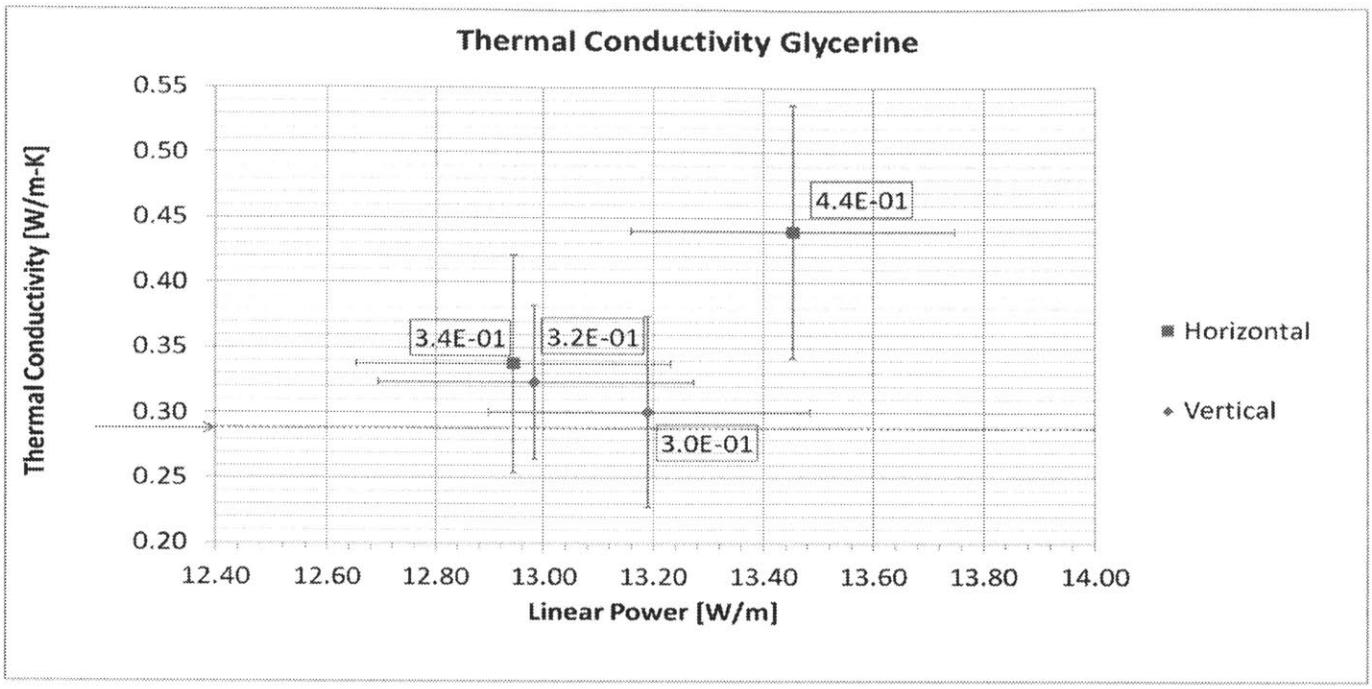

Figure A-2: Inset of glycerine data for low linear power, with an arrow indicating the standard value for thermal conductivity (0.289 W/m-K). Data appear to be within error of the published quantity.

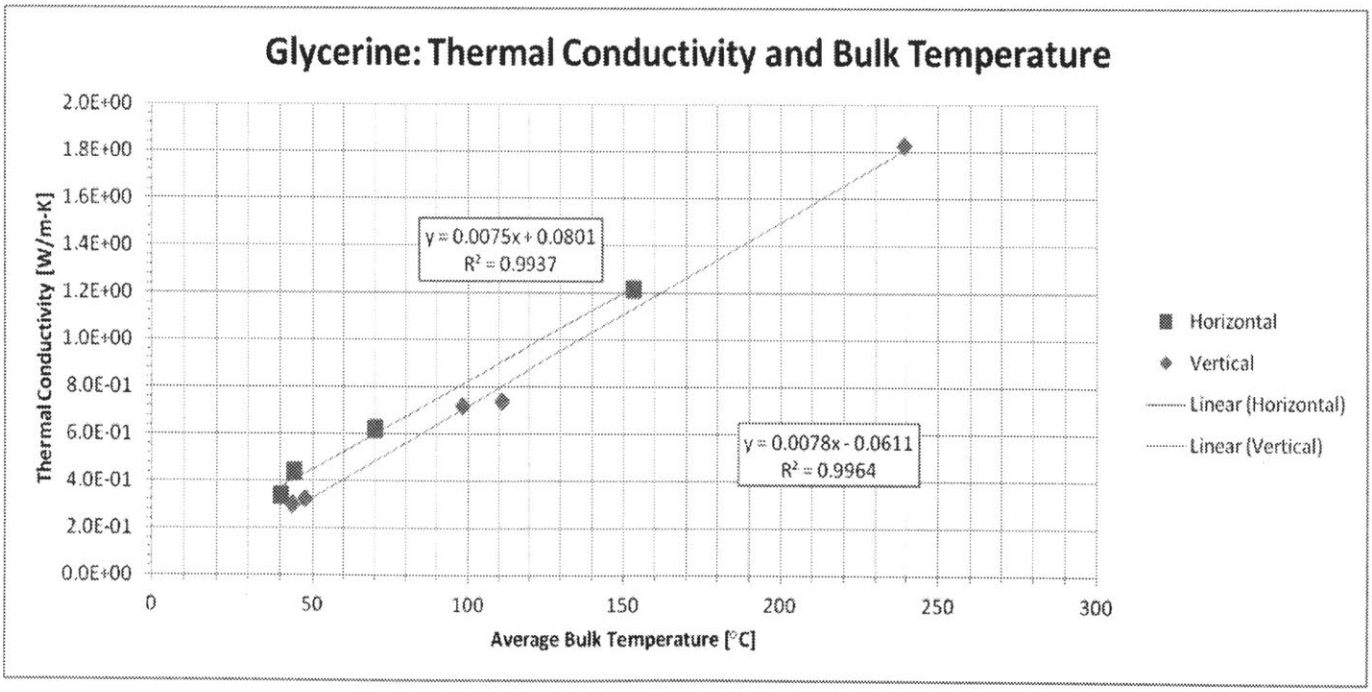

Figure A-3: Thermal conductivity of glycerine with respects to average bulk temperature of the fluid.

A.2 Air

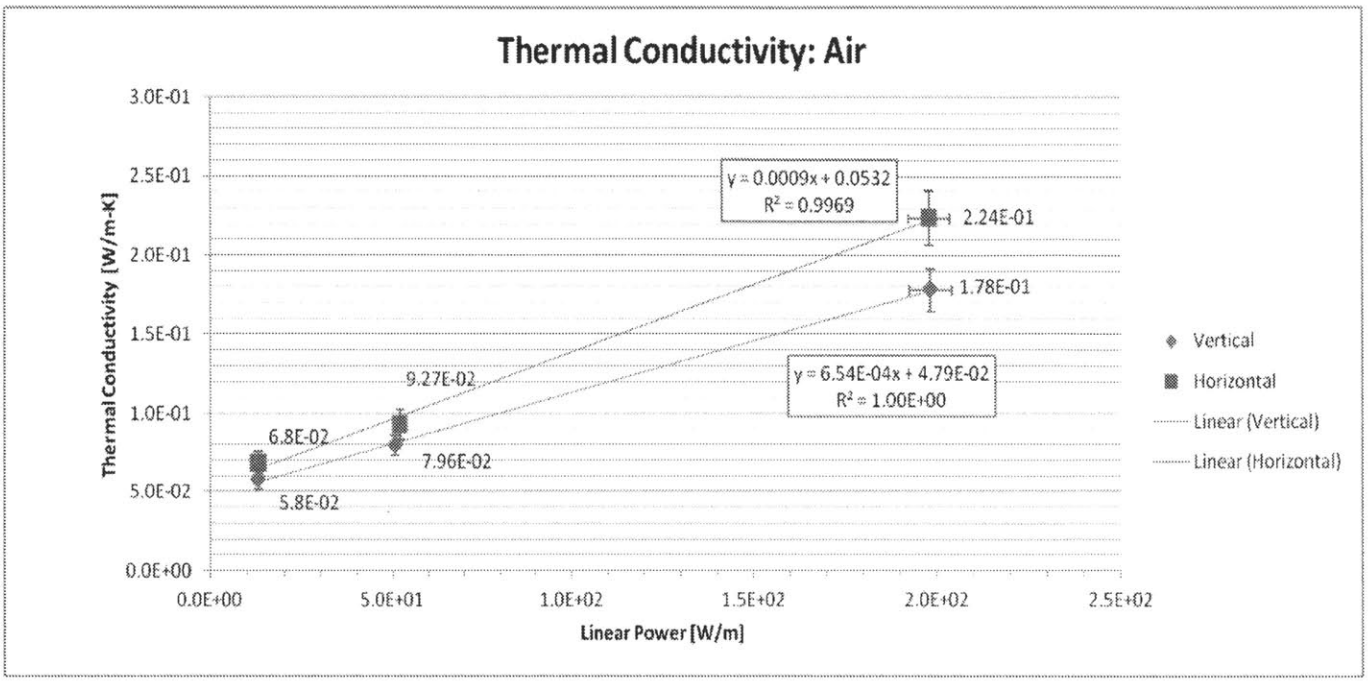

Figure A-4: Thermal conductivity of air in terms of linear power.

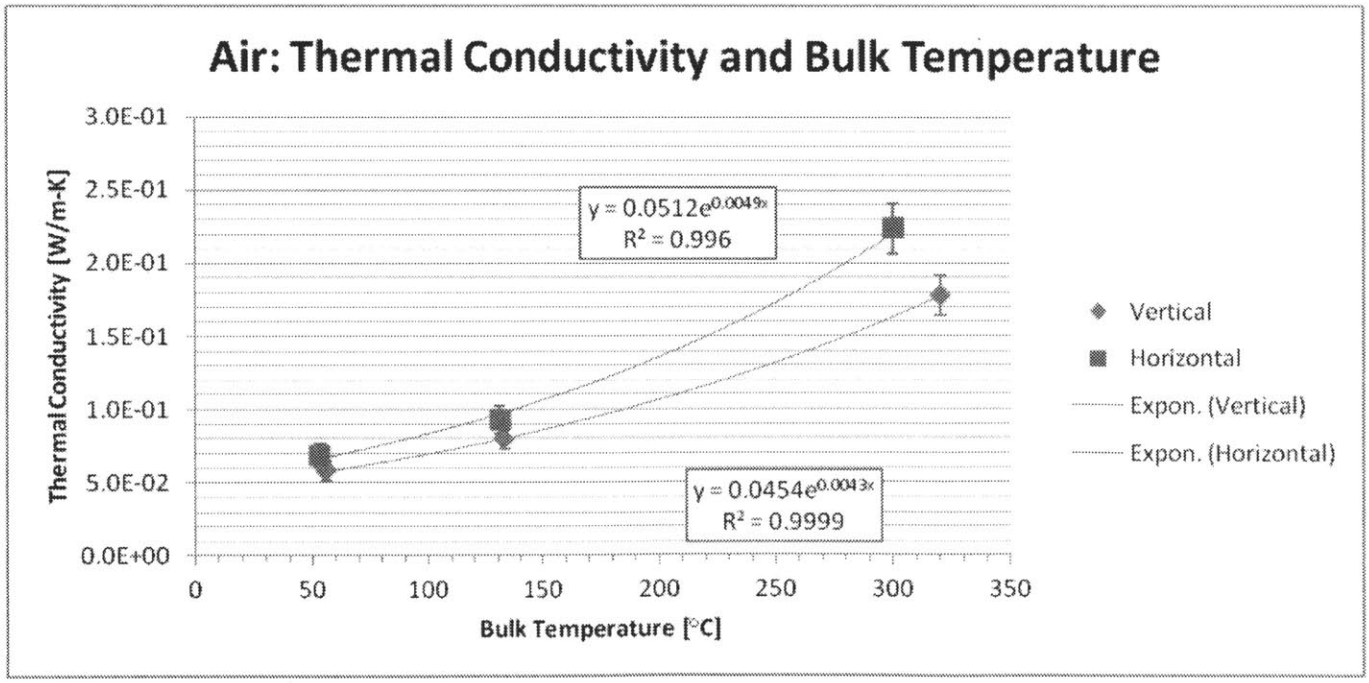

Figure A-5: Thermal conductivity of air in terms of bulk temperature.

A.3 Bentonite Clay

A mixture of 70% wt. Bentonite and 30% water was tested in the apparatus in the vertical orientation. Clay was prepared externally in a batch and then applied by hand around the heater rod. Once enough clay was applied, it was shaped with a paint scraper into a cylinder and then inserted into the outer pipe. This was the most involved process in regards to inserting material into the annulus and is not recommended for future work unless a softer clay (i.e. a 50/50 ratio) is used instead.

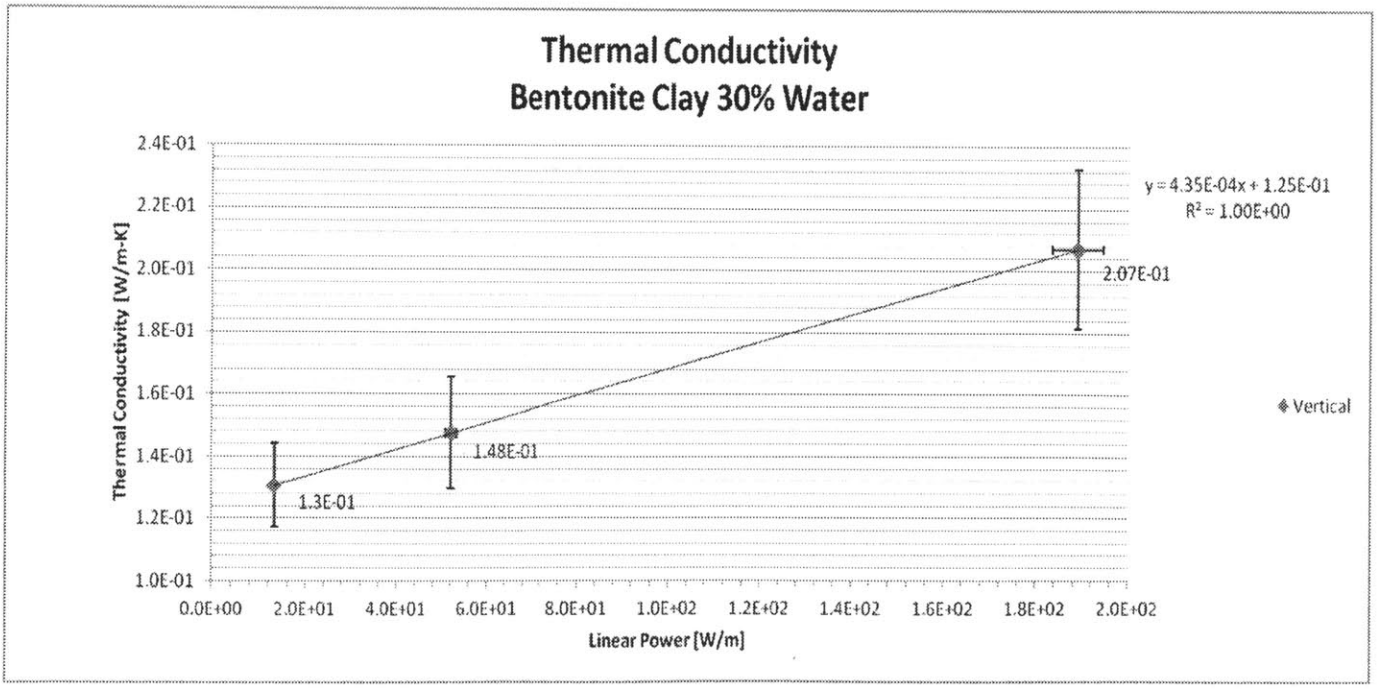

Figure A-6: Thermal conductivity of Bentonite Clay

A.4 Granite Filings

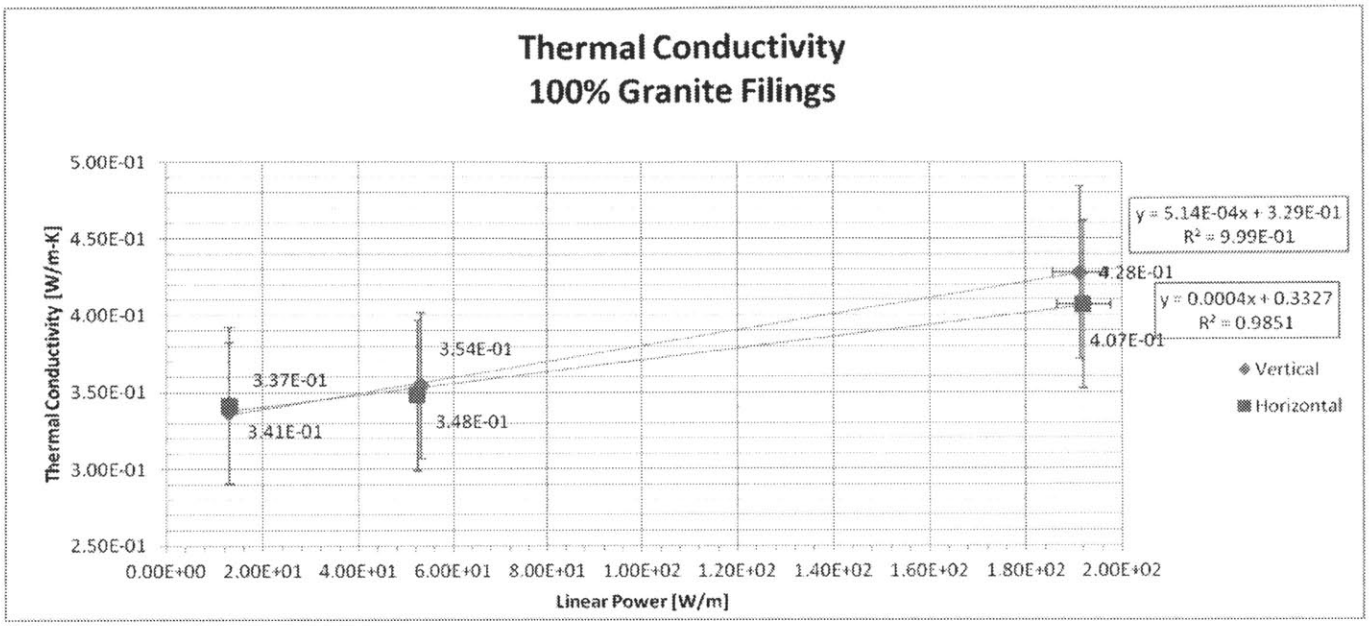

Figure A-7: Thermal conductivity of Granite filings

A.5 30% Bentonite, 70% Granite

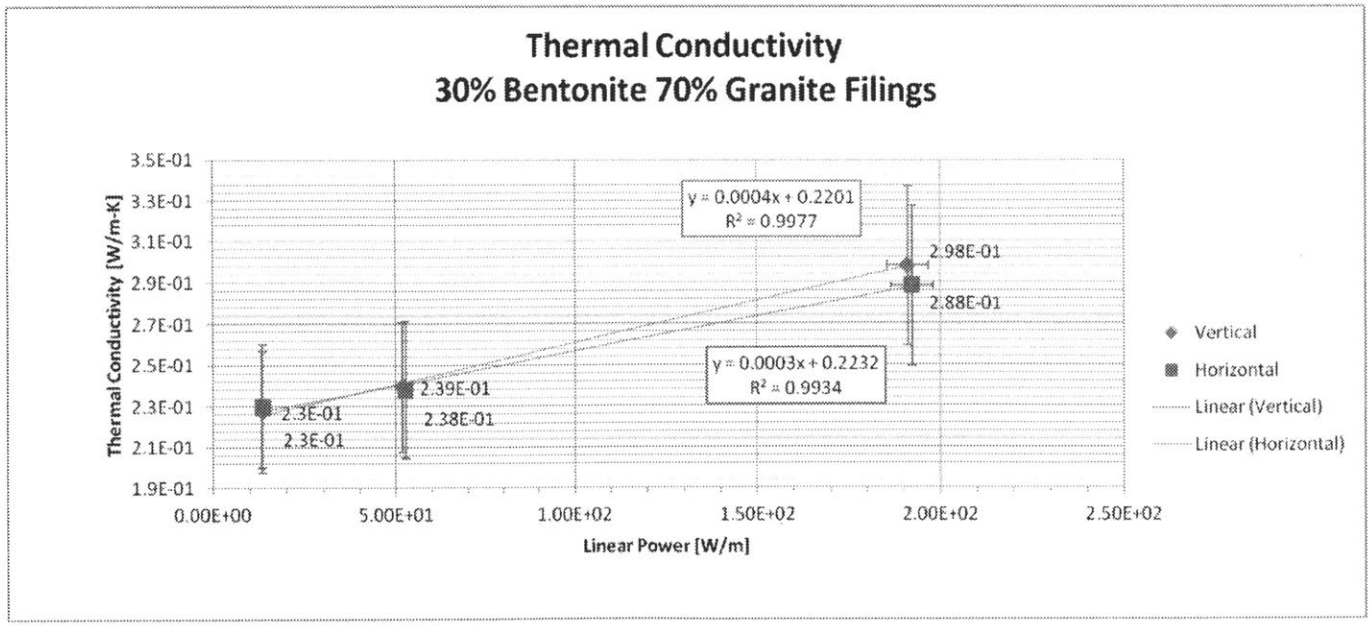

Figure A-8: Thermal conductivity of 30/70 Bentonite/Granite Mix

A.6 50% Bentonite, 50% Granite

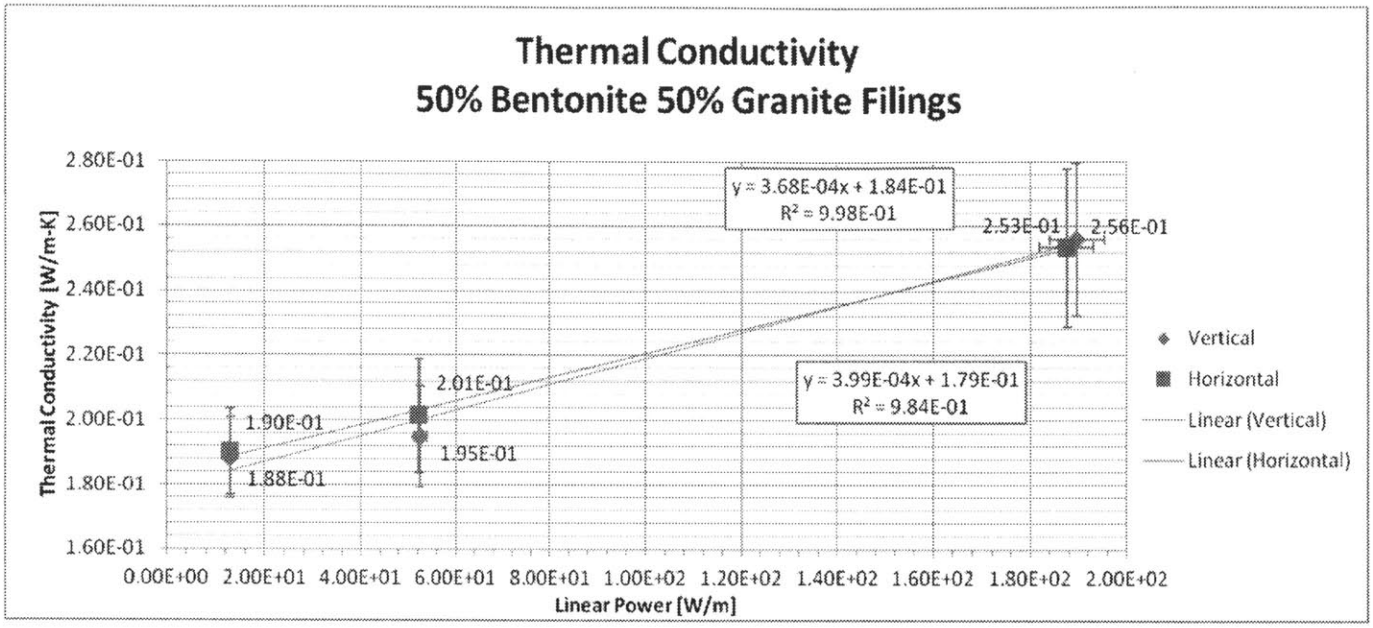

Figure A-9: Thermal conductivity of 50/50 Bentonite/Granite Mix

A.7 70% Bentonite, 30% Granite

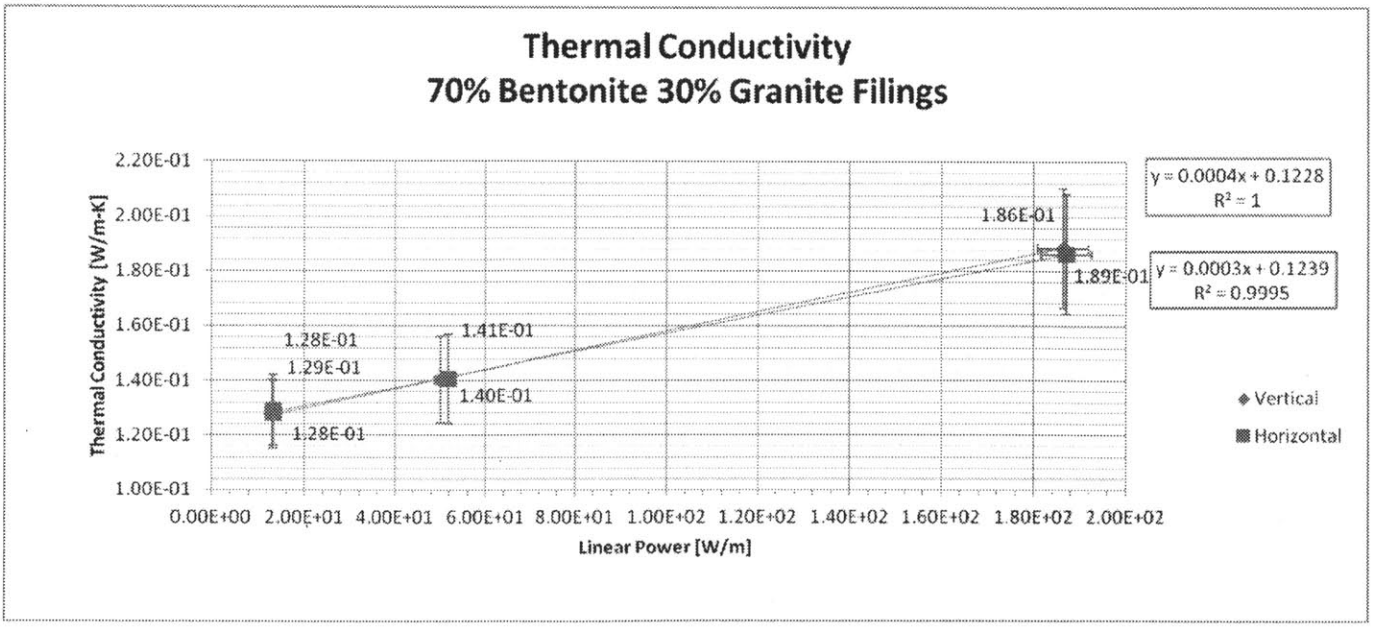

Figure A-10: Thermal conductivity of 70/30 Bentonite/Granite Mix

A.8 Dry Bentonite

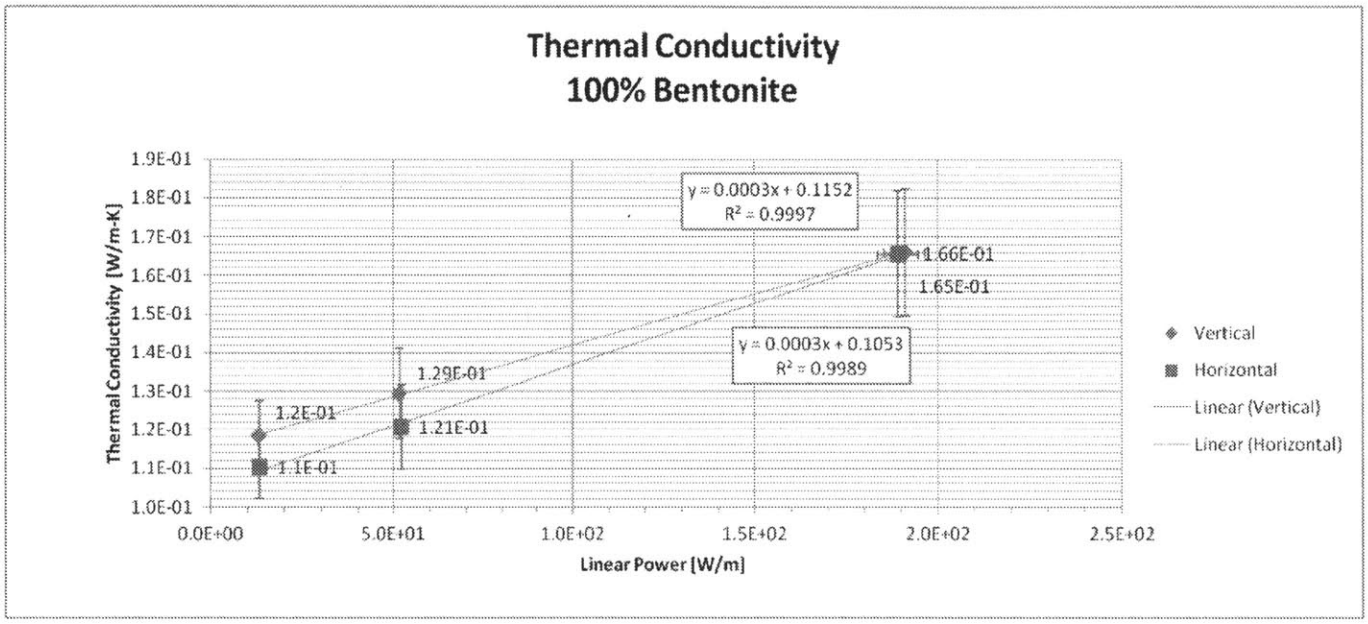

Figure A-11: Thermal conductivity of Bentonite Powder

A.9 Sodium Tetraborate

Experiments with sodium tetraborate were conducted with the pore space filled with air and helium and in vertical and horizontal orientations. Data from these iterations are shown together in figure A-12 The effects of using the horizontal orientation are more negligible for air than helium. In either case, the thermal conductivity of helium is easily a factor of 1.5 to 1.9 above that of air.

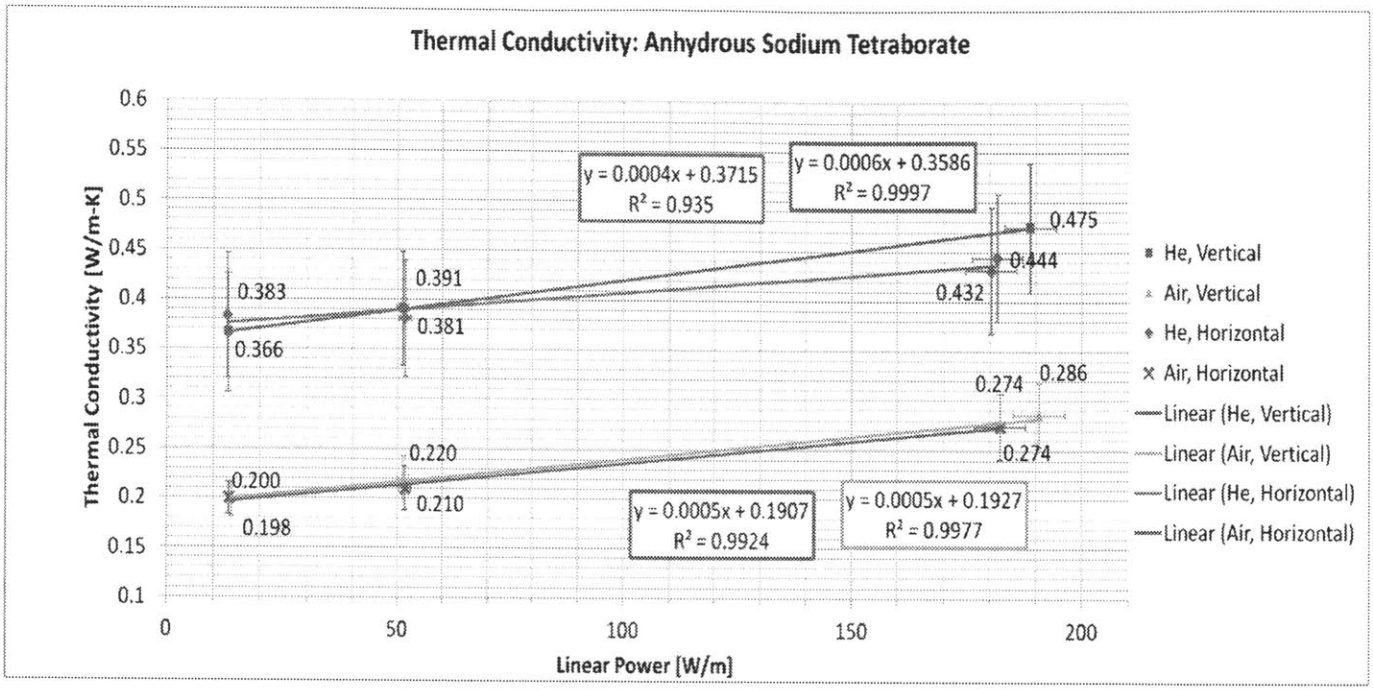

Figure A-12: Thermal conductivity of sodium tetraborate filled with either air or helium.

Appendix B

Permeability Auxiliary Data

This appendix provides details on the samples used in the EAPS permeameter and useful photographs.

B.1 Samples Cured Under Room Temperature

#	Description	L (mm)	D (mm)	M (g)	ρ	ϕ
8	Cut Samples	25.52	12.67	6.1926	1.925	0.125
7		25.6	12.68	5.8715	1.816	0.175
6		25.56	12.7	6.2318	1.925	0.125
5		25.49	12.7	5.8741	1.819	0.173
4		25.5	12.69	6.185	1.918	0.129
3		25.44	12.68	5.8704	1.827	0.170
2'	After permeability test at up to 150C and 400b at 100b pore pressure	28.39	13.59	6.3618	1.545	0.298
2	Cut Sample	25.53	12.7	5.8635	1.813	0.176

Table B.1: Homogeneous samples drilled from bulk laboratory preparation at atmospheric temperature. Compare the densities to the compacted sample in table B.2.

B.2 Samples Cured Under Pressure

All permeability measurements for the pressurized sample were conducted at room temperature. ϕ refers to porosity.

#	Description	L [mm]	D [mm]	M [g]	ρ [g/cc]	ϕ
$C2$	Sample was exposed to P_p=100 bar and P_c=200, 300, 400 bar	27.15	12.5	7.332	2.201	0.000
$C2'_i$	Sample was exposed to P_p=100 bar and	22.07	12.5	5.1798	1.912	0.131
$C2'_f$	P_c=200, 300, 400, 500, 600 bar	21.69	12.15	5.1675	2.055	0.066

Table B.2: Samples cured under pressure, with C2 documenting state before first run and C2i/C2f documenting before/after parameters for second run at higher pressures.

B.3 Permeameter Components Spread Out

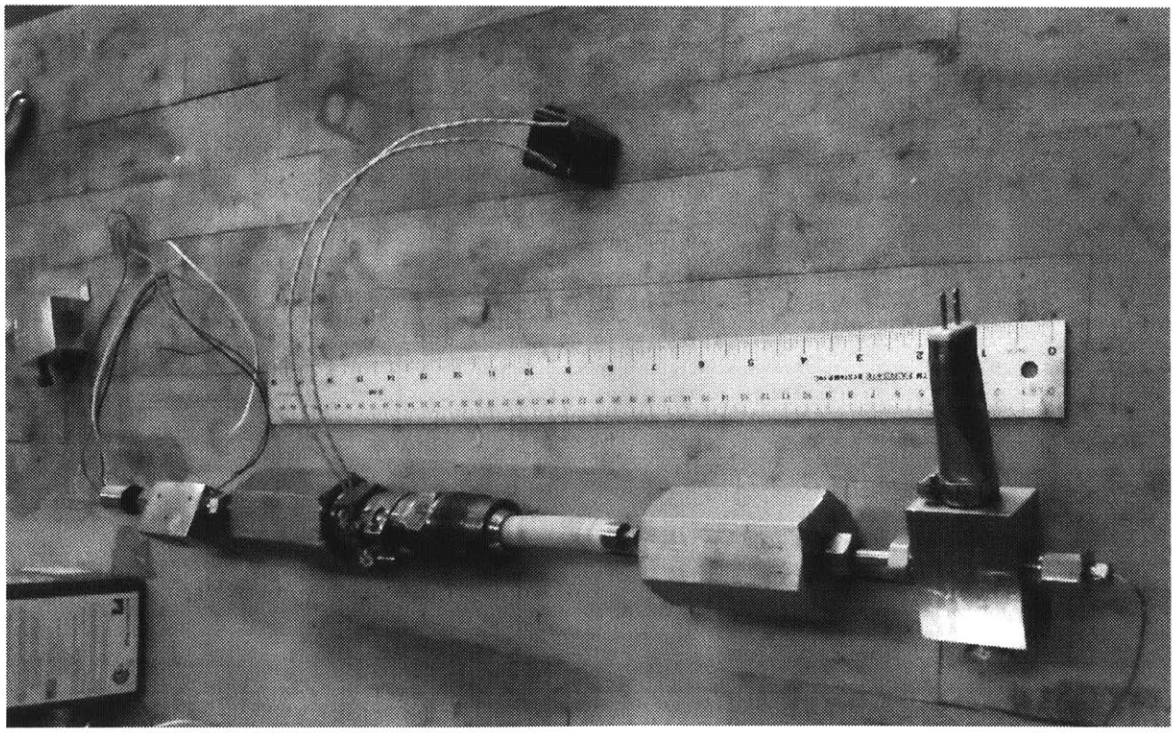

Figure B-1: The permeameter disassembled to view sample.

B.4 Permeameter for Heating Experiment

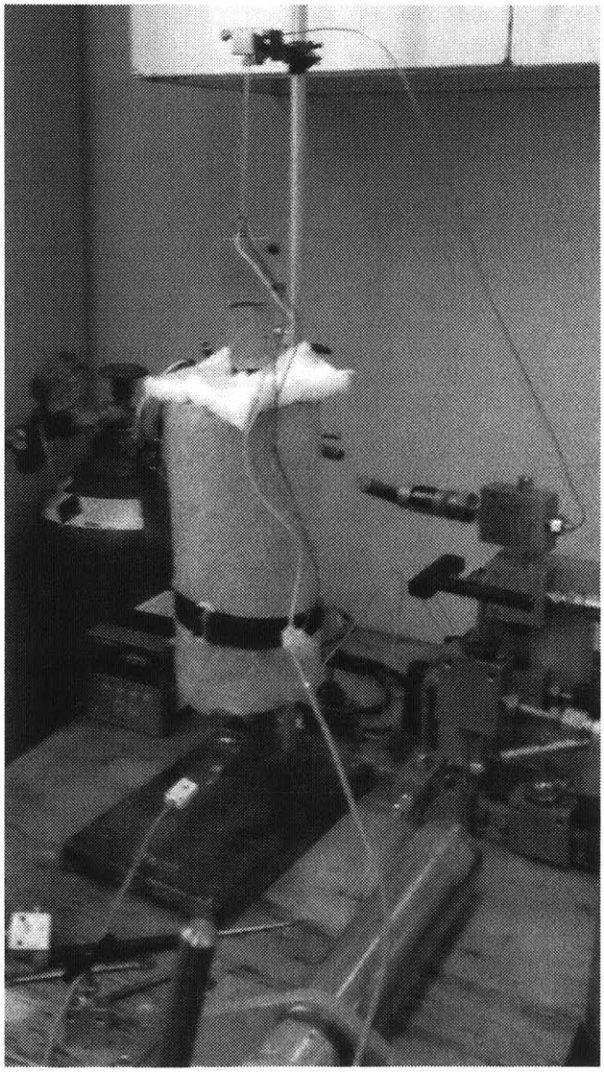

Figure B-2: Insulation applied to the outside of the permeameter to allow for accurate temperature readings when heating the sample. The pore pressure and confining pressure systems are visible in the foreground.

References

[1] J. Novak, Conception and experimental investigation of thermal switches, Tech. rep., M.S. Thesis, Massachusetts Institute of Technology, Dept. of Nuclear Engineering, Dept. of Mechanical Engineering, Cambridge, MA (1995).

[2] F. P. Incopera, D. P. Dewitt, T. L. Bergman, A. S. Lavine, Fundamentals of Heat and Mass Transfer, 7th Edition, John Wiley and Sons, 2011.

[3] E. A. Bates, Borehole meeting 2-29-2012, Tech. rep., Massachusetts Institute of Technology (2012).

[4] U. Mok, Y. Bernabé, B. Evans, Permeability, porosity and pore geometry of chemically altered porous silica glass, Journal of Geophysical Research 107 (B1,2015).

[5] R. Kranz, J. Saltzman, J. Blacic, Hydraulic diffusivity measurements on laboratory rock samples using an oscillating pore pressure method, Int. J. Rock Mech. Min. Sci. & Geomech. 27 (5) (1990) 345–352.

[6] M. Moss, M. A. Molecke, Thermal conductivity of bentonite/quartz high-level waste package backfill, in: D. G. Brookins (Ed.), Scientific Basis for Nuclear Waste Management, Vol. VI, Materials Research Society, North-Holland, 1982, pp. 719–726.

[7] R. Alvarez, What about the spent fuel?, Bulletin of the Atomic Scientists 58 (2002) 45–47.

[8] L. H. Hamilton, B. Scowcroft, M. H. Ayers, V. A. Bailey, A. Carnesale, P. V. Domenici, S. Eisenhower, C. Hagel, J. Lash, A. M. Macfarlane, R. A. Meserve, E. J. Moniz, P. F. Peterson, J. W. Rowe, P. Sharp, Blue Ribbon Commission on America's Nuclear Future:

Final Report to Secretary of Energy, Blue Ribbon Commission on America's Nuclear Future, 2012.

[9] E. A. Bates, A drop-in concept for deep borehole canister emplacement, Master's thesis, Department of Nuclear Science and Engineering, Massachusetts Institute of Technology (2011).

[10] R. L. Garwin, Reactor-grade plutonium can be used to make powerful and reliable nuclear weapons: Separated plutonium in the fuel cycle must be protected as if it were nuclear weapons., Draft, Council on Foreign Relations, New York (August 1998).

[11] B. W. Arnold, P. V. Brady, S. J. Bauer, C. Herrick, S. Pye, J. Finger, Reference design and operations for deep borehole disposal of high-level radioactive waste, Tech. Rep. SAND2011-6749, Sandia National Laboratories (October 2011).

[12] H. F. Wang, B. P. Bonner, S. R. Carlson, B. J. Kowallis, H. C. Heard, Thermal stress cracking in granite., Journal of Geophysical Research 94 (B2) (2012) 1745–1758.

[13] P. Wersin, L. Johnson, I. McKinley, Performance of the bentonite barrier at temperatures beyond 100 °c: A critical review, National Cooperative for the Disposal of Radioactive Waste (NAGRA) 32 (8-14) (207) 780–788.

[14] D. Powley, Pressures and hydrogeology in petroleum basins, Earth Science Reviews 29 (1990) 215–226.

[15] G. Zimmermann, A. Korner, H. Burkhardt, Hydraulic pathways in the crystalline rock of the ktb, Geophys J Int 142 (1) (2000) 4–14.

[16] C. Clauser, Permeability of crystalline rocks, EOS Transactions, American Geophysical Union 73 (21) (1992) 233–240.

[17] K.-B. Min, J. Rütqvist, C.-F. Tsang, L. Jing, Thermally induced mechanical and permeability changes around a nuclear waste repository: a far-field study based on equivalent properties determined by a discrete approach, International Journal of Rock Mechanics & Mining Sciences 42 (2005) 765–780.

[18] J. Rütqvist, B.Freifeld, K.-B.Min, D.Elsworth, Y. Tsang, Analysis of thermally induced changes in fractured rock permeability during 8 years of heating and cooling at the yucca mountain drift scale test, International Journal of Rock Mechanics & Mining Sciences 25 (2008) 1373–1389.

[19] W. Brace, Permeability of crystalline and argillaceous rocks, Int.J. Rock Mech. Min. Sci. & Geomech Abstr. 17 (1980) 241–251.

[20] A. Batchelor, Permeability enhancement studies in southwest england, Tech. Rep. 1st Annual Report, Camborne School of Mines, Cornwall, 70 Pages (1978).

[21] C. L. Fenton, M. A. Fenton, The Rock Book, Courier Dover Publications, 1940.

[22] A. Genter, H. Traineau, B. Ledésert, B. Bourgine, S. Gentier, Over 10 years of geological investigations within the hdr soultz project, france, Proceedings World Geothermal Congress (2000) 3707–3712.

[23] I. Stober, K. Bucher, Hydraulic properties of the crystalline basement, Hydrogeology Journal 15 (2007) 214–224.

[24] C. I. Hoag, Canister design for deep borehole disposal of nuclear waste, Master's thesis, Department of Nuclear Science and Engineering, Massachusetts Institute of Technology (2006).

[25] ARPA-E, Laser-mechanical drilling for geothermal energy, Online (2010).
URL `http://arpa-e.energy.gov/?q=arpa-e-projects/laser-mechanical-drilling-geothermal-energy`

[26] H. Carlsson, Update: The international stripa project, IAEA Bulletin 28 (1) (1986) 25–28.

[27] W. Weart, Wipp: A bedded salt repository for defense radioactive waste in southeastern new mexico, Tech. Rep. 10.1021/bk-1979.ch002, Sandia Laboratories, Albuquerque, NM (April 1979).

[28] Quickrete cements material safety data sheet, Online, accessed April 8, 2013 (July 2012). URL http://www.quikrete.com/PDFs/MSDS-K1-Cements.pdf

[29] H. C. McLaughlin, Preparation and use of sodium silicate gels (1965).

[30] D. K. Smith, Cementing, Vol. 4 of Harry L. Dougherty Series, Society of Petroleum Engineers, Richardson, TX, 1989.

[31] B. L. Todd, T. M. Jr., Downhole wellbore tools having deteriorable and water-swellable components thereof and methods of use (2010).

[32] R. Courland, Concrete Planet, Prometheus Books, New York, 2011.

[33] Standard specification for portland cement (C150/C150m-12) (October 2012).

[34] Y. Xu, D. Chung, Effect of sand addition on the specific heat and thermal conductivity of cement, Cement and Concrete Research 30 (2000) 59–61.

[35] F. Sabins, P. Sennier, L. Watters, Study produces supercement for annular seal and long-term integrity in deep, hot wells, Drilling Contractor Magazine.

[36] P.-S. Cheung, Expanding addtive for cement composition (1999).

[37] K. Hossain, Volcanic ash and pumice as cement additives: pozzolanic, alkali-silica reaction and autoclave expansion characteristics, Cement and Concrete Research 35 (2005) 1141–1144.

[38] H. Binici, O. Aksogan, Sulfate resistance of plain and blended cement, Cement & Concrete Composites 28 (2006) 39–46.

[39] F. Massazza, Pozzolanic cements, Cement & Concrete Composites 15 (1993) 185–214.

[40] E. J. Mayhew, Oil and gas well cementing composition, u.S. Patent 3036633 (May 1962).

[41] J. P. Pendrys, Biodegradation of asphalt cement-20 by aerobic bacteria, Applied and Environental Microbiology 55 (6) (1989) 1357–1362.

[42] M. V. Swain, J. T. Hagan, Indentation plasticity and the ensuing fracture of glass, Journal of Physics D: Applied Physics 9 (15) (1976) 2201.
URL http://stacks.iop.org/0022-3727/9/i=15/a=011

[43] S. Shaikh, Effective thermal conductivity measurements relevant to deep borehole nuclear waste disposal, S.m. thesis, S.M. Thesis, Massachusetts Institute of Technology, Department of Nuclear Science and Engineering, Cambridge, MA (2007).

[44] Westinghouse, AP1000 brochure, Online Brochure (2007).
URL http://www.westinghousenuclear.com/docs/AP1000_brochure.pdf

[45] C. Bailey, Stainless steel thermal properties, Online (January 2013).
URL http://www.mace.manchester.ac.uk/project/research/structures/strucfire/materialInFire/Steel/StainlessSteel/thermalProperties.htm

[46] J. Brisson, MIT Course 2.006: Property data tables, Booklet (Spring 2008).

[47] J. Kim, Analysis of laminar mixed convection in vertical tube annulus with upward flow, ASME HTD 42 (1985) 91–98.

[48] J. Z. R.K. Goel, Bhawani Singh, Underground Infrastructures: Planning Design and Construction, Butterworth-Heineman, Waltham, MA, 2012.

[49] U.S. National Research Council Subcommittee for Review of the KBS-II Plan, A review of the Swedish KBS-II Plan for disposal of spent nuclear fuel, National Academy of Sciences, 1980.

[50] D. Dixon, M. Gray, A. Thomas, A study of the compaction properties of potential clay-sand buffer mixtures for use in nuclear fuel waste disposal, Engineering Geology 21 (1985) 247 – 255. doi:10.1016/0013-7952(85)90015-8.
URL http://www.sciencedirect.com/science/article/pii/0013795285900158

[51] J. Rydberg, Groundwater chemistry of a nuclear-waste repository in granite bedrock, UC-70 UCRL-53155, Lawrence Livermore National Laboratory (1981).

[52] R. Hall, D. Martin, The thermal conductivity of powder beds. a model, some measurements on uo, vibro-compacted microspheres, and their correlation, Journal of Nuclear Materials 101 (1981) 172–183.

[53] J. Bear, Hydraulics of Groundwater, McGraw-Hill Series in Water Resources and Environmental Engineering, McGraw-Hill Inc., Jerusalem, Israel, 1979.

[54] J. Galíndez, J. Molinero, J. Samper, C. Yang, Simulating concrete degradation processes by reactive transport models, J. Phys. IV France 136 (2006) 177–188.

[55] Z. E. Heineman, Fluid Flow in Porous Media, University of Leoben, 2005.

[56] M. Jooss, H. W. Reinhardt, Permeability and diffusivity of concrete as function of temperature, Cement & Concrete Research 32 (2002) 1497–1504.

[57] W.-S. Kuo, Evaluation of deep drillholes for high level nuclear waste disposal, Master's thesis, Department of Nuclear Science and Engineering, Massachusetts Institute of Technology (1991).

[58] G. Ondrey, Nuclear-waste sponge?, Chemical Engineering (2013) 12.

[59] Omega, Thermocouples: An introduction, Online (May 2013).
URL `http://www.omega.com/thermocouples.html`

[60] H. Akgün, An assessment of borehole sealing performance in a salt environment, Environmental Geology 31 (1/2) (1997) 34–41.

[61] G. S. Was, Fundamentals of Radiation Materials Science, Springer-Verlag Berlin Heidelberg, New York, 2007.

[62] P. L. Hoffman, J. J. Breslin (Eds.), The Technology of High-Level Nucear Waste Disposal, Vol. 1, Technical Information Center, U.S. Department of Energy, 1981, prepared for the Department of Energy National Waste Terminal Storage Program Office.

[63] Glycerine: an overview, Tech. rep., The Soap and Detergent Association, Glycerine & Oleochemical Division, New York (1990).